2008

Synthesis and Surface Characterization of Silica-Polypeptide Composite Particles

Erick Isael Soto-Cantu
Louisiana State University and Agricultural and Mechanical College, esotoc1@lsu.edu

SYNTHESIS AND SURFACE CHARACTERIZATION OF SILICA-POLYPEPTIDE COMPOSITE PARTICLES

A Dissertation

Submitted to the Graduate Faculty of
Louisiana State University and
Agricultural and Mechanical College
in partial fulfillment of the
requirements for the degree of
Doctor of Philosophy
in
The Department of Chemistry

By
Erick Isael Soto-Cantu
B.S. Universidad Autónoma de Nuevo León, México, 2001
December, 2008

To my family

ACKNOWLEDGEMENTS

First, I would like to thank my research advisor Prof. Paul Russo. He provided me with scientific guidance but at the same time gave me freedom to explore and try to solve the problems using my ideas. His critique was always constructive and intended to foster scientific thinking. He nurtured a “can do” attitude towards problem solving.

I am thankful to the members of my advisory committee. I often had informal meetings with Prof. Robin McCarley to discuss the progress of my research. He provided valuable suggestions and his time in the laboratory. Prof. Ioan Negulescu trained me and allowed me to use the thermal analysis instruments in his lab. Prof. William Daly who has extensive experience in polymer science helped and me to reason and solve questions about my research. I thank Prof. Donghui Zhang for serving in my advisory committee and for all her helpful comments. I would also like to thank Prof. Harris Wong for serving as the Dean’s representative.

I am in debt to Cindy Henk and Ying Xiao of the Socolofsky Microscopy Center at LSU. Cindy had always an attitude of help and provided valuable advice result of her long experience. She was a great contributor for obtaining the TEM images of stained silica-polypeptide composite particles. Dr. Rafael Cueto trained me on the use of equipment such as gel permeation chromatography, asymmetric flow filed-flow fractionation, zetasizer, autotitrator, UV-vis. He provided his time and advice for a number of experiments. Dr. Dale Treleaven trained me and helped me with NMR characterization. Prof. Qinling Wu allowed me to use the thermal analysis instrument in his lab on times of high need. I would like to acknowledge Prof. Timothy Deming for allowing me to visit his lab at UCLA in order to learn

valuable synthetic tools. I am thankful to Dr. Alfonso Davila for helping me to set up and build laboratory hardware as well as for his help and comments on infrared data acquisition.

I appreciate the help of my colleagues in Dr. Russo's group. Garrett Doucet, Nadia Edwin, Jirun Sun, Derek Dorman, Brandon Curtis, Sreelatha Balamurugan, Katie Vance, Matt Seamster, Cecile Pitot, Amanda Steffens, Melissa Collins, Javoris Hollinsworth, Cornelia Rosu and Xiaowei Tong. I am particularly thankful to Sibel Selcuk, Jianhong Qiu and Jerome Koch for their teamwork in our common research goals. I value the help of members of the Deming's research group: Jarod Hanson, Jennifer Yang and Zhibo Li.

I would like to acknowledge the National Science Foundation and Louisiana State University for funding this work. I am thankful to the Coates Travel Award and APTEC for funding trips to present my work and to visit Prof. Deming's lab.

My family has always been with me in my decision making and I am extremely thankful for their support. My sister Gabriela is majoring in graphic design and helped me to adapt some of the figures in this document.

TABLE OF CONTENTS

ACKNOWLEDGEMENTS iii

LIST OF TABLES vii

LIST OF FIGURES viii

ABBREVIATIONS AND SYMBOLS xiii

ABSTRACT xvi

CHAPTER 1 GENERAL INTRODUCTION 1
1.1 Introduction 1
1.2 Dissertation Overview 2

CHAPTER 2 LITERATURE REVIEW 4
2.1 Introduction 4
2.1.1 Colloidal Silica 4
2.1.2 Surface Modification 7
2.1.3 Surface Characterization 13
2.1.4 Core-Shell Particles 16
2.1.5 Polymer Brushes 20
2.1.6 Polypeptides 22
2.1.6.1 PBLG and PLGA 25
2.1.6.2 PCBL and PLL 27
2.1.6.3 PEG-Lysine 28

CHAPTER 3 EXPERIMENTAL 30
3.1 Synthesis 31
3.1.1 Silica Cores 31
3.1.1.1 Original Stöber Method 31
3.1.1.2 Modified Method 32
3.1.1.3 Etching with HF 32
3.1.2 Functionalization 32
3.1.3 *N*-Carboxyanhydrides 33
3.1.4 Silica-Polypeptide Composite Particles 34
3.1.4.1 Silica-PBLG Composite Particles 34
3.1.4.2 Silica-PLGA Composite Particles 35
3.1.4.3 Silica-PCBL Composite Particles 36
3.1.5 Poly(N_ε-carbobenzyloxy-L-lysine) 36
3.2 Characterization 37
3.2.1 Dynamic Light Scattering 37
3.2.2 Asymmetric Flow Field-Flow Fractionation 38
3.2.3 Electron Microscopy 38

3.2.4 Quantification of Amino Groups 39
3.2.5 Zeta Potential 40
3.2.6 Thermogravimetric Analysis 40
3.2.7 Gel Permeation Chromatography 40
3.2.8 Nuclear Magnetic Resonance 43

CHAPTER 4 RESULTS AND DISCUSSION 44
4.1 Silica Cores 44
4.1.1 Control of Size 44
4.1.2 Control of Polydispersity 48
4.1.3 Quantification of Amino Groups 54
4.1.4 Relationship Between Amino Group Surface Density and Zeta Potential 62
4.2 Polypeptide Shell 63
4.2.1 Sequential Growth of Polypeptide 63
4.2.2 Shell Visualization by Positive Staining Transmission Electron Microscopy 69
4.2.3 pH Behavior of PLGA-SiPCPs 88
4.2.4 NMR Study of PCBL-SiPCPs 91

CHAPTER 5 CONCLUSIONS AND FUTURE WORK 105
5.1 Conclusions 105
5.2 Future Work 107
5.2.1 Measurement of the Molecular Weight of PBLG 107

REFERENCES 109

APPENDIX A SUPLEMENTAL MATERIAL FOR CHAPTER 5 127

APPENDIX B PERMISSION 134

VITA 136

LIST OF TABLES

Table 3.1 Composition of low molar mass cocktail 42

Table 3.2 Composition of medium molar mass cocktail..... 42

Table 3.3 Composition of high molar mass cocktail 42

Table 4.1 Size of P/F silica particles measured by TEM at different accelerating voltages..... 81

Table 4.2 Size of silica-PBLG composite particles measured by TEM at different accelerating voltages. 84

Table 4.3 Comparison of the core hydrodynamic radius and shell thickness of silica-PBLG composite particles measured by dynamic light scattering and TEM. 87

Table 4.4 Comparison of the hydrodynamic radius and shell thickness of silica-PCBL composite particles of low initiator surface density (ES.4.53A) at 15 °C and 40 °C in *m*-cresol measured by dynamic light scattering. 103

Table 4.5 Comparison of the hydrodynamic radius and shell thickness of silica-PCBL composite particles of high initiator surface density (ES.4.53A) at 15 °C and 40 °C in *m*-cresol measured by dynamic light scattering. 104

LIST OF FIGURES

Figure 2.1 Scheme of the synthesis of colloidal silica by the Stöber process (drawings not to scale). 5

Figure 2.2 General structure of a silane used in surface functionalization. Variables appear in color and constants in black. 8

Figure 2.3 Representation of the population of silanol groups on a silica surface. 8

Figure 2.4 Mechanism of silane monolayer formation. 10

Figure 2.5 Reaction mechanism of ninhydrin with an amino acid. 14

Figure 2.6 a): Basic structure of an amino acid. b): A dipeptide. 23

Figure 2.7 a): Structure of the α-helix conformation. b): Structure of the random coil conformation. 24

Figure 2.8 Scheme of the "amine" mechanism for polymerization of NCAs. Adapted from reference 175. 25

Figure 2.9 Scheme of the "activated monomer" mechanism for polymerization of NCAs. Adapted from reference 175. 26

Figure 2.10 General structure of poly-L-glutamates. 28

Figure 2.11 General structure of poly-L-lysines. 29

Figure 2.12 Structure of PEG-lysine. The PEG moiety appears in red. 29

Figure 4.1 Graph of hydrodynamic radius *vs* water/TEOS w/w, Samples ES.3.3A-H. Observed (●) and fitted (—) data. 45

Figure 4.2 Graph of hydrodynamic radius *vs* water/TEOS w/w, Samples ES.3.3A-H. Observed (●), Bogush's (—) and Razink's (—) predictions. 47

Figure 4.3 TEM images of silica particles. a): Before HF etching, sample ES.4.37A (image 90081). b): After HF etching, sample ES.4.41A (image 90095). 49

Figure 4.4 TEM images of silica particles. a): Prepared by pre-dissolving reagent grade TEOS in ethanol, sample ES.4.37A (image 90081). b): Certified standard silica, sample ES.3.181A (image 89830). 50

Figure 4.5 TEM images of silica particles. a): Prepared by pre-dissolving reagent grade TEOS in absolute ethanol, sample ES.4.37A (image 90081). b): Prepared using traditional Stöber procedure, sample ES.3.111B (image 89766). 50

Figure 4.6 AF4 trace of colloidal silica, hydrodynamic radius. a): Prepared by pre-dissolving TEOS in ethanol, sample ES.4.47A. b): Prepared using traditional Stöber procedure, sample ES.3.111A. Left axis (black curve), relative intensity of the light scattering detector at 90°. Right axis hydrodynamic radius (blue curve). 52

Figure 4.7 AF4 trace of colloidal silica, geometric radius. a): Prepared by pre-dissolving TEOS in ethanol, sample ES.4.47A. b): Prepared using traditional Stöber procedure, sample ES.3.111A. Left axis (black curve), relative intensity of the light scattering detector at 90°. Right axis geometric radius (blue curve). 53

Figure 4.8 Chemical structures of (3-aminopropyl) trimethoxysilane (APS) and methyl-trimethoxysilane (MTMS). 55

Figure 4.9 Scheme of the reaction of ninhydrin with P/F silica cores. 57

Figure 4.10 Calibration curve for quantification of amino groups. 58

Figure 4.11 Graph of surface density of amino groups measured by the ninhydrin method *vs* mol fraction of APS in the APS/MTMS solution used for surface modification (asumming monolayer formation and that the parking area of APS and MTMS is 4 molecules per nm^2). 59

Figure 4.12 Enlarged version of the graph of surface density of amino groups measured by the ninhydrin method *vs* mol fraction of APS in the APS/MTMS solution used for surface modification. 59

Figure 4.13 Scheme of the distribution of amino groups on the surface of a colloidal silica particle at low concentration 60

Figure 4.14 Scheme of the distribution of amino groups on the surface of a colloidal silica particle at high concentration. 60

Figure 4.15 Graph of zeta potential (ζ) *vs* the logarithm of the surface density of amino groups as measured using ninhydrin method. 62

Figure 4.16 TGA curves of silica-PBLG composite particles (ES.3.186B-ES.3.188C) obtained by the sequential addition of monomer (BLG-NCA) to amino-functionalized silica cores (ES.3.186A). Inner figure (bottom left) is the TGA curve of neat PBLG. 64

Figure 4.17 Graph of the %weight difference between 200 and 600 °C (Δ600-200) for silica-PBLG composite particles (ES.3.186B-ES.3.188C) obtained by the sequential addition of monomer (BLG-NCA) to amino-functionalized silica cores (ES.3.186A). 66

Figure 4.18 Graph of $R_{h,app}$ *vs* monomer added for silica-PBLG composite particles (ES.3.186B-ES.3.188C) obtained by the sequential addition of monomer (BLG-NCA) to amino-functionalized silica cores (ES.3.186A) in THF. DLS measurements were performed in pyridine. 67

Figure 4.19 Graph of polypeptide shell thickness *vs* monomer added for silica-PBLG composite particles (ES.3.186B-ES.3.188C) obtained by the sequential addition of monomer (BLG-NCA) to amino-functionalized silica cores (ES.3.186A). 68

Figure 4.20 Graph of $R_{h,app}$ *vs* q^2 for silica cores (□ ES.3.79A in water) and silica-PBLG composite particles (■ ES.3.128A in pyridine). 71

Figure 4.21 TGA curves of silica cores (ES.3.79A) and silica-PBLG composite particles (ES.3.128A). 71

Figure 4.22 a): Picture of the staining setup, b): depiction of the staining setup (not drawn to scale). 76

Figure 4.23 TEM images of silica-PBLG composite particles (ES.3.128A) stained with osmium tetroxide vapors. a): 15 minutes of exposure (image 89734), b): 30 minutes of exposure (image 89736). 77

Figure 4.24 TEM images of P/F silica cores (ES.3.111B) at different accelerating voltages. a): 40 kV, b): 60 kV, c): 80 kV, d): 100 kV (images 89385-88). 79

Figure 4.25 TEM image of P/F silica cores (ES.3.111B) chosen for image analysis (from Figure 4.24). The yellow line is the straight line selection over which the plot profile was analyzed. ... 79

Figure 4.26 Plot profiles of TEM images of P/F silica cores (ES.3.111B) at different accelerating voltages. a): 40 kV, b): 60 kV, c): 80 kV, d): 100 kV. 80

Figure 4.27 TEM images of silica-PBLG composite particles (ES.3.128A) at different accelerating voltages. a): 40 kV, b): 60 kV, c): 80 kV, d): 100 kV (images 89389-92). 82

Figure 4.28 TEM images of silica-PBLG composite particle (ES.3.128A) chosen for image analysis (from Figure 4.27). The yellow line is the straight line selection over which the plot profile was analyzed. 83

Figure 4.29 Plot profiles of TEM images of silica-PBLG (ES.3.128A) at different accelerating voltages. a): 40 kV, b): 60 kV, c): 80 kV, d): 100 kV. 83

Figure 4.30 TEM image of P/F silica-coated cobalt nanoparticles to be used as internal negative control (image 86330). 85

Figure 4.31 TEM images of silica-PBLG composite particles (ES.3.128B) with Co@silica particles (ES.3.114A) as internal negative control. a): 100 kX, b): 160 kX (images 89761-62). 86

Figure 4.32 TEM image of silica-PBLG composite particles (ES.3.128B) with Co@silica particles (ES.3.114A) as internal negative control. The corona was digitally colored for visual enhancement (image 89761). 87

Figure 4.33 Combined graph of hydrodynamic radius (■) on left axis and zeta potential (●) on right axis *vs* pH for silica-PLGA composite particles (ES.4.59A). [NaCl] ~ 0.1. Hydrodynamic radii data obtained from Malvern Zetasizer instrument. 89

Figure 4.34 Combined graph of hydrodynamic radius (■) on left axis and zeta potential (●) on right axis *vs* pH for silica-PLGA composite particles (ES.3.105B). [NaCl] ~ 0.1. Hydrodynamic radii data obtained from Malvern Zetasizer instrument. 90

Figure 4.35 Graph of hydrodynamic radius of Co@silica-PCBL composite particles *vs* temperature in *m*-cresol. (Copied with permission from reference 1) 92

Figure 4.36 GPC trace of PCBL for conformational studies (ES.4.33A). Mobile phase 0.1 M LiBr in DMF. Differential refractive index (DRI) signal (□) and light scattering at θ = 90° (LS_90°) (●) signal. 93

Figure 4.37 Conformation plot (log(R_g) *vs* log(molar mass)) of PCBL for conformational studies (ES.4.33A). Mobile phase 0.1 M LiBr in DMF. 94

Figure 4.38 NMR spectra of PCBL at temperatures below and above the reported transition temperature (15 °C and 50 °C respectively). 95

Figure 4.39 a): ^{1}H-NMR spectra of PCBL in *m*-cresol-d_8 at 15 (—) and 50 °C (—) (rescaling of Figure 4.38 focusing on the α and ε protons), b): graph of chemical shift, δ, *vs* temperature for the ε-CH_2 of PCBL. 96

Figure 4.40 Graphs of $R_{h,\,app}$ vs q^2. a): silica cores (ES.4.47A), b): silica-PCBL composite particles (ES.4.53A in *m*-cresol at 20 °C). 97

Figure 4.41 TGA curves of silica cores (ES.4.47A)(●) and silica-PCBL composite particles (ES.4.53A)(□). 98

Figure 4.42 TEM images. a): silica cores (ES.4.47A), b): silica-PCBL composite particles (ES.4.53A in pyridine). 99

Figure 4.43 ^{1}H-NMR spectra of silica-PCBL in *m*-cresol-d_8 at 15 (—) and 40 °C (—). 100

Figure 4.44 Graph of chemical shift, δ, *vs* temperature for the amide of silica-PCBL composite particle in *m*-cresol-d_8. 101

Figure 4.45 Graphs of the approximate derivative $\Delta\delta$ / ΔT *vs* temperature for the amide protons of silica-PCBL composite particles in *m*-cresol-d_8 (with data from Figure 4.44). a): heating direction, b): cooling direction. 102

Figure A1 Graph of R_g *vs* molar mass of PBLG in different mobile phases: anhydrous DMF (●), 0.1 M LiBr in DMF (★) and 0.1 M LiBr in DMF + 1% water added (■). The red line is the predicted curve for a rod. 130

Figure A2 Graph of R_h *vs* molar mass of PBLG in different mobile phases: anhydrous DMF (○), 0.1 M LiBr in DMF (△) and 0.1 M LiBr in DMF + 1% water added (□). The red line is the expected curve for a rod. 131

Figure A3 Graph of R_g or R_h *vs* molar mass of PBLG (merged) in different mobile phases: R_g in anhydrous DMF (□), R_g in 0.1 M LiBr in DMF (○), R_g in 0.1 M LiBr in DMF + 1% water added (△), R_h in anhydrous DMF (▽), R_h in 0.1 M LiBr in DMF (◇) and Rh in 0.1 M LiBr in DMF + 1% water added(◁). 132

Figure A4 Mark-Houwink plot of PBLG in different mobile phases: anhydrous DMF (●), 0.1 M LiBr in DMF (★) and 0.1 M LiBr in DMF + 1% water added (■). 133

ABBREVIATIONS AND SYMBOLS

η_0	Solvent viscosity
$[\eta]$	Intrinsic viscosity
AFFF	Asymetric flow field-flow fractionation
AFM	Atomic Force Microscopy
Ag	Silver
APS	(3-aminopropyl) trimethoxysilane
Au	Gold
BLG	λ-benzyl-L-glutamate
CBL	N_ε-carbobenzyloxy-L-lysine
Co	Cobalt
CO_2	Carbon dioxide
Cu	Copper
δ	Chemical shift
d	Diameter
dn/dc	Specific refractive index increment
DCA	Dichloroacetic acid
DCE	1,2-dichloroethane
DLS	Dynamic light scattering
DMA	2(dimethylamino)ethyl methacrylate
DMF	*N,N*-dimethylformamide
DRI	Differential refractive index
Et	Ethyl group, $-C_2H_5$
EtOAc	Ethyl acetate
FITC	Fluorescein isothiocyanate
Gd	Gadolinium
GPC	Gel permeation chromatography
H_2O	Water
HBr	Hydrogen bromide

HCl	Hydrogen chloride
HF	Hydrogen fluoride
k	Boltzmann's constant
λ	Wavelength
LiBr	Lithium Bromide
LS_90	Light scattering signal at 90 degree
M	Molar, mol/liter
$MgSO_4$	Magnesium sulfate
min	Minute
MTMS	methyl-trimethoxysilane
n	Solvent refractive index
$NaHCO_3$	Sodium bicarbonate
$NaNO_3$	Sodium nitrate
NaOH	Sodium hydroxyde
NCA	*N*-carboxyanhydride
NH_3	Ammonia
NMR	Nuclear magnetic resonance
OsO_4	Osmium tetroxide
π	Number pi, 3.1416
P/F	Passivated/functionalized
PBLG	Poly(λ-benzyl-L-glutamate)
PCBL	Poly(N_ε-carbobenzyloxy-L-lysine)
PEG-lysine	Poly(*N*-2-[2-(2-methoxyethoxy)ethoxy]acetyl-lysine)
PEO	Poly(ethylene oxide)
PLGA	poly(L-glutamic acid)
PLL	Poly(L-lysine)
PNIPAM	poly(*N*-isopropylacrylamide)
PS	Polystyrene
PTFE	polytetrafluoroethylene

q	Scattering vector
θ	Scattering angle
R_g	Radius of gyration
$R_{h,\ app}$	Apparent hydrodynamic radius
RPM	Revolutions per minute
s	Second
SEM	Scanning electron microscopy
Si	Silicon
$SiCl_4$	Silicon tetrachloride
SiF_4	Silicon tetrafluoride
SiO_2	Silicon dioxide, silica
SLS	Static light scattering
T	Absolute temperature
TEM	Transmission electron microscopy
TEOS	Tetraethyl orthosilicate
TFA	Trifluoroacetic acid
TGA	Thermogravimetric analysis
THF	Tetrahydrofuran
TiO_2	Titanium dioxide, titania
V	Volt
XPS	X-ray photoelectron spectroscopy

ABSTRACT

The synthesis and sequential surface characterization of silica-polypeptide composite particles is described. Nearly monodisperse colloidal silica cores were obtained by the alkaline hydrolysis of tetraethyl orthosilicate (TEOS). The hydrodynamic radius can be easily controlled in the range of ~ 20-140 nm by the water/TEOS ratio in the starting reaction mixture. The surface of the synthesized silica cores was further passivated/functionalized (P/F) by a mixture of (3-aminopropyl) trimethoxysilane (APS) and methyl-trimethoxysilane (MTMS). The amino groups were quantified using UV-Vis spectrometry after reaction with ninhydrin. The use of zeta potential measurements of the P/F silica particles at low pH is presented as a potential alternative for the quantification of surface amino groups.

The amino groups on the P/F silica cores were used as initiators for the polymerization of *N*-carboxyanhydrides (NCAs) yielding silica-polypeptide composite particles. The polypeptide content of silica-PBLG (silica-poly(γ-benzyl-L-glutamate)) was controlled when the synthesis was performed by sequential addition of *N*-carboxyanhydride (monomer). The polypeptide shell in a "wet" state was visualized by using positive staining with osmium tetroxide (OsO_4) vapors when the particles were dispersed in pyridine. The stained composite particles were observed using transmission electron microscopy (TEM). They appear as spheres with a light corona around them. The use of an internal negative control that can be easily observed in the same field presents a compelling argument for the hypothesis that the observed corona is the polypeptide shell. The benzyl groups of PBLG on silica-PBLG composite particles were removed by reaction with hydrogen bromide yielding silica-PLGA (poly(L-glutamic acid)) particles. The hydrodynamic radii and zeta potential were studied as function of pH. The silica-PLGA composite particles

appear extended and negatively charged at high pH and compact and neutral at low pH. This can be attributed to the changes on the PLGA shell. Silica-PCBL (poly(carbobenzyloxy-L-lysine)) composite particles were synthesized by the reaction of P/F silica cores with the respective NCA. The PCBL shell apparently undergoes a temperature-induced conformation transition as suggested by nuclear magnetic resonance and dynamic light scattering measurements.

CHAPTER 1 GENERAL INTRODUCTION

1.1 Introduction

Colloidal particles are scientifically appealing for two primary reasons: they are essential in a number of applications and they are key components in fundamental studies. The current and potential applications range from fields of nanomedicine and nanodetection to colloidal stabilization of paints, food and cosmetics. Colloidal particles play an important role in fundamental studies such as colloidal crystallization, probe diffusion and phase transitions. Because of their large size as compared to atoms or molecules, colloidal particles are considerably easier to purify and handle. Also because of their size, they are easier to track and visualize. The work by Turksen[1] contains a detailed review of practical aspects of colloidal particles with emphasis on the core-shell type. The work by Qiu[2] provides a review of fundamental aspects of colloidal particles with stress on probe diffusion.

The importance of the core-shell architecture of some designed colloidal particles is discussed in this dissertation. Biomedical applications such as bioimaging and cell labeling are reviewed by Sounderaya and Zhang.[3] Other important fields of application of colloidal particles are catalysis,[4] encapsulation of active components,[5;6] drug, gene and DNA delivery,[3;7-13] capture and release of particles such as viruses,[14] biomarking,[15;16] bioseparation, bioanalysis,[17-19] electronics,[20] optoelectronic devices[21] and reinforcing agents.[22]

The inclusion of magnetic particles inside the colloidal particles adds a degree of complexity. Salgueriño-Maceira and Correa-Duarte reviewed the status of magnetic core/shell particles for biological applications.[23] In 2006 Martel *et al.* reported the manipulation of colloidal magnetic beads at speeds in the order of 8 μm/s along preplanned paths by

magnetotactic bacteria.[24] Then in 2007, Martel *et al.*, were able to control a 1.5 mm ferromagnetic particle in the carotid artery of a living swine using a clinical magnetic resonance imaging platform.[25] The above-mentioned particles are out of the colloidal range but the study can be used as a proof concept that magnetic particles can be manipulated inside of a living organism.

In addition to the myriad of applications of colloidal particles they are good models to perform fundamental studies. For example they can be used to gain a better understanding of crystallization of atoms and molecules. Monodisperse colloidal spheres can form colloidal crystals of different structures depending on the interactions between the particles.[26;27] Also when colloidal particles of different shape are mixed, rods and spheres for example, they can form other phases such as columnar and lamellar.[28] Tagged colloidal particles can be used as tracers in order to understand diffusion in colloidal dispersions or in very viscous liquids.[29-33] Therefore, it is important to have the ability to synthesize colloidal particles in which the size, presence or absence and sign of charge, content and distribution of components such as soft and hard moieties can be easily tailored.

1.2 Dissertation Overview

The goal of this dissertation is to describe the in-depth surface characterization of silica-polypeptide composite particles. Particles of this nature have been synthesized earlier by our group. However, some parameters have to be known better in order to gain an understanding of the behavior the particles and the phases they may form.

Chapter 2 provides a comprehensive literature review including:

- The synthesis of colloidal silica and the factors that influence size and polydispersity

- The functionalization of silica surfaces using different silane agents
- The quantification of functional groups on surfaces with emphasis on amino groups
- A description of the different types of core-shell particles
- An introduction to polymer brushes
- An overview of characteristics and synthesis of homopolypeptides

Chapter 3 describes the experimental part of the synthesis and sequential characterization of silica-polypeptide composite particles. The polypeptides include PBLG, PLGA and PCBL. Chapter 4 presents the experimental results and discussion thereof. The results can be divided in 6 categories:

- Synthesis of silica cores: control in size by modification of a simple parameter and by etching with HF
- Functionalization of silica cores and quantification of amino groups on the silica surface
- Synthesis of silica-PBLG composite particles of different polypeptide content formed by sequential addition of monomer
- Visualization of the polypeptide shell of silica-PBLG composite particles by positive staining transmission electron microscopy
- Synthesis of silica-PLGA composite particles and their response to changes in pH
- Synthesis of silica-PCBL composite particles and their response to changes in temperature studied by dynamic light scattering and nuclear magnetic resonance

Chapter 5 presents the conclusions derived from this work and suggests paths for future work in this area.

CHAPTER 2 LITERATURE REVIEW

2.1 Introduction

2.1.1 Colloidal Silica

Colloidal silica is a dispersion of silicon oxide particles in the size range of roughly 1 nm to 1 μm.[34] Silica has several advantages over other inorganic materials. The difference of refractive index between silica and non polar liquids is small, which minimizes multiple scattering. The chemistry of silica and silicon compounds is very well known, and as a consequence, a large amount of reported literature on surface modification exists. The solubility of silica in a hydrofluoric acid makes HF suitable for the preparation of hollow particles. The sol-gel process by which colloidal silica is obtained is simple and robust.

A number of publications report on the preparation and characterization of colloidal silica.[35-61] The work by Stöber *et al.* published in 1968 is one of the first reports on the synthesis of colloidal silica.[35] Their work, probably the most cited in the subject, explored the formation of colloidal silica by the hydrolysis of alkyl silicates using linear alcohols as solvents, ammonia as catalyst in the presence or absence of water. A readily available and widely used alkyl silicate is tetraethyl otrhosilicate (TEOS). It can be obtained by the reaction of tetrachlorosilane ($SiCl_4$) with ethanol. A number of chemical suppliers offer different grades of TEOS as a commodity. Therefore, it is more convenient to buy it than to synthesize it. The silicon atom in TEOS carries a partial positive charge which makes it susceptible to nucleophilic attack. The molecule has a functionality of four. In the presence of water the Si-OEt bonds are hydrolyzed; EtOH and a new Si-OH (silanol) bond are produced. The silanol part of the molecule can further react with another TEOS molecule producing a Si-O-Si bond; the chemical union of the two molecules is a

dimer. The polymerization reaction proceeds further and gives cyclic molecules. Additional growing produces particles which condense to the most compact state, leaving –OH groups on the outside. These hydrolysis condensation reactions can occur on a wide range of pH; however, at pH between 7-10 and salts absent, all the condensed species are more likely to be ionized and, hence, mutually repulsive. Growth occurs primarily by the addition of monomers to more highly condensed particles.[62] TEOS and water are not miscible. For this reason a small alcohol in which both components are soluble is added. Figure 2.1 depicts the process.

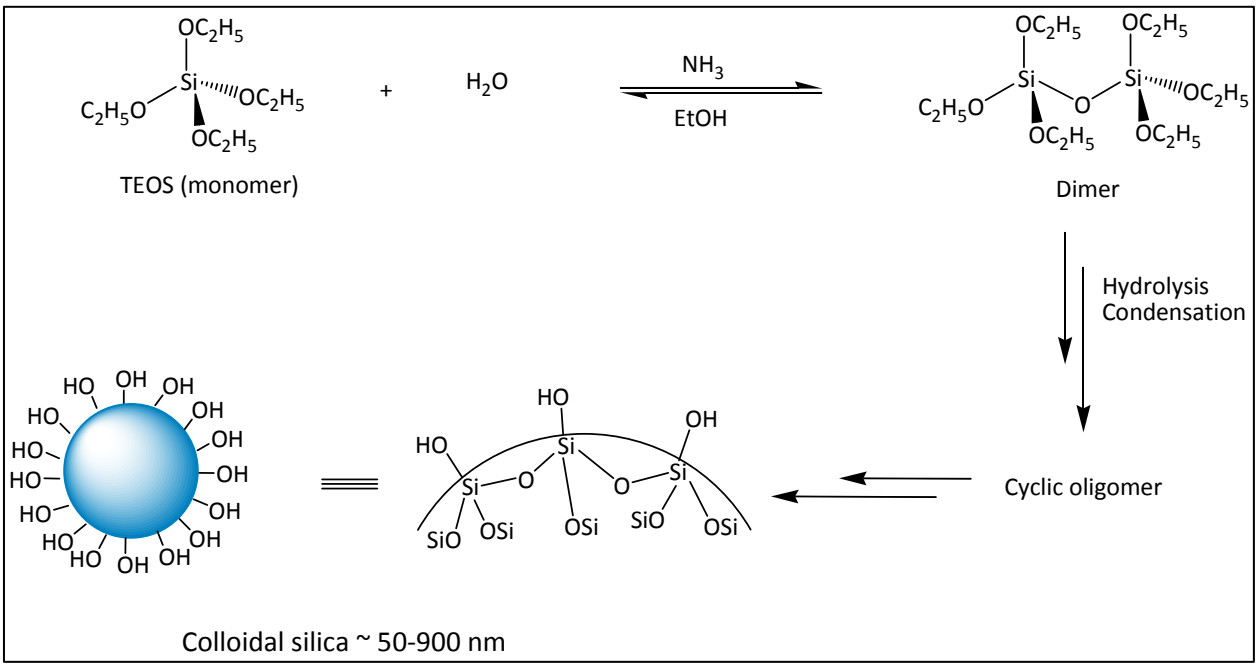

Figure 2.1 Scheme of the synthesis of colloidal silica by the Stöber process (drawings not to scale).

The effects of the concentration of components,[43;50] temperature,[44] solvent, *etc.* are well explored. Most of the factors were briefly explored in the original Stöber work. In general, an increase in either the water or ammonia concentration produces larger particles. On the other hand, an increase in temperature has the opposite effect. Alcohols of higher molecular weight yield larger particles but an increase in size polydispersity as well. In most studies

colloidal silica is obtained by the direct addition of TEOS to an ammonia/alcohol solution. Conversely, a number of different approaches has also been explored. In most cases the synthesis is carried on in batch mode. Howard and Khdary sprayed TEOS onto a methanol/ammonia solution. [41] The resulting particles have low polydispersity depending on the reaction conditions. Colloidal silica has also been obtained in water in oil emulsion and microemulsion media.[46;48] Particle size can be related to droplet size when ammonia is the catalyst. Other pathways include precipitation methods. Silica gel or olivine(a silicon-containing mineral) have been dissolved in strong base and colloidal silica formation occurs when the pH is slowly neutralized.[51;53] A similar approach includes the condensation of silicic acid in the presence of oligo-lysine.[54] Anionic surfactants have been used at low concentrations and have an effect on the particle size of the resulting silica.[56] Other self-assembled surfactants have been used as templates for the synthesis of mesoporous silica.[38] Dumbbells have been obtained by the destabilization and application of shearing to spherical colloidal silica.[39] The majority of the reports refer to batch processes; nevertheless, there have been efforts oriented to developing colloidal silica by continuous processes. Bonamartini Corradi *et al.* used a Teflon tube where the premixed reagents were passed by while irradiated by microwaves.[49] Kahn *et al.* performed the synthesis in microfluidic channels. [40]

Colloidal silica obtained by these means tends to be spherical and to posses relatively low polydispersity. This desired feature facilitates study by scattering methods, makes the particles usable for the calibration of instruments and simplifies the analysis of results for fundamental studies. Small polydispersity values are also required for the close packing of spheres into two- or three-dimensional colloidal crystals.[26;63-65] Monodisperse colloidal silica coated onto a glass surface has been used as an antireflective film for solar energy

applications.[66] A variety of metals and oxides have been used for coating or growing silica. One of priciest components of paints is titanium dioxide which is also used as a paper whitener among other uses. Hsu *et al.* reported the titania coating of silica. [67]

2.1.2 Surface Modification

Modification of surfaces is done in different fields for a variety of purposes. For example, Claesson and Philipse modified silica colloids with thiol functional groups for the irreversible adsorption of metal and oxide particles.[68] Bagwe *et al.* modified silica nanoparticles with different functional groups to reduce aggregation and nonspecific binding.[69] Matoussevitch *et al.* modified metallic cobalt nanoparticles for stabilization.[70] Csogor *et al.* modified the surface of colloidal silica particles with different basic groups for gene delivery.[8] Similarly, Kneuer *et al.* used amino-modified silica nanoparticles as carriers for plasmid DNA.[9] Chen *et al.* was able to reversibly capture and release bacteriophage viruses using similarly modified particles.[14] Kurth and Bein modified an oxidized aluminum surface for immobilization of pepsin.[71] Possibly one of the most common uses of surface modification is simply to produce colloidal stability.[72;73]

Silica (SiO_2), silicon (Si), iron, mica, among other surfaces are commonly modified by taking advantage of the rich silane chemistry. Silanization reactions have been researched extensively. Brunner *et al.* reported the substrate effects in the functionalization of mica, native silicon and silica coated silicon using octadecyltrichlorosilane.[74] Figure 2.2 shows the general structure of a silane used in surface modification. It is color coded; variables appear in color and constants appear in black.

- Silane molecules have invariably a central silicon (Si) atom

- They possess an anchoring group (A) generally chloro or alkoxy, the number of anchoring groups (m) is 1, 2 or 3
- They bear a non-anchoring group (N) which is almost invariably methyl, the number of non-anchoring groups is 0, 1 or 2
- They have an alkyl chain $-(CH_2)_n-$ of n carbons varying normally from 0 to 20
- An R group such as –H, -X, -OH, -COOH, -CN, $-N_3^+$, $-NH_2$ among others is attached to the alkyl chain (or to the Si atom if n = 0)

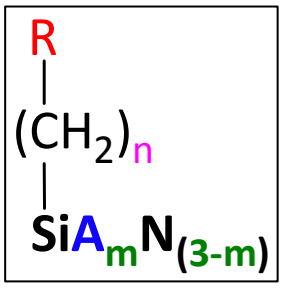

Figure 2.2 General structure of a silane used in surface functionalization. Variables appear in color and constants in black.

The anchoring group is normally chloro or alkoxy.[75-80] Chlorosilanes are relatively more reactive than alkoxysilanes. They are more sensitive to water present in the solvent or substrate.[76] The silica substrate has naturally occurring hydroxyl groups, geminal and single as depicted in Figure 2.3.

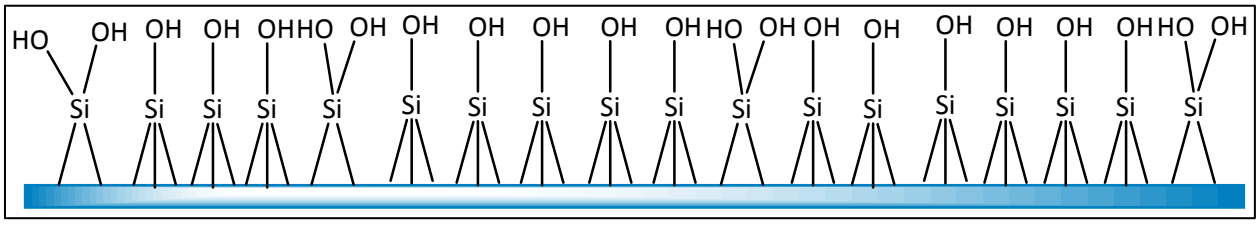

Figure 2.3 Representation of the population of silanol groups on a silica surface.

The total surface concentration of hydroxyl groups has been measured by thermogravimetry and nuclear magnetic resonance (NMR) spectroscopy. The most accepted value[74;81] is around 4-5 hydroxyl groups/nm^2. The mechanism for monolayer formation is depicted on Figure 2.4. It starts by the hydrolysis of the labile groups attached to the silicon atom (chloro or alkoxy). Once those groups become hydroxyl, they hydrogen bond to hydroxyl groups of neighbor silane molecules or to the hydroxyl groups on the surface (non-hydrolyzed alkoxy groups are also capable). Covalent bonds are formed after the condensation of water (or alcohol if the alkoxy group was not hydrolyzed previously). The formation of Si-O-Si bonds between neighbor silane molecules is known as lateral polymerization. Bieraum *et al.* reported that films obtained from trichlorosilanes are more ordered than the ones obtained from trialkoxysilanes.[78] That is probably due to incomplete lateral polymerization. The presence of non-labile groups, generally methyl, attached to the silicon atom gives less anchoring points as well as lower probability or impossibility of lateral polymerization. It has been reported that alkoxysilanes bearing one or two methyl groups on the silicon atom yield more uniform thin layers than the ones bearing only labile groups.[75]The presence of more anchoring points (chloro or alkoxy) brings the possibility for the formation of 3-D networks that can extend to thicknesess of up to tens of nanometers.[82] In general, trichlorosilanes or trialkoxysilanes produce thicker layers than the di- or mono- counterparts. Chain length is key factor in the formation of thin films of silane molecules.[78-80;82] It has been reported that longer alkyl chains tend produce more ordered films.[78] Bieraum *et al.* concluded that the optimal chain length in terms of order is 18 carbons. The water contact angle of the films is almost independent of the alkyl chain length. This indicates that the packing of the films does not allow the penetration of liquid water.

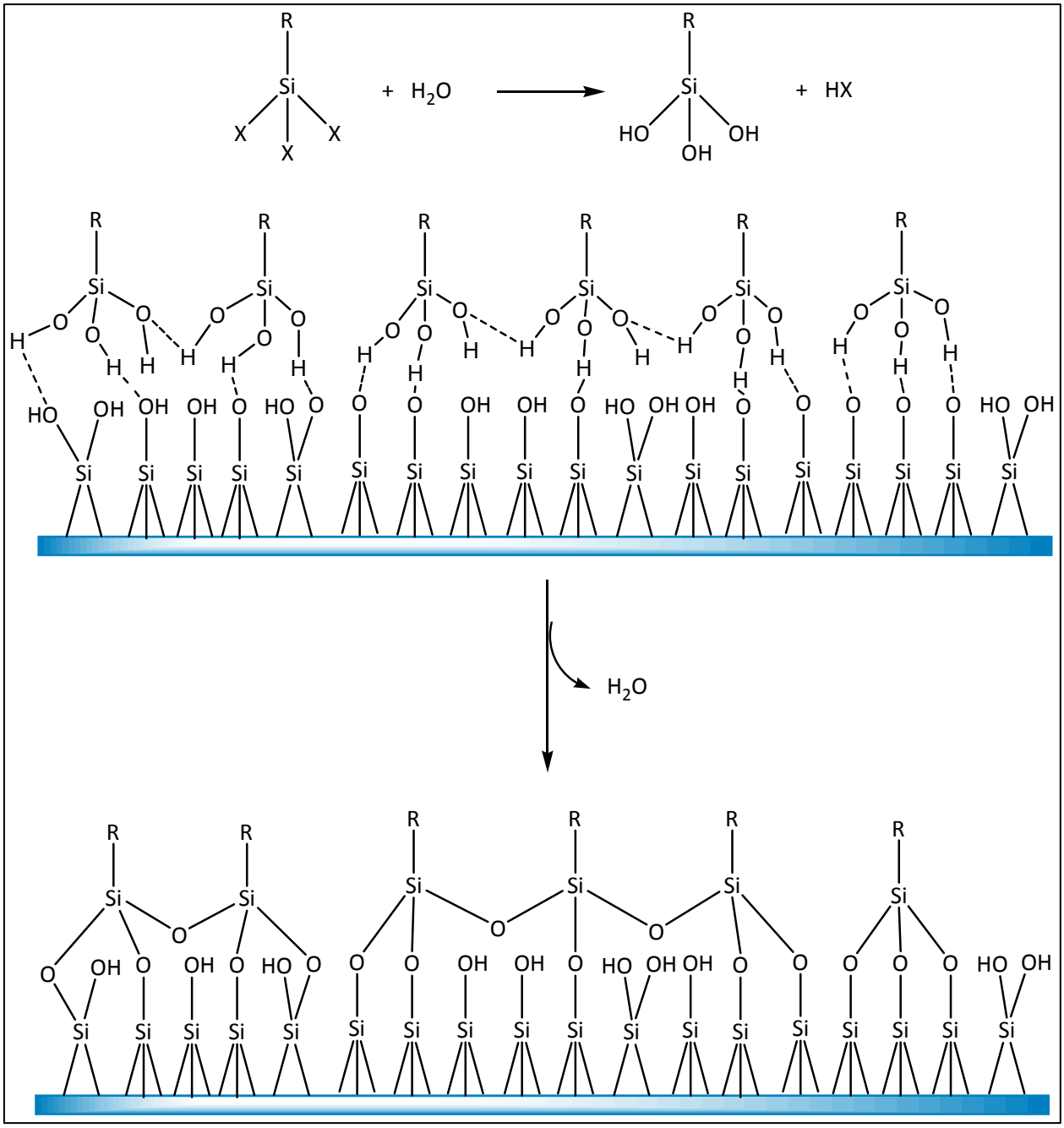

Figure 2.4 Mechanism of silane monolayer formation.

In one of the earliest reports of the functionalization of surfaces using alkoxysilanes, Haller reported conducting the reaction in the vapor phase.[83] The author claimed that strictly monolayers are formed. Later, Fadeev and McCarthy reported that dichloro- and trichloroalkylsilanes yield more oriented films by reaction in solution than in the vapor phase

using ehytldiisopropylamine as a catalyst.[82] Other amines such as triethylamine[84] and ethylenediamine[85] have been used as catalysts for reactions of this nature. Amines can act as bases and weakly bind to the acidic protons of the naturally occurring hydroxyl groups on silicon or silica surfaces. It is possible to think of it as the amine molecule saving the space for the incoming silane molecule and therefore yielding a more ordered assembly. The effect of water on the substrate surface or in the solvent has also been studied. Krasnoslobodtsev and Smirnov reported the effect that water has on silanization of silica by trimethoxysilanes.[86] They concluded that monolayers are formed when water is absent. In a previous study, McGovern *et al.* reported the role of solvent in the silanization of glass using octadecyltrichlorosilane.[87] They investigated different solvents that have different affinity for water. It was found that solvents that have low water content lead to incomplete monolayer formation whereas in solvents with high water contentration, polymerization occurs in the bulk solvent phase. Solvents such as benzene or toluene can have a water concentration (~ 1.5 ppm) that is optimum for the formation of closely-packed monolayers. It has been reported that liquid and supercritical carbon dioxide is also a good solvent for silanization reactions.[88]

The presence or absence of a functional group in the alkyl chain is another variable that plays a role in the silanization reaction. For example, it was found that the interactions between the amino groups of trichloro or trimethoxysilanes, lead to the formation of disordered films.[78] On the contrary, the alkyl chain of alkyltrichloro or aklyltrimethoxysilanes without a functional group does not interact with the silanol groups on the surface. This lack of interaction permits only the anchoring groups (hydrolyzed chloro or alkoxy) to interact with the surface yielding oriented films.

A number of terminal functional groups can be covalently attached to a variety of surfaces. Vinyl, alcohol, carboxylic acid, amine bromine, azide are just a few examples of end-functionalities that can be attached to surfaces by taking advantage of silane chemistry.[71;75-78;80;84;85;89-92] Balachander and Sukenik made chlorosilanes of different functionalities (-NH_2, -N_3^+, -Br, -CN) using ω-undecenyl alcohol and self-assembled them on glass or silicon surfaces.[77] In one of the most comprehensive reports on the modification of silicon surfaces using alkylchlorosilanes, Wasserman from the Whitesides group created different functionalities by modifying the terminal double bond of the assembled monolayers.[80] The amino functionality is of particular importance for this project because amines are known to initiate the ring-opening polymerization of *N*-carboxyanhydrides.[93]

Initially, Fong and Russo reported the synthesis of silica-polypeptide composite particles using only (3-aminopropyl) trimethoxysilane (APS) for the functionalization of colloidal silica.[94;95] Later, Turksen found that using only APS for the functionalization may lead to the formation of polypeptide that has steric hindrance constraints.[1] In order to overcome this, the introduction of a non-reactive group that acts as a spacer was necessary. Methyl-trimethoxysilane (MTMS) was used as spacer. Functionalization with a solution of APS and MTMS can lead to particles that have the amino groups that can as as initiators but also have passive methyl groups that act as spacers. The idea of using a mixture of passive and active moieties was explored by Heise *et al*.[89] They used a mixture of 1-bromo-11-(trichlorosilyl)undecane and 1-trichlorosilylundecane in order to modify silicon substrates. The bromo group was transformed to amino *in situ*. They further used the amino groups as initiators for the polymerization of γ-benzyl-L-glutamate-*N*-carboxyanhydride. A similar concept has been applied on colloidal particles.[69;96]

2.1.3 Surface Characterization

The knowledge of the surface concentration of initiator (amino groups) is essential.Ring-opening polymerizations of *N*-carboxyanhydrides normally behave as *living*, so it is essential to know the exact amount of initiators. The monomer to initiator ratio can be used to predict the molecular weight of the resulting polymer. Also, by knowing the concentration of initiators, it is possible to perform kinetic studies on the polymerization reaction. Another reason why it is important to know the surface concentration of initiators is to calculate steric constraints.

Most of the methods for surface characterization such as X-ray photoelectron spectroscopy (XPS), ellipsometry, contact angle, atomic force microscopy (AFM) either work best or exclusively on flat surfaces. Extensive characterization of silane films has been done using above-methods. [71;74;78-80;82;83;86-88;91;92;97-102]

The solid-phase synthesis of peptides has required methods to verify the presence of amino groups. In 1970 Kaiser *et al.* reported a simple method for testing the completion of the reaction in the Merrifield solid-phase synthesis. They reported that the method is sensitive to 5 μmol/g .[103] It involves the reaction of ninhydrin with a terminal primary amine which produces a bright purple complex. The reaction mechanism is shown in Figure 2.5 (adapted from reference 104). The colored product formed has the "stolen" nitrogen of the amine that was tested. In other words, the nitrogen that was "immobilized" on the solid substrate is extracted by the ninhydrin molecule and becomes part of the colored molecule in solution.

In 1973 Felix and Jimenez reported the use of fluorescamine as a qualitative method for the detection of completeness in solid-phase coupling reactions.[105] The authors claim that the method is capable of detecting pmol quantities of primary amines. A key difference between the ninhydrin and the fluorescamine methods is that in the latter the fluorescent product is

attached to the solid surface. This is potentially a drawback if the method is to be used for quantification on colloidal particles due to scattering.

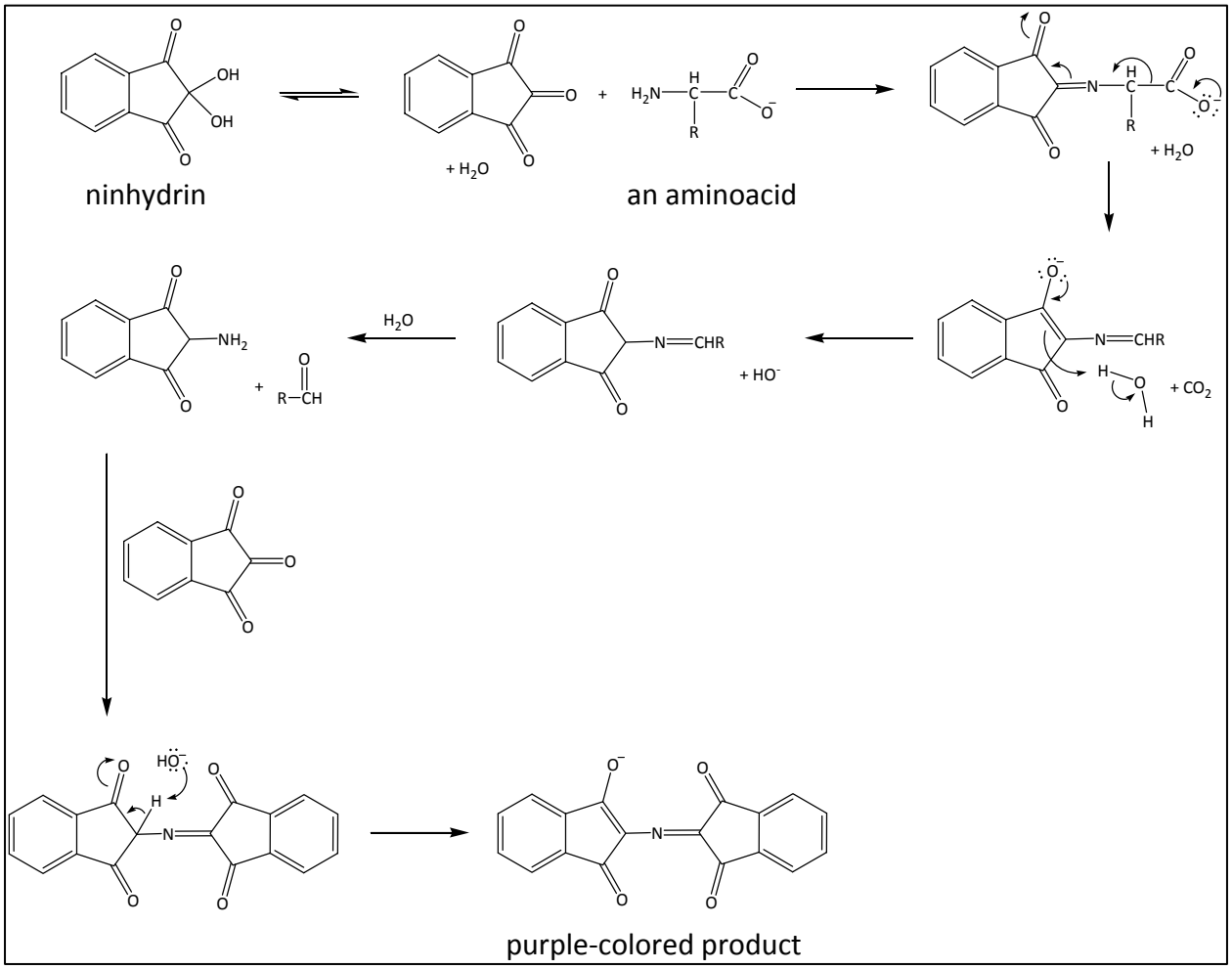

Figure 2.5 Reaction mechanism of ninhydrin with an amino acid.

In 1976 Hancock and Battersby reported the use of 2,4,6-trinitrobenzenesulphonic acid for the qualitative analysis of free amines in solid-phase peptide synthesis.[106] The authors claimed that the method is more sensitive than the ninhydrin method. The red-orange product is attached to the solid phase and has to be observed under the microscope. Like the fluorescamine method, this is a potential drawback if the method is to be used quantitatively. In 1990 Flegel and Sheppard reported the use of bromophenol blue as a quantitative method

for the monitoring of continuous flow solid-phase peptide synthesis.[107] The method is indeed quantitative but only for the synthesized peptide. It is qualitative for the amino groups. Kay *et al.* wrote a review of qualitative methods for monitoring solid-phase synthesis.[108]

In 1992 Kurth and Bein described experiments designed to monitor the reaction of 3-aminopropyltriethoxy silane on an aluminum oxide surface.[109] They were able to quantify the amount of deposited silane using a quartz crystal microbalance. Ganachaud *et al.* reported the quantification of amino groups on the surface of polystyrene latex particles.[110] The method involves adding an excess of 3-(2pyridyldithio) propionic acid to the particles. The excess reagent is removed by centrifugation, and pyridine-2-thione is released in solution after reaction with dithiotritol. Saitoh *et al.* added an excess of fluorescein isothiocyanate (FITC) to a dispersion containing bacteria in order to quantify the amino groups on their surface.[111] Even though the method uses a fluorescent dye, it is relies on measuring the absorbance of the FITC in excess. They also reported another spectrophotometric method using dithiobis(5-nitropyridine). Locascio-Brown *et al.* used a radiometric and a fluorometric method for the quantification of amines on soda-lime glass spheres.[112] The radiometric method consisted of reacting ^{14}C-acetyl chloride with the surface amino groups. The acetyl amide was then cleaved from the particles using trisodium phosphate and the spheres were centrifuged. The radioactivity of the supernatant was measured and related to the amine concentration. The fluorometric method used a similar approach. The amino groups were first removed by hydrolysis with trisodium phosphate and the colloidal spheres were removed by centrifugation. The supernatant containing amine was then reacted with fluorescamine.

Ninhydrin has been used mostly for quantitative analysis. Nevertheless, Henry *et al.* used ninhydrin for the quantification of amines on the surface of an amino-modified

polymer.[113] In an example of the use of ninhydrin for quantitative purposes on particles, Sarin *et al.* were able to measure the amino group concentration on polystyrene beads used for solid-phase peptide synthesis.[114] The report includes a proposed mechanism that explains the presence of blue color on the beads and a way to overcome it.

2.1.4 Core-Shell Particles

Core-shell particles can be divided, by the nature of their components, into inorganic-inorganic, organic-organic and organic-inorganic. One of the advantages of their morphological nature relies in the fact that is possible to control the overall properties by controlling the size or composition of the components.

The inorganic-inorganic type normally consists of hard and dense particles of high refractive index. Grasset *et al.* reported the synthesis of CeO_2@SiO_2 particles by a water-in-oil microemulsion approach. These particles have potential applications as components of anti-UV films and catalysis.[115] Kobayashi *et al.* was able to produce SiO_2-Gd-SiO_2 nanoparticles that exhibit good properties as magnetic resonance contrast agents.[116] Kobayashi and Sakuraba reported the synthesis of Cu@SiO_2 particles.[117] The silica coating improved the stability of copper. The concept of applying a silica coating over a transition metal in order to improve its stability has also been applied to cobalt yielding Co@silica particles.[118;119] These particles have potential applications in recording media, drug delivery, among others. Liz-Marzán *et al.* reported the synthesis of Au@SiO_2 particles.[120] They demonstrated that dispersions of different colors can be obtained by controlling the thickness of the silica shell and the refractive index of the dispersant. Kim *et al.* reported the preparation of SiO_2@Au particles using an alcohol reduction method.[121] Ag@SiO_2 particles have been synthesized using a similar approach.[122] Chou and Chen reported a similar kind of particles but in this case the silica shell

was porous.[123] The protective coat was helpful against sintering effects. Kalele *et al.* synthesized SiO_2@Ag particles and used them for the optical detection of antibodies.[124] Lee *et al.* reported the synthesis of TiO_2@SiO_2 particles with controlled shell thickness.[125] Because of the titanium dioxide coating, these particles have potential applications in photocatalysis, and in the coatings industry as white pigments. All of the above particles are spherical in shape. Core-shell rod particles of adjustable aspect ratios have also been produced.[126]

Core-shell particles of organic-organic nature are generally soft and one or both components are stimuli responsive such as temperature, salt concentration or pH. Nevertheless, in some instances, the function of the shell is to improve dispersibility or reduce aggregation. For example, Giani *et al.* reported the synthesis of PTFE particles with a polystyrene (PS) coating.[127] pH-responsive core-shell particles have been synthesized using copolymers as building blocks. The controlled aggregation of a triblock copolymer of poly[(ethylene oxide)-*block*-2(dimethylamino)ethyl methacrylate-*block*-2-(diethylamino)methacrylate] (PEO-DMA-DEA) resulted in "onionlike" micelles of DEA cores, DMA inner shells and PEO outer shells.[128] Using a different approach, Zhang *et al.*, reported the preparation of pH-responsive core-shell particles using poly(ε-caprolactone) as the core and poly(acrylic acid) as the shell.[129] A substantial difference lies in the fact that the polymers are not covalently connected. After core biodegradation or dissolution, the core-shell particles can become hollow. A very commonly used polymer in the synthesis of core-shell particles is poly(*N*-isopropylacrylamide) (PNIPAM) due to its dramatic volume changes at around 32 °C. This phase transition is reversible and it is the reason why PNIPAM is widely used in the synthesis of temperature-responsive particles.[130-135] Chu *et al.* reported the synthesis of core-shell microcapsules with PNIPAM chains acting as thermoresponsive gates.[134] They used those

particles for the controlled release of sodium chloride and vitamin B_{12}. By taking advantage of the temperature responsiveness of PNIPAM as well as other pH sensitive polymers, it has been possible to synthesize core-shell particles that are both temperature and pH responsive. Cores of PNIPAM and shell of poly(4-vinylpyridine)[130] or poly(2-vinylpyridine)[135] have been reported. In both instances the pH sensitive polymer is a base. Jones and Lyon synthesized poly(*N*-isopropylacrylamide-*co*-acrylic acid) cores, in this case the copolymer is an acid.[132] They grew a PNIPAM shell on top of the core; that resulted in its restricted sweling. Poly(ethylene oxide) (PEO) is another very popular polymer due to its biocompatibility. Qiu and Wu synthesized PNIPAM grafted with PEO and took advantage of the reversible temperature-induced phase transition of PNIPAM in order to form core-shell particles.[133]

Core-shell particles of hybrid nature, *i.e.* organic/inorganic, commonly have a hard inorganic core and a soft organic shell. One of the advantages over the organic/organic type is that the cores are normally better defined. The presence of organic and inorganic materials makes them more versatile. A metal used frequently as core is gold. Marinakos *et al.* reported the preparation of Au@poly(*N*-methylpyrrole) particles.[136] The gold cores were etched, hence producing poly(*N*-methylpyrrole) hollow particles. They were able to load the gold cores with guest molecules and they remained after the shell was formed and the core was etched away. This principle can be extended to other molecules such as enzymes, proteins, DNA and the hollow particles can work as carriers. Mariankos *et al.* reported the synthesis of a similar kind of particles with a conductive polymer shell.[137] Shan *et al.* grafted pre-made PNIPAM and PS to gold nanoparticles.[138] They were able to control the hydrophobic/hydrophilic character of the particles by controlling the ratio of PNIPAM to PS. There are instances in which the gold core has served as seed for the growth of a silica shell that works as the anchor for polymer

attachement.[139;140] Silica is one of the most frequently used materials as a core due to the rich silane chemistry discussed earlier in this chapter. For example, Yang *et al.* polymerized pyrrole on the surface of colloidal silica.[141] Luo *et al.* deposited a coating of polyaniline on the surface of an electrode in order to improve its sensitivity.[142] Polystyrene has been grown from colloidal silica particles.[143] Wu and Ke studied the effect of silica-PS core-shell particles on the crystallization of poly(ethylene terephtalate) (PET).[144] They found that the particles improve the crystallization rate and temperature of PET. Polyisobutene has been grafted onto colloidal silica particles making them potentially useful as model systems for colloids in non-polar systems.[145] Qi *et al.* reported the growth of poly(methyl methacrylate) and poly(butyl acrylate) onto silica nanoparticles providing them better dispersibility in polymer matrices.[146] There are instances in which silica plays the role of shell. Fluorescent dyes such as fluorescein isothiocyanate[147] (FITC) and rhodamine 6G[148] have been trapped in colloidal silica. Core-shell particles of silica and PEG have also been reported. Pacard *et al.* attached pre-made PEG to colloidal silica and form networks that proved to be useful for oligonucleotide synthesis.[149] Zhang *et al.* published on the attachment of PEG to colloidal silica.[150] They claimed that the new method provides improved stability in aqueous and several organic solvents. Yagüe *et al.* compared the viability of bare and silica-PEG particles as potential drug carriers.[151]

Not much attention has been paid to the core-shell particles in which a polypeptide acts as the shell. In 1974 Dietz *et al.* reported the polymerization of L-alanine and L-leucine *N*-carboxyanhydrides on silica.[152] Tsubokawa *et al.* polymerized λ-methyl-L-glutamate *N*-carboxyanhydride onto carbon black nanoparticles.[153] Fong *et al.* synthesized silica-poly(λ-benzyl-L-glutamate)[94] (PBLG) and silica-poly(ε-carbobenzyloxy-L-lysine) (PCBL)[95] core-shell particles. Soto-Cantu *et al.* reported the synthesis and pH behavior or silica-poly(L-glutamic

acid) (PLGA) core-shell particles.[154] Polypeptides have desirable features to offer for example chirality, pH, temperature and solvent composition sensitivity. They possess well-defined secondary structures in several common solvents.

2.1.5 Polymer Brushes

The covalent attachment of polymers to surfaces has drawn attention because of the potential and current applications of such systems. A polymer chain that is grafted on or grown from one end to a surface is known as a polymer brush. They have applications as drug carriers, colloid stabilizers, friction reducers among others.

Two approaches are used for the preparation of polymer brushes. The *grafting to* approach consists of the binding of a functional end of the polymer to a functional surface. Bridger *et al* reported the attachment of anionically-initiated, pre-made polystyrene on the surface of chloro- and non functionalized colloidal silica.[155] The polystyrene polymer brushes gave colloidal stability in non-aqueous solvents. The Ballauff group has several publications on the polymer brushes field. In 2005 Mei *et al.* reported the attachment of long chains of poly(2-methylpropenoyloxyethyl)trimethylammonium chloride on polystyrene latexes.[156] Platinum was formed on the polymer brushes and proved to have a high catalytic activity on the reduction of *p*-nitrophenol by sodium borohydride. In 2006 Lu *et al.* reported the synthesis of similar polymer brushes. The surface was also polystyrene latex but they attached poly(ethylene glyclol) methacrylate.[157] Alcantar *et al.* formed silica surfaces by the chemical vapor deposition of silane and oxygen gases on surfaces of different shapes. The silica surfaces were then activated by water plasma. Then the hydroxyl end-groups of PEG were reacted with the silica.[158] The PEG brushes were intended to give biocompatibility to the silica surfaces. It is also possible to attach isocyanate-capped PEO on silica surfaces. The resulting urethane linkage

is more hydrolytically stable.[159] Tokareva *et al.* attached carboxyl group terminated poly(2-vinylpryridine) to a silicon surface that was modified by gold evaporation and polyglycidyl methacrylate spin-coating.[160] They deposited gold nanoparticles on top of the pH responsive polymer brushes and used it as a nanosensor.

In the *grafting from* approach, an initiator moiety is attached to the surface. The functionalized surface is then reacted with the monomer hence the polymer is formed *in situ*. Lu *et al.* reported the synthesis of cross-linked PNIPAM brushes on functionalized latex spheres by photoemulsion polymerization.[161] Zhou *et al.* used living anionic surface-initiated polymerization in order to grow polystyrene brushes on silica nanoparticles.[162] Similarly, Fan *et al.*, reported the synthesis of polystyrene brushes grafted from modified clay surfaces.[163] Zhang *et al.* was able to grow poly(2-(dimethylamino)ethyl methacrylate) on the surface of modified polystyrene latex. [164] The resulting brushes are pH and temperature responsive.

The *grafting to* and *grafting from* approaches have been used in the formation of polypeptide brushes mostly to flat surfaces. The former has the advantage that the polymer can be characterized well prior to attachment. This cannot be done in the *grafting from* approach because the polymer is formed on the surface. Though it is possible to characterize the polymer after the polymerization, sometimes the reactions used for detachment may affect the polymer hence bringing error to the characterization. The *grafting from* approach has the advantage that it produces higher surface coverage and it is faster. Miura *et al.* reported the attachment of several polypeptides that were synthesized using an initiator with a disulfide moiety that later was used for anchoring the polymers on gold surfaces.[165] Chang and Frank reported the attachment of PBLG on flat silicon surfaces using the *grafting to* and the *grafting from* approaches.[166] Later Heise *et al.* reported the attachment of PBLG on modified silicon

substrates.[89] The silicon surface was modified with a mixture of bromoalkyltricholoro silane and alkyltrichlorisilane. The bromo groups were transformed to amino groups; the latter served as initiators for the polymerization of γ-benzyl-L-glutamate-*N*-carboxyanhydride (BLG-NCA). Wieringa *et al.* synthesized PBLG and poly(γ-methyl-L-glutamate) on flat silicon substrates previously modified with APS.[167] The amino moiety of APS served as initiator for the polymerization of NCAs. In these examples, the polymerization reactions were performed in solution. In 1998 Chang and Frank introduced the vapor deposition-polymerization of an NCA.[168] Under high vacuum and a temperature of ~ 100 °C they were able to evaporate BLG-NCA. They had an amino-functionalized silicon wafer. The amino groups were able to start the polymerization of the NCA in a solvent-free environment. Later Wang and Chang modified the method and reported the formation of block co-polypeptides.[169] Lee *et al.* extended the method to several other amino acid NCAs yielding a variety of conformations.[170] Wang and Chang reported that the formed PBLG and poly(N_ε-carbobenzyloxy-L-lysine) (PCBL) can be deprotected yielding poly(L-glutamic acid) and poly(L-lysine) respectively.[171;172] The resulting polymer brushes are responsive to changes in pH, surfactant and ion concentration.

2.1.6 Polypeptides

Polypeptides and proteins are one of the predominant kinds of polymers found in nature.[104] They are macromolecules formed by amino acids linked through amide bonds also called peptide bonds. Figure 2.6 shows the basic structure of an amino acid and illustrates the peptide bond in a dipeptide. About 20 different R groups can be found in nature. Polypeptides can be arranged in different structures. Some of the most common are α-helix, random coil and β-sheet.

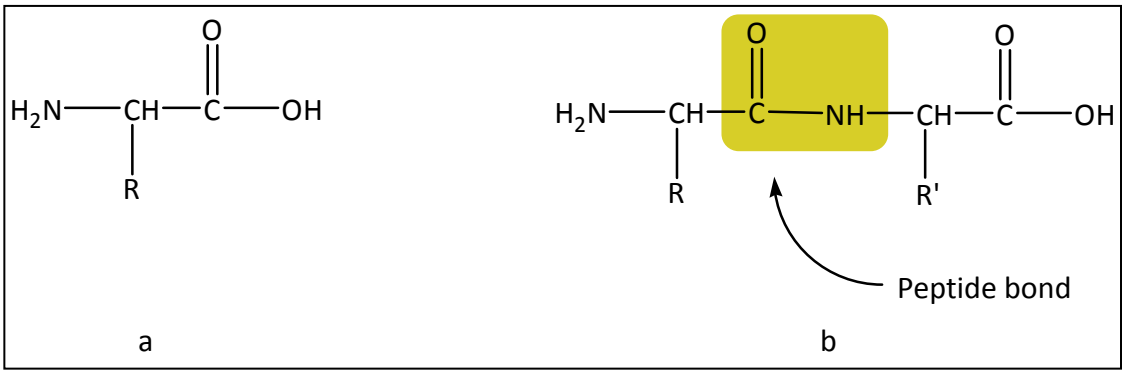

Figure 2.6 a): Basic structure of an amino acid. b): A dipeptide.

The α-helix first proposed by Pauling and Corey[173] is a very robust structure that polypeptides commonly adopt. The intramolecular hydrogen bonding that is present in the α-helical structure gives it its long range order. Figure 2.7 shows a scheme of the arrangement of atoms in the α-helical and random-coil conformations. The α-helix has been well characterized. The amino acid residues are on a spiral pitch of approximately 0.54 nm, it is right-handed for L-α-aminoacids and has about 3.6 residues per turn (18 residues in 5 turns).[93]

Polypeptides and oligopeptides with a defined sequence of amino acid residues, *i.e.* a specific sequence in with the R groups may be the same or different, are commonly synthesized using the solid-phase Merrifield method.[174] Nonetheless, the most common technique used for the large scale synthesis of polypeptides is *N*-carboxyanhydride anhydride (NCA) polymerization.[175] Although NCA polymerization lacks the sequence control that the solid-phase synthesis has, it can produce random, block and homopolypeptides in a relatively faster, easier and cheaper way. The ring-opening polymerization of NCAs can be initiated by nucleophiles. Primary amines are often used as nucleophile initiators. Figure 2.8 shows a scheme of the reaction mechanism. In this so-called "amine" mechanism, the nucleophile is not basic enough

to pull the acidic proton that is attached to the nitrogen in the ring. Following this mechanism, the polymer grows linearly with monomer conversion in the absence of side reactions.[93;175]

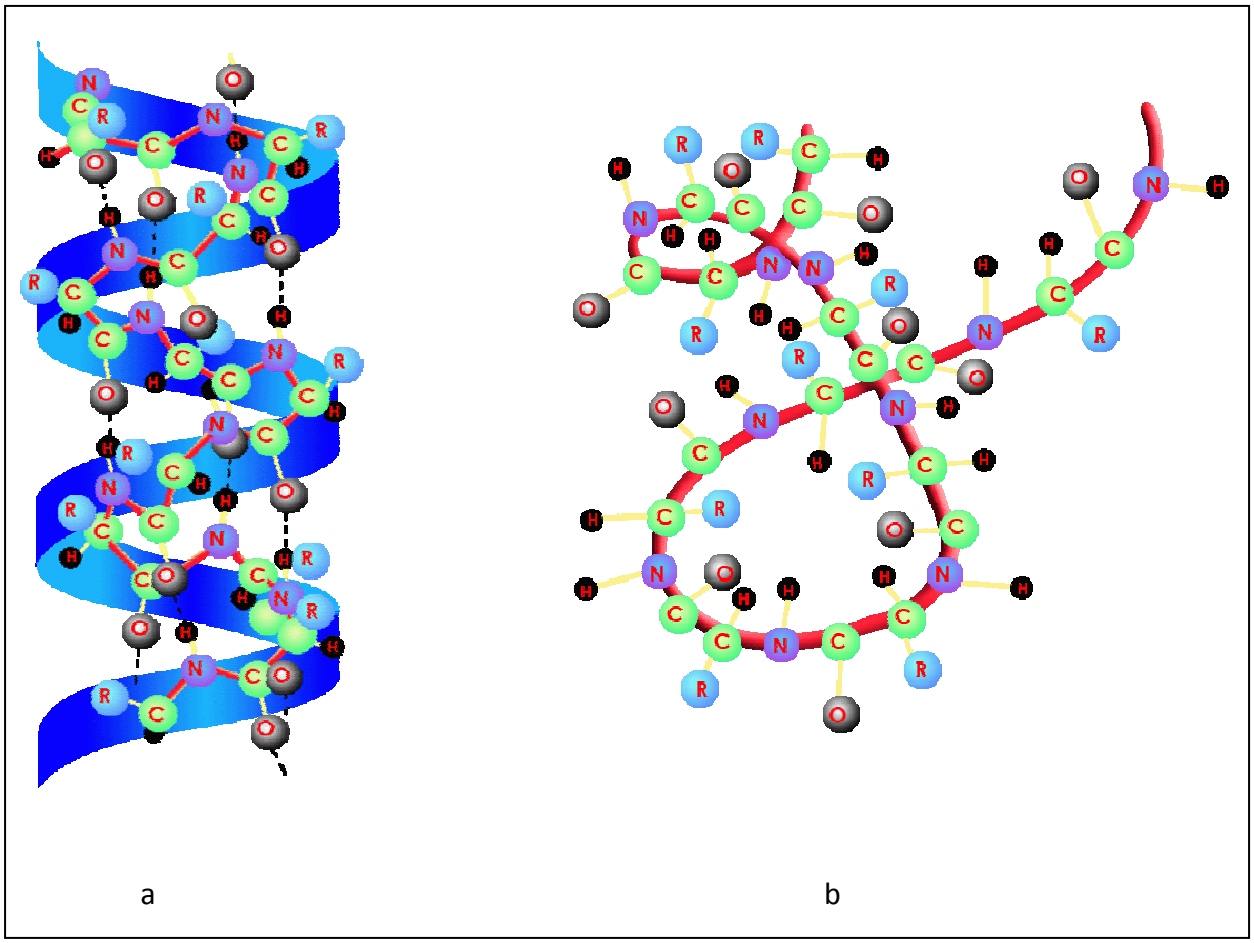

Figure 2.7 a): Structure of the α-helix conformation. b): Structure of the random coil conformation.

When a more basic compound such a tertiary amine or an alkoxide is used as initiator, the reaction mechanism follows a different path: the "activated monomer" mechanism. Figure 2.9 shows a scheme of the reaction mechanism. Initially an acid-base reaction occurs in which the base pulls out the acidic proton of the NCA ring. The deprotonated NCA then becomes a nucleophile that initiates chain growth. Further deprotonation of another NCA continues the activated monomer mechanism. The polymerization follows a step-growth behavior in which

high molecular weight are only obtained when the monomer conversion approaches 100%.[93;175;176]

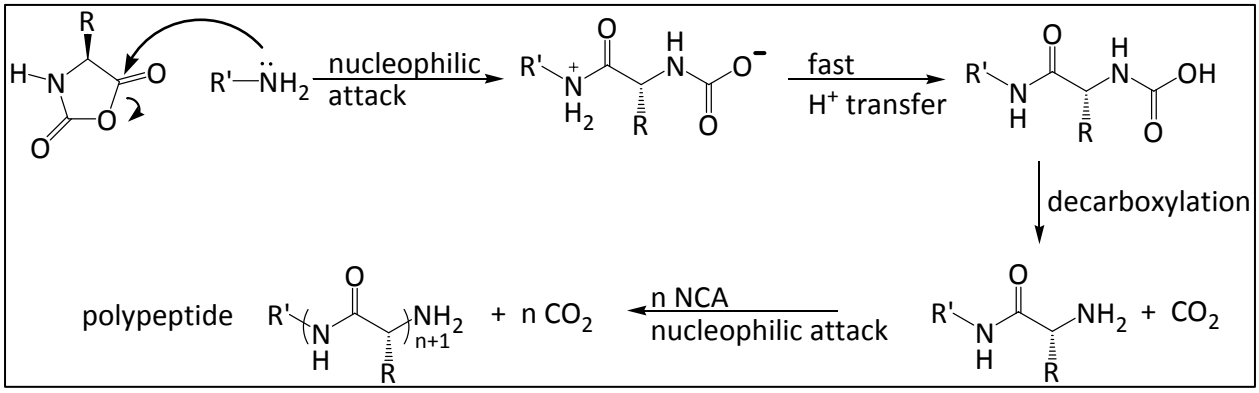

Figure 2.8 Scheme of the "amine" mechanism for polymerization of NCAs. Adapted from reference 175.

A new class of initiators for the polymerization of NCAs was developed by Deming.[177] Some of the positive characteristics of this class of initiators are:

- Molecular weight increases linearly with monomer to initiator ratio
- Low polydispersity indices (<1.1) are obtained
- Block copolymers can be synthesized in a single pot through sequential monomer addition

This kind of initiators are complexes of a transition metal such as cobalt, nickel, copper, palladium, zinc, platinum, ruthenium, iron and iridium with electron donors such as primary amines, cyclic alkenes and phosphines.[177-184] One of the most used is tetrakis(trimethylphosphine)cobalt, $(PMe_3)_4Co$.[185-187]

2.1.6.1 PBLG and PLGA

Poly(γ-benzyl-L-glutamate) (PBLG) is the most studied homopolypeptide. The structure of PBLG is shown in Figure 2.10, where R is the benzyl group ($-CH_2C_6H_5$). It possesses a well-defined alpha-helical structure in a variety of solvents.[93] Nevertheless, only in a few pure

solvents PBLG does not aggregate while maintaining its helical structure; those are: pyridine, DMF, *m*-cresol and nitrobenzene.[188] Because of its alpha-helical structure, PBLG can be considered a rod-like polymer whose diameter is 16 Å.[189] Each repeating unit contributes 1.5 Å to the length of the rod.[93] Therefore its length can be estimated if the degree of polymerization (DP) is known by simply multiplying DP times 1.5 Å. Several investigations report different persistence lengths for PBLG.[189] . Regardless of the possible disagreements in the persistence length value of PBLG, all of them are relatively long when compared to other polymers.

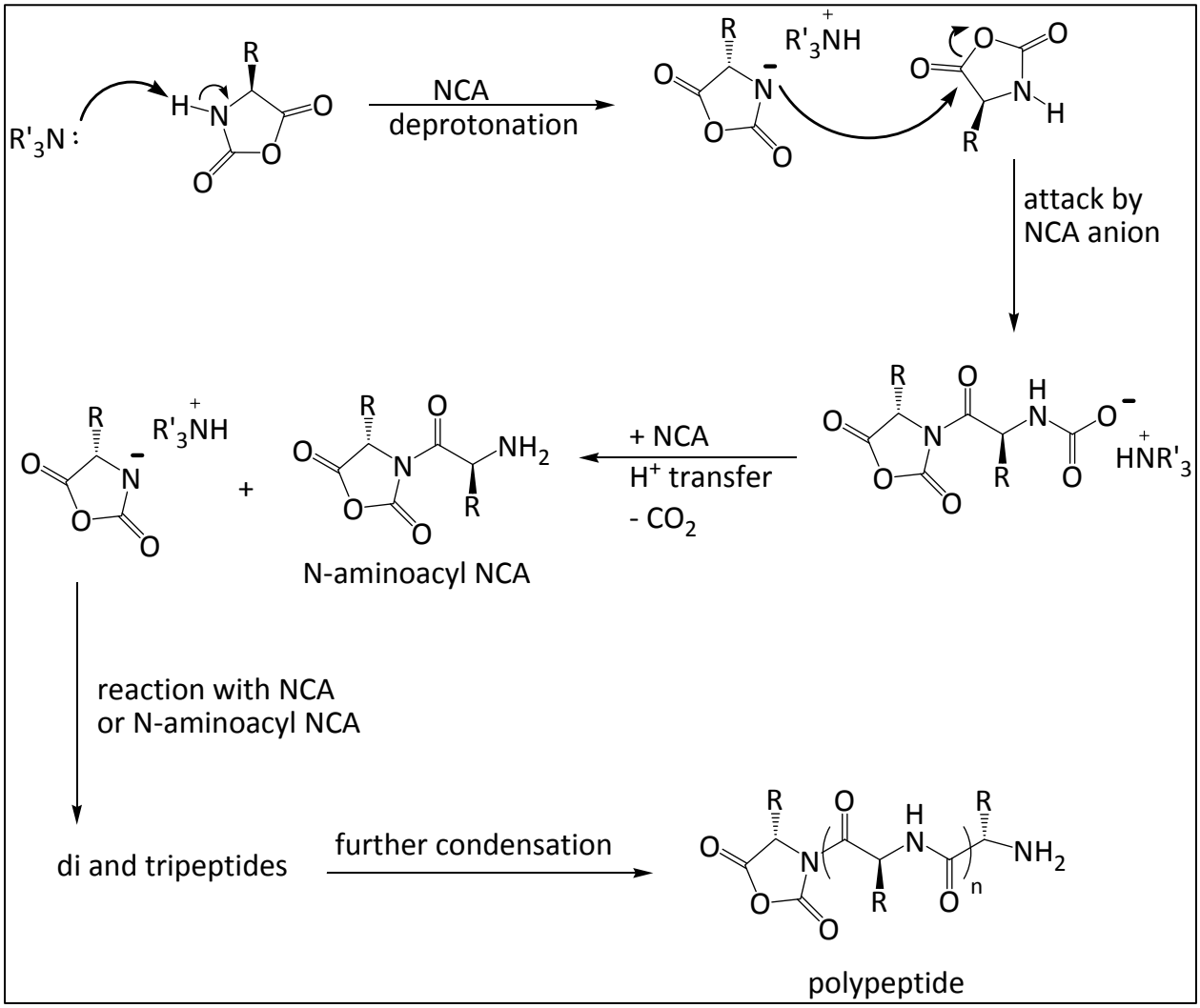

Figure 2.9 Scheme of the "activated monomer" mechanism for polymerization of NCAs. Adapted from reference 175.

Another interesting feature of PBLG is that it can experience a reversible coil→helix transition in solvent mixtures.[190-194] The transition can be triggered by the increase in concentration of trifluoroacetic acid (TFA) in chloroform.[190] TFA disrupts the intramolecular hydrogen bonds that stabilize the alpha-helical structure. In a solution of dichloroacetic acid (DCA) and 1,2-dichloroethane (DCE) the transition can be triggered by changes in temperature or composition.[191-194]

Poly-L-glutamic acid (PLGA) can be obtained by removal of the benzyl group on the repeating units of PBLG. The structure of PLGA is shown in Figure 2.10, where R is a hydrogen atom. The benzyl group is often used as a protecting group in peptide synthesis, so its removal also can be called deprotection. Several approaches have been used in order to achieve deprotection without racemization or cleavage of peptide bonds. Reagents such as alkaline aqueous alcohol, sodium in liquid ammonia, hydrogen with catalyst, have failed or produced racamization. Dry hydrogen bromide in glacial acetic or benzene acid has been effective in removing the benzyl protecting groups.[195;196]

Like PBLG, PLGA cal also exhibit a reversible coil→helix transition.[197] This transition can be triggered by changes in pH. At high pH the side-chain carboxyl groups are deprotonated, hence charged, and the polypeptide chain adopts a random coil conformation. At low pH the carboxyl groups are uncharged; the intramolecular hydrogen bonding prevails leading to a alpha-helix conformation.[197;198] Wang and Chang studied the helix→coil of tethered PLGA on silica induced by pH, decylammonium chloride and calcium ion.[171]

2.1.6.2 PCBL and PLL

Poly(ε-carbobenzyloxy-L-lysine) (PCBL) is a well studied polypeptide. The structure of PCBL is shown in Figure 2.11, where R is the carbobenzyloxy group (-$COOCH_2C_6H_5$), also

abbreviated Cbz or Z. Like PBLG, PCBL can exist in the alpha-helix conformation. It also has a long persistence length. PCBL exhibits a temperature-induced coil→helix transition in *m*-cresol at around 27 °C.[199-203] This is of particular interest because unlike PBLG that exhibits the coil→helix transition in solvent mixtures, PCBL does it in a single solvent and therefore is composition independent. The transition can also be induced by TFA which acts in a similar way as in PBLG.[204]

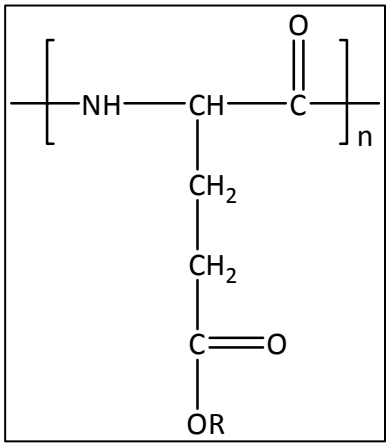

Figure 2.10 General structure of poly-L-glutamates.

Poly-L-lysine (PLL) can be obtained by removal of the carbobenzyloxy groups of the side chains of PCBL. The structure of PLL is shown in Figure 2.11, where R is a hydrogen atom. The removal of the protecting groups can be conducted similarly to the removal of the protecting groups in PBLG: treatment with dry hydrogen bromide in acetic acid or benzene.[195]

2.1.6.3 PEG-Lysine

Poly(*N*-2-[2-(2-methoxyethoxy)ethoxy]acetyl-lysine) (PEG-lysine) is a rigid, water-soluble, uncharged, alpha-helical homopolypeptide. The structure of PEG-lysine is shown in Figure 2.12 in which the PEG moiety appears in red. The synthesis and characterization of PEG-lysine was reported by Yu *et al.*.[187] PEG-lysine combines interesting features of PCBL and PLL.

For example PEG-lysine possesses characteristics of PCBL such as rigidity, absence of charge and ability to form alpha-helices but PEG-lysine is soluble in water and PCBL is not. Similarly, PEG-lysine possesses characteristics of PLL such as rigidity, ability to for alpha-helices and water solubility but PEG-lysine is uncharged and PLL may or may not be charged depending on pH. The rigidity and length of PEG-lysine allows it to form aqueous cholesteric liquid crystals.[185] PEG-lysine is synthesized from the respective *N*-carboxyanhydride. Therefore it presents the advantage that the PEG chain is attached to every repeating unit.

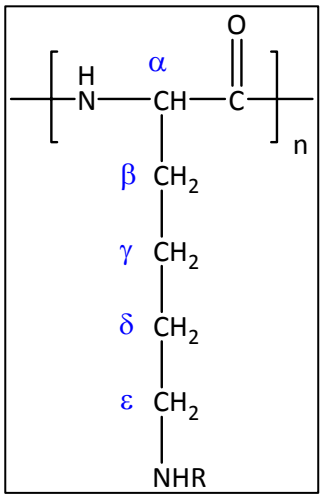

Figure 2.11 General structure of poly-L-lysines.

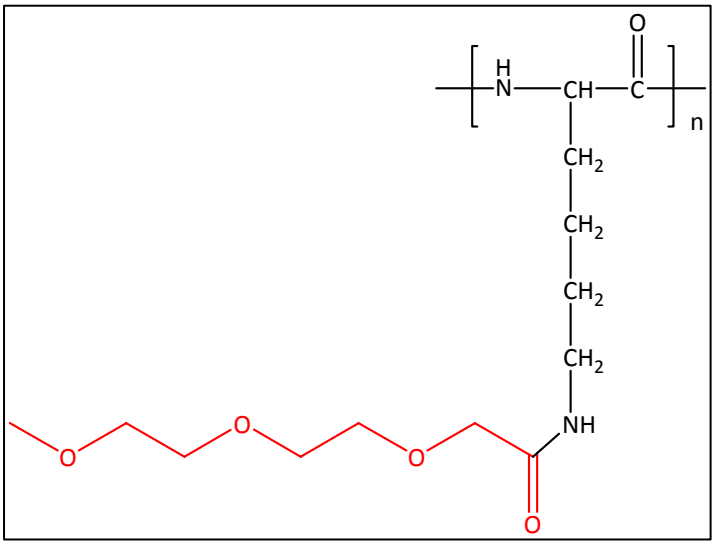

Figure 2.12 Structure of PEG-lysine. The PEG moiety appears in red.

CHAPTER 3 EXPERIMENTAL

This chapter provides the experimental information for the synthesis and characterization of the core-shell silica-polypeptide composite particles. The synthesis component includes the description of the steps necessary to obtain and control the size of the silica cores as well as their passivation/functionalization. The monomers: γ-benzyl-L-glutamate-*N*-carboxyanhydride (BLG-NCA) and N_{ε}-carbobenzyloxy-L-lysine-*N*-carboxyanhydride (CBL-NCA) were synthesized from their respective protected amino acids BLG and CBL by reaction with triphosgene. The synthesis of the NCAs is described. The *grafting to* approach was used for the preparation of the silica-PBLG composite particles. The procedures by *one-time addition* or *sequential addition* are delineated. Silica-PLGA composite particles were obtained by debenzylation of the PBLG shell on silica-PBLG composite particles. PCBL and silica-PCBL composite particles were synthesized in order to investigate the possibility of a coil

The characterization of silica-polypeptide composite particles at each stage is described. The hydrodynamic radius of colloidal silica of different sizes was measured by dynamic light scattering (DLS). The surface amino groups of the passivated/functionalized (P/F) silica cores were quantified using the ninhydrin method. The zeta potential of the P/F silica cores was measured at low pH in order to search for a relationship to the surface density of amino groups. The hydrodynamic radius of silica-polypeptide was measured by DLS. The polypeptide content was quantified using thermogravimetric analysis (TGA). The PBLG shell of silica-PBLG composite particles was visualized using transmission electron microscopy (TEM) after positive stainig with osmium tetroxide. The hydrodynamic radius and zeta potential of silica-PLGA composite particles was measured at different pH values. PCBL and silica-PCBL composite particles were

synthesized in order to study the coil→helix transition of the tethered PCBL. Results by Turksen suggest the occurrence of a temperature-induced coil→helix transition.[1]

3.1 Synthesis

TEOS reagent grade 98% was purchased from Sigma-Aldrich, absolute ethanol 200 proof was purchased from AAPER, concentrated ammonia (29%) and, hydrofluoric acid 48% in water were purchased from EMD, water was obtained from a Barnstead Nanopure™ purification system. Anhydrous Tetrahydrofuran (THF), anhydrous *N,N*-dimethylformamide (DMF) and anhydrous hexanes were obtained from a Pure-Solv™ system. (3-aminopropyl)trimethoxysilane (97%), methyl-trimethoxysilane (MTMS) (98%), γ-benzyl-L-glutamate (≥ 99%) , N_{ε}-carbobenzyloxy-L-lysine (98%), triphosgene (98 %), anhydrous magnesium sulfate, sodium bicarbonate (reagent), sodium methoxide solution in ethanol (30%), 2-propanol (≥ 99.5%), acetone (ACS reagent), methanol (HPLC), chloroform (HPLC), chloroform-d, *m*-cresol-d_8, the following solvents of anhydrous grade: ethyl acetate (EtOAc), benzene, pyridine, and 1,4-dioxane were purchased from Sigma-Aldrich and used without further purification, unless otherwise specified.

3.1.1 Silica Cores

3.1.1.1 Original Stöber Method

350 mL of absolute ethanol, 10-25 mL of concentrated ammonia and 0-9 mL of water were mixed in a 500 mL round-bottom flask. They were vigorously stirred using a magnetic bar for 10-20 minutes in order to reach homogeneity. After that, 25 mL of TEOS were added from graduated cylinder. The addition was done rapidly (~ 3-5 seconds) while the mixture was being stirred. The reaction was allowed to proceed at room temperature for 24 hours. Then the

colloidal dispersion was centrifuged at 7600 *g* for 60 minutes. The silica pellet was subsequently re-dispersed in absolute ethanol. This centrifugation-dispersion or washing procedure was repeated at least 5 times.

3.1.1.2 Modified Method

The procedure by Zhang *et al.*[205] was scaled up. Solution I was prepared by adding 230-260 mL of absolute ethanol and 20-50 mL of concentrated ammonia to a 500 mL round bottom flask. This solution was magnetically stirred vigorously for 10-20 minutes. Solution II was prepared in a 50 mL beaker by dissolving 5 mL of TEOS in 20 mL of absolute ethanol. Solution II was loaded into a 50 mL polypropylene syringe and added rapidly (~ 0.8 s) into solution I while vigorous stirring was kept at all times. The reaction was allowed to proceed at room temperature for 2 hours. The resulting colloidal silica was centrifuged at 3000 *g* for 30 minutes. The silica pellet was subsequently re-dispersed in absolute ethanol. This centrifugation-dispersion or washing procedure was repeated at least 5 times.

3.1.1.3 Etching with HF

10 mL of colloidal silica obtained by the modified method (conc. 8.6 mg/mL) was placed in a 50 mL polypropylene tube. Then 10 mL of a 1% HF solution was added to the silica dispersion. The mixture was magnetically stirred and allowed to react at room temperature for 9 hours. After that, the resulting colloidal silica was centrifuged at 5900 *g* for 30 minutes. The silica pellet was subsequently re-dispersed in absolute ethanol. This centrifugation-dispersion or washing procedure was repeated at least 5 times.

3.1.2 Functionalization

Dispersions of colloidal silica cores in absolute ethanol (concentration approximately 10%) were placed in 200 mL Erlenmeyer flasks. Solutions of APS and MTMS were freshly

prepared in Eppendorf tubes. The solutions had predetermined compositions and the total volume of solution was typically 100 µL. The amount of silanes (APS and MTMS) added was calculated considering the estimated total surface area of the silica cores (assuming spherical shape, radius = $R_{h,\ app}$ from DLS measurements, density of colloidal silica[94] 1.96 g/cm^3) and assuming that the parking area of a silane molecule[84;98] is 4 molecules per nm^2. An excess of typically 10-20% of the estimated amount was added. The APS/MTMS solution was added rapidly to the colloidal silica cores dispersion while stirring. The functionalization reaction was allowed to proceed at room temperature for around 12 hours. The resulting passivated/functionalized (P/F) colloidal silica particles were centrifuged at 3000 *g* for 45 minutes. The supernatant was tested for amines using ninhydrin. The pellet of P/F particles was re-dispersed in absolute ethanol. This washing procedure was repeated until the supernatant tested negative for amines (absence of blue coloration after ~ 10 mg of ninhydrin were added and placed in a water bath at ~ 65 °C for ~ 30 minutes). Typically more than 5 washes were required to remove all the unreacted APS.

3.1.3 *N*-Carboxyanhydrides

The procedure by Daly and Poché was used for the synthesis[206] and purification[207] of γ-benzyl-L-glutamate-*N*-carboxyanhydride (BLG-NCA) and N_ε-carbobenzyloxy-L-lysine-*N*-carboxyanhydride (CBL-NCA). Typically, 10 grams of the protected amino acid γ-benzyl-L-glutamate or N_ε-carbobenzyloxy-L-lysine were suspended in 300 mL of anhydrous ethyl acetate in a 500 mL round bottom flask. The addition took place inside of a glove bag with a dry nitrogen atmosphere. Subsequently, the flask was equipped with a reflux condenser and dry nitrogen was passed through the system for at least 10 minutes. The slurry was brought to

reflux and one third equivalent of triphosgene were added rapidly. The reaction was allowed to proceed under nitrogen a atmosphere for 4-5 hours. After that the soluble *N*-carboxyanhydride was formed making the reaction mixture clear. In cases where the reaction mixture was not completely clear, a small quantity of triphosgene was added. The resulting NCA solution was then cooled down to – 5 °C in the stoppered flask. The cold solution was then transferred to a separatory funnel and washed first with 100 mL of water chilled to 0 °C and then with 100 mL of 0.5 % $NaHCO_3$ solution chilled to 0 °C. The NCA solution in ethyl acetate was then treated with anhydrous $MgSO_4$ until no clumping was observed. The solution was then gravity filtered and concentrated to about one third of its original volume in a rotary evaporator. Afterward, about 100 mL of anhydrous hexanes was added to the solution causing the precipitation of the monomer. The slurry was then chilled to -5 °C and kept at that temperature overnight. The NCA crystals were then collected by suction filtration in a dry nitrogen environment. The crystals were subsequently dried in a vacuum oven for 24 hours. The yield is typically 70%.

3.1.4 Silica-Polypeptide Composite Particles

3.1.4.1 Silica-PBLG Composite Particles

The *grafting from* approach was used. The composite particles were prepared by *sequential addition* or *one-time addition* of monomer.

Sequential addition: 100 mL of anhydrous THF (from a Pure-Solv™ system) was placed in a 200-mL round bottom flask. Then 2.000 grams of BLG-NCA was added. After the monomer was dissolved, 17-mL passivated/functionalized colloidal silica in THF was added (total weight of silica = 0.86 gram, functionalization surface density = 0.72 $–NH_2$ grpups/nm^2). An immediate production of CO_2 was observed by bubbling it in mineral oil. The reaction is allowed to proceed until the rate of evolution of CO_2 was inappreciable (1-2 days). 4 mL of sample was taken out of

the reaction mixture and washed 3 times with anhydrous pyridine and dried for TGA analysis. 2.163 more grams of BLG-NCA was added and allowed to react as the first step. The sampling and addition procedure (1.978, 1.894 and 2.007 grams respectively) was repeated until a total mass of 10 grams of BLG-NCA was added. After the total amount of BLG-NCA was added and the rate of production of CO_2 was inappreciable, the sample was centrifuged at 7600 *g* for 60 minutes. The supernatant was removed and the pellet was re-dispersed in pyridine. This centrifugation-dispersion or washing procedure was repeated at least 5 times.

One-time addition: 100 mL of anhydrous THF (from a Pure-Solv™ system) was placed in a 200-mL round bottom flask. Then 11 grams of BLG-NCA was added. After the monomer was dissolved, 16 grams of passivated/functionalized colloidal silica in THF was added (total weight of silica = 0.945 gram, functionalization surface density = 0.72 $–NH_2$ grpups/nm^2). An immediate production of CO_2 was observed by bubbling it in mineral oil. The reaction was allowed to proceed until the rate of evolution of CO_2 is inappreciable (~6 days). After that, the sample was centrifuged at 7600 *g* for 60 minutes. The supernatant was removed and the pellet was re-dispersed in pyridine. This centrifugation-dispersion or washing procedure was repeated at least 5 times.

3.1.4.2 Silica-PLGA Composite Particles

1 gram of silica-PBLG composite particles was dispersed in benzene inside a polytetrafluoroethylene (PTFE) tube. Then 4 mL of a 33% HBr solution in acetic acid were added. The reaction was allowed to proceed under stirring and sonication for 30 minutes. The silica-PLGA composite particles were then extracted using a 5% $NaHCO_3$ solution followed by a wash of the aqueous layer using chloroform in order to remove any benzyl bromide present. The dispersion was then dialyzed against water.

3.1.4.3 Silica-PCBL Composite Particles

The N_ε-carbobenzyloxy-L-lysine-*N*-carboxyanhydride was prepared following the same procedure as for the synthesis of BLG-NCA (see 3.2.1.1).

The composite particles were prepared as follows: 4.75 grams of CBL-NCA were dissolved in 100 mL of anhydrous THF (from a Pure-Solv™ system). Then 74 mL of passivated/functionalized colloidal silica particles were added (total weight of silica = 0.90 gram, functionalization surface density = 0.29 $-NH_2$ grpups/nm^2). The reaction proceeded for 4 days at room temperature until the rate of evolution of CO_2 was inappreciable. After that, the sample was centrifuged at 7600 *g* for 60 minutes. The supernatant was removed and the pellet was re-dispersed in pyridine. This centrifugation-dispersion or washing procedure was repeated at least 5 times.

3.1.5 Poly(N_ε-carbobenzyloxy-L-lysine)

The monomer, N_ε-carbobenzyloxy-L-lysine-*N*-carboxyanhydride, CBL-NCA, was prepared following the same procedure as for the synthesis of BLG-NCA (see 3.1.3). 3.065 grams of N_ε-carbobenzyloxy-L-lysine-*N*-carboxyanhydride, CBL-NCA were dissolved in 60 mL of anhydrous THF (from a Pure-Solv System). Then 8 μL of a 30% sodium methoxide solution in ethanol were added. The reaction is allowed to proceed until the rate of evolution of CO_2 is inappreciable (2 days). At this point the molecular weight was around 200,000 g/mol and the polydispersity index around 1.3. The PCBL solution was poured in acetone/methanol. Then the wet PCBL was dried in a vacuum oven for 5 days. 2.1 grams of dry PCBL were collected. The molecular weight was 202,200 g/mol and the polydispersity index 1.086.

3.2 Characterization

3.2.1 Dynamic Light Scattering

Dynamic light scattering (DLS) measurements were conducted in a custom built apparatus using a He-Ne laser as the source of light (632.8 nm). An ALV-5000 digital autocorrelator was used. Measurements were made in homodyne mode[208] at different scattering angles from 30° to 90° in 15° increments. The apparent diffusion coefficient is defined as:

$$D_{app} = \frac{\Gamma}{q^2} \qquad \text{Equation 3.1}$$

where Γ is the decay rate of the electric field autocorrelation function $g^{(1)}(t)$ and q is the scattering vector defined as:

$$q = \frac{4 n \pi \sin\frac{\theta}{2}}{\lambda_0} \qquad \text{Equation 3.2}$$

n is the solvent refractive index, θ is the scattering angle and λ_0 is the wavelength of the incident light. D_{app} become D_0 in the limit of zero concentration. The hydrodynamic radius (R_h) of the sample can be calculated by applying the Stokes-Einstein equation:

$$R_h = \frac{kT}{6\pi\eta_0 D_0} \qquad \text{Equation 3.3}$$

where k is Boltzmann's constant, T is the absolute temperature and η_0 is the viscosity of the solvent. Multi-angle measurements were performed in order to verify the size-independence on scattering angle. Once this was confirmed, a Malvern Zetasizer Nano-ZS ZEN3600 was used

for routine measurements. The instrument performs backscatter DLS measurements at θ = 173° using a 4 mW He-Ne laser of λ = 633 nm. The hydrodynamic radii obtained from multi-angle measurements and from the Malvern Zetasizer Nano-ZS were statistically the same.

3.2.2 Asymmetric Flow Field-Flow Fractionation

Asymmetrical Flow Field Flow Fractionation (AF4) system (Eclipse 2, Wyatt Technology Corp., Santa Barbara, CA). An Agilent 1100 HPLC system (Agilent 1100 isocratic pump, Agilent 1100 autosampler, and Agilent 1100 degasser, Agilent Technologies, Palo Alto, CA) was used to inject the samples and deliver the mobile phase to the AF4 system. The AF4 channel was assembled with a 350 µm-thick Mylar spacer. The membrane used was made of regenerated cellulose with a 10 kDa molecular weight cutoff (Wyatt). AF4 parameters: channel length, 24 cm; channel width at inlet, 2.15 cm; channel width at outlet, 0.6 cm, channel flow, 0.75 mL/min; focus flow, 1.5 mL/min, 2 minutes. Injection: 100 µL of sample were injected at an injection flow of 0.2 mL/min with a focus flow of 1.5 mL/min for 3 minutes, focus at 1.5 mL/min for 3 minutes, and then focus at 0.25 mL/min for 7 minutes. Separation: channel flow, 0.75mL/min. cross flow, 0.2mL/min, constant for 2 minutes, ramp 30 minutes to 0.01 mL/min. Detectors used: Heleos, Multi Angle Light Scattering (MALS), with a QUELS (DLS) detector (Wyatt Technology Corp., Santa Barbara, CA). The source is a GaAs 50 mW laser at λ = 658 nm. Optilab rEX Differential Refractive Index detector (Wyatt Technology Corp., Santa Barbara, CA) at 658nm. Data acquisition and data analysis were performed using the Astra V software (Wyatt).

3.2.3 Electron Microscopy

For routine transmission electron microscopy (TEM) measurements, approximately 2 µL of sample were placed on top of a 400-mesh, carbon-coated, copper grid from Electron

Microscopy Sciences. A positive staining technique was developed with the help of Cindy Henk in the Socolofsky Microscopy Center at LSU. The silica-polypeptide samples were dispersed in pyridine at a concentration around 1%. Approximately 2 µL of sample were placed on top of a grid (specifications above). After that, while the solvent still was present, the sample-containing grid was place inside of a 2 inch Petri dish. A small cylinder containing 1 mL of a 1% (w/v) OsO_4 solution and a filter paper soaked with the same OsO_4 solution were placed inside the Petri dish. The sample was exposed to only the vapors of the OsO_4 solution inside the Petri dish, the solution at any point was in contact with the sample. The time of exposure was 15 minutes. After that the sample was taken out of the Petri dish and was allowed to air dry. The dry samples were then explored using a JEOL 100-CX TEM working at an accelerating voltage of 80 kV unless indicated otherwise. The resulting images were analyzed using ImageJ 1.38x from the National Institutes of Health, USA. In instances of particle sizes obtained from TEM a sample of 80-170 particles were counted.

3.2.4 Quantification of Amino Groups

A 0.35 % (w/v) ninhydrin solution in absolute ethanol was freshly prepared. Standard hexylamine solutions were freshly prepared in order to build the calibration plot. The concentration range was 0.12 to 0.87 mM. Samples were dried at 120 °C for 4-6 hours. 0.2 g of sample was placed in a capped vial along with 4 mL of absolute ethanol. The mixture was placed in a Branson ultrasonicator for 30 minutes. After that, 1 mL of ninhydrin solution was added to the vial containing the sample and it was sonicated for 10 more minutes. The ninhydrin-sample dispersion was then placed in a water bath at 65 °C for 30 minutes. The samples were allowed to cool down for 10-15 minutes. Once the samples were at about room temperature they were centrifuged at 7600 *g* for 30 minutes. Approximately 1 mL of

supernatant was pipetted out and the absorbance at 588 nm was measured in a Hewlett Packard 8453 spectrophotometer. Measurements were repeated 3 times. Some measurements were performed by Jerome Koch.

3.2.5 Zeta Potential

Zeta potential measurements were performed in a Malvern Zetasizer Nano-ZS ZEN3600. The instrument is described in section 3.2.1 but the scattering angle for zeta potential measurements is θ = 17°. Clear polycarbonate disposable capillary zeta potential cells from Malvern were used. The P/F silica cores were dispersed in 0.1 M HCl and 1 mM $NaNO_3$ at concentrations ~ 0.1% (w/v). Measurements were performed by Jerome Koch. For the silica-PLGA composite particles the starting pH was reached by addition of 0.1 and 1 M NaOH. The changes in pH were achieved by adding 0.1 M HCl using the multi-purpose titrator MPT-2 attached to the Zetasizer.

3.2.6 Thermogravimetric Analysis

Thermogravimetric analysis was performed in a TA Instruments TGA Q50 under nitrogen atmosphere or in a TA Instruments TGA 2950 under air atmosphere. In both cases the heating rate was 10°C/min. The results were comparable.

3.2.7 Gel Permeation Chromatography

Two Phenogel 300 x 7.8 mm columns (Phenomenex, Torrance, CA), connected in series were used: (1) 10µ, 105Å (10K-1000K); (2) 10µ, MXM (100-10,000K) and a guard column (5 µ, 50x7.8mm) were used. The GPC instrumentation consisted of an Agilent 1100 pump (Agilent Technologies, Palo Alto, CA), and an Agilent 1100 autosampler. For detection 3 detectors connected on series were used: A Wyatt Heleos Multi Angle Light Scattering (MALS) (Wyatt Technology Corp., Santa Barbara, CA) with a GaAs 50 mW laser at λ = 658 nm, a Wyatt ViscoStar

viscosity detector, and a Wyatt rEX Differential Refractive Index detector, with a 658nm light source. A volume of 50 µL of concentration 6 mg/mL was injected. The mobile phase was either anhydrous grade DMF, 0.1 M LiBr in DMF or 0.1 M LiBr in DMF + 1% (v/v) water. The flow rate was 1 mL/minute. Data acquisition and molecular weight (MW) calculations were performed using the Astra V software (Wyatt).

Poly(γ-benzyl-L-glutamate) (PBLG) was purchased from Sigma-Aldrich (formerly known as Sigma) and Polysciences. PBLG was dried in a vacuum oven at 60 °C for at least 12 hours until the weight was constant. Polystyrene was purchased from TSK standards. *N,N*-dimethylformamide (DMF) of HPLC grade and DMF anhydrous grade were purchased from Sigma-Aldrich and used without further purification. Dry DMF was obtained from a Pure-Solv™ solvent purification system. Lithium bromide (LiBr) reagent grade was purchased from Sigma-Aldrich.

Cocktails of low, medium and high molecular weight (MW) PBLG were prepared. All the nominal molecular weights are averages provided by the vendor. The low MW range was from 34,600 to 100,000 g/mol. The medium MW range was from 105,300 to 231,000 g/mol. The high MW range was 225,000 to 318,000 g/mol. The solutions had concentrations of 4.6, 5.3 and 6.9 mg/mL for the high, medium and low MW respectively. Cocktails of low medium and large molecular weight were used in order to have a broad range of molecular weights. In principle, a broadly polydisperse sample could have been injected instead. Nevertheless, in order to have a good signal, a large amount of polymer would have to be injected causing overloading of the column. The average molecular weights provided by the vendors and the respective percentage in each cocktail are shown in Table 3.1, 3.2 and 3.3.

Table 3.1 Composition of low molar mass cocktail

Average MW of component	Weight %
34,600	25.6
45,600	23.6
91,000	25.1
100,000	25.6

Table 3.2 Composition of medium molar mass cocktail

Average MW of component	Weight %
105,300	25.8
200,000	30.1
218,000	25.8
231,000	18.3

Table 3.3 Composition of high molar mass cocktail

Average MW of component	Weight %
225,000	17.3
250,000	23.8
277,000	17.3
293,500	19.2
318,000	22.4

The water content of DMF of various grades was measured using a Metler Toledo DL32 Karl-Fisher coulometric titrator. DMF HPLC grade had 107 ppm, anhydrous grade DMF had 37.8 ppm and dry DMF had 17.8 ppm. The manufacturer specification for dry DMF is water content lower than 30 ppm. The dry DMF had the lowest water content. However, because it is passed through alumina in the Pure-Solv system, it has to be filtered. The filtration process was carried out with extreme care inside or a glove bag with dry nitrogen atmosphere. The process is relatively slow (~ 50 mL/min). During the filtration time the DMF can absorb water from the

environment. After filtration, the water content increased more than 300 ppm. In contrast, DMF anhydrous grade has slightly larger water content than the original dry DMF from the Pure-Solv™ system. Because it also has very low dust content and that saves the filtration step that can lead to an increase in the water content.

The specific refractive index increment (*dn/dc*) value for PBLG in anhydrous DMF[189] was 0.118 mL g^{-1}. The *dn/dc* value for PBLG in 0.1 M LiBr[177] in DMF was 0.104 mL g^{-1}. The same value of 0.104 mL g^{-1} was assumed for the PBLG in 0.1 M LiBr + 1% water. The refractive index increment *dn/dc* for PCBL in 0.1 M LiBr[177] in DMF was 0.123 mL g^{-1}.

3.2.8 Nuclear Magnetic Resonance

Routine measurements were done in a Bruker 250-DPX NMR spectrometer. Samples were dissolved in deuterated chloroform, $CDCl_3$. Experiments at variable temperatures were conducted in a Bruker AVANCE 400 MHz NMR spectrometer. A fraction of the resulting silica-PCBL composite particles was transferred to THF by centrifugation-dispersion. The composite particles once in THF were mixed with *m*-cresol-d_8. The THF was then removed in the vacuum oven. The final concentration (based on CBL repeating unit) was approximately 5 mM. The dry PCBL prepared by the initiation with sodium methoxide was directly dissolved in *m*-cresol-d_8, the concentration was approximately 5 mM. Approximately 0.1 % of TMS v/v was added. Spectra of the untethered PCBL was collected by Jerome Koch and Dr. Dale Treleaven. Spectra were analyzed using MestRe-C.

CHAPTER 4 RESULTS AND DISCUSSION

4.1 Silica Cores

4.1.1 Control of Size

A number of factors can influence the size and polydispersity of the resulting colloidal silica formed by the sol-gel process. Some of them include temperature, the nature and concentration of the components (alkoxy silane, alcohol, ammonia, and water), surfactants or electrolytes added, rate of mixing, pre-dilution of components. Having control over the particle size is essential. The potential applications and multiple properties of colloidal silica are size-dependent. Temperature is a factor that has a great influence on the resulting size of the produced silica.[44] However, temperature control is not always trivial. Maintaining isothermal conditions is relatively complicated when the area/volume ratio of the vessel is small (large vessels). From the point of view of chemistry it is easier to vary initial concentrations of the reactants or catalyst in order to obtain the desired result. Water is known for having a sensitive effect over the final size of the colloidal silica obtained by the Stöber method. It is also readily available and cheap among other virtues. The effect the ratio of water/TEOS was studied. The concentration of TEOS had an approximate constant value of 0.35 M. Water was added to the ethanol, ammonia solution. In addition, the concentrated ammonia solution was a source of water itself. Figure 4.1 shows a graph of hydrodynamic radius (R_h) *vs* water/TEOS w/w. The observed hydrodynamic radii data was fitted by an exponential curve. The curve fits the data relatively well (R^2=0.993). The intention of fitting the data is mostly to serve as a size predictor rather than explaining the growth phenomenon.

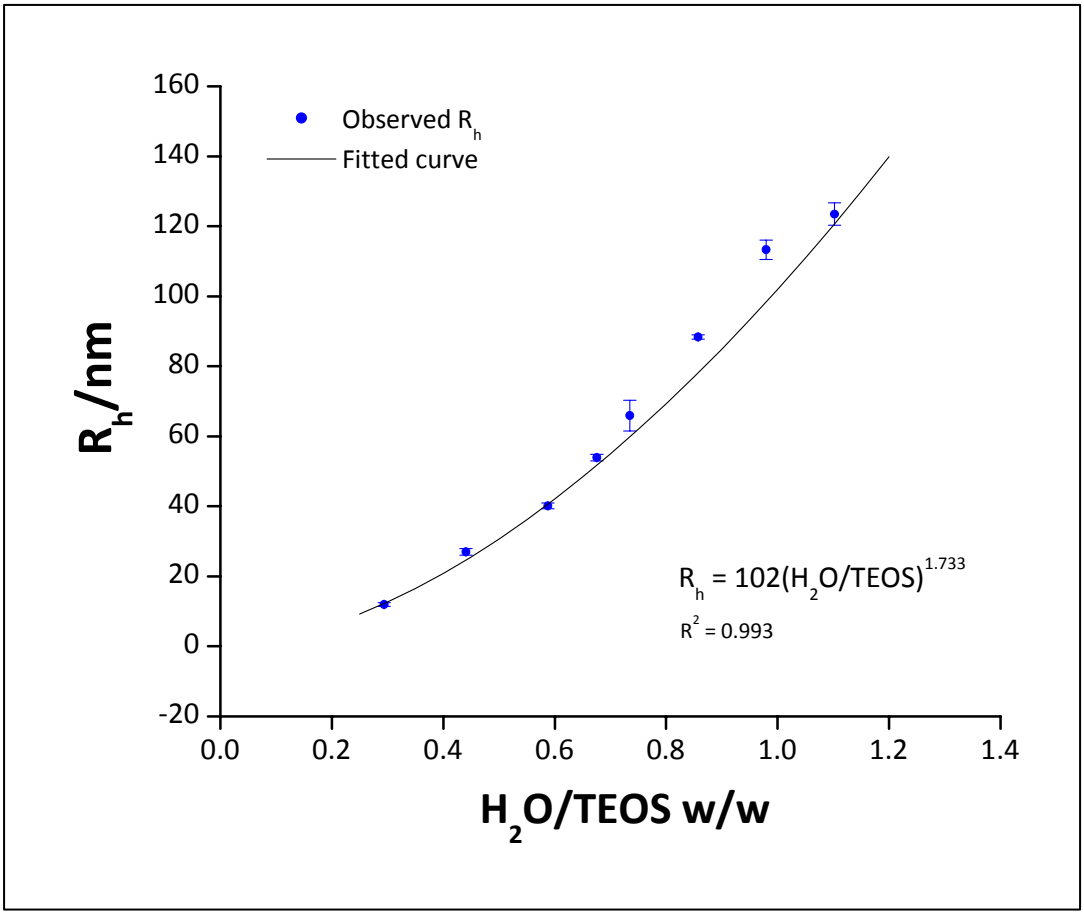

Figure 4.1 Graph of hydrodynamic radius *vs* water/TEOS w/w, Samples ES.3.3A-H. Observed (●) and fitted (—) data.

In 1988 Bogush *et al.* explored the resulting colloidal silica obtained by the hydrolysis of TEOS.[43] The researched concentration ranges were 0.1-0.5 M TEOS, 0.5-17.0 M H_2O and 0.5-3.0 NH_3 all using ethanol as the reaction solvent. They developed an expression to fit the experimental data; thus, it did not contain mechanistic information. The expression is:

$$d = A[H_2O]^2 \exp\left(-B[H_2O]^{\frac{1}{2}}\right) \qquad \text{Equation 4.1}$$

with

$$A = [TEOS]^{\frac{1}{2}}\left(82 + 151[NH_3] + 1200[NH_3]^2 - 366[NH_3]^3\right) \qquad \text{Equation 4.2}$$

$$B = 1.05 + 0.523[NH_3] - 0.128[NH_3]^2$$ Equation 4.3

where *d* is the average diameter in nanometers and the reagent concentration is given in mol/L.

Equation 4.2 includes the correction proposed by Razink and Schlotter.[209] The error is only typographical apparently. On Equation 4.2 the sign before 151 should be plus instead of minus. The corrected equation predicts larger diameters and fits the experimental data reported by Bogush. Neither the expression published first by Bogush nor the correction by Razink predict the hydrodynamic radius of the obtained colloidal silica as can be observed in figure 4.2.

The predicted values by both equations observed in Figure 4.2 are obtained by substituting all the actual molar concentrations (TEOS, H_2O and NH_3) in the equations (4.1-4.3). The independent variable in Figure 2.8 is H_2O/TEOS. It is possible to have the same H_2O/TEOS ratio for a number of TEOS, H_2O, NH_3, and ethanol combinations that would yield silica of different R_h. Using a given H_2O/TEOS ratio it is possible to make the predicted curves fit the experimental data by changing NH_3 and ethanol concentrations. By doing so, the resulting concentrations of components may go to the limits or fall out of the experimental threshold reported by Bogush. This suggests that the empirical equations may be modified and expanded to fit a wider range of experimental conditions.

Another possible reason for the disagreement between the observed and the predicted results may be due to the purity of the TEOS. Bogush, as in most publications, used high purity, freshly distilled TEOS. The results in the present work were obtained using TEOS reagent grade (98%). The nature of the impurities is unknown since the vendor would not provide that information and investigating that is out of the scope of the present study. It is possible that

strong-interacting impurities may have a considerable effect in the initial stages of TEOS condensation. A qualitative and quantitative analysis of the impurities in the TEOS as well as in the resulting silica can lead to the study of the effect of them on particle size. This would result in an even broader understanding of the mechanistic aspects of TEOS condensation. The resulting hydrodynamic radii satisfy the size range and uniformity of particles needed in this project.

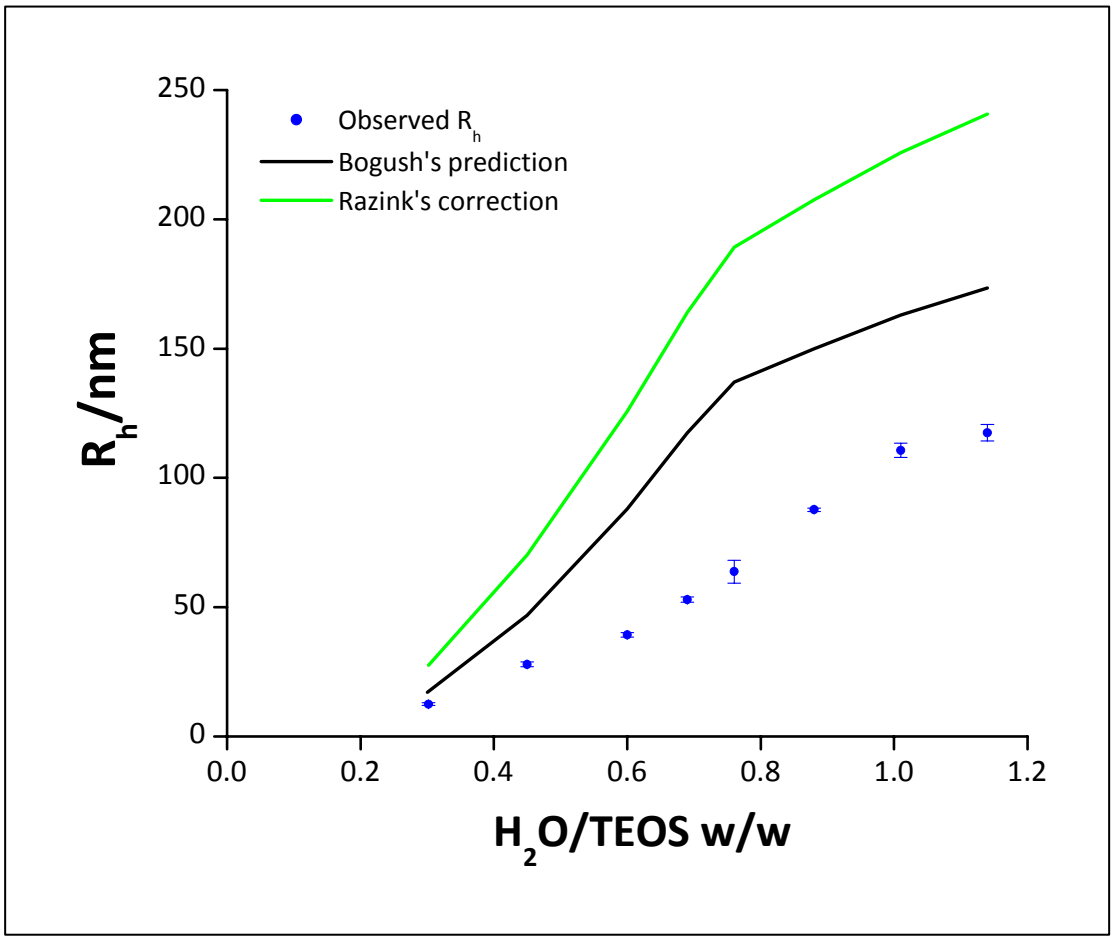

Figure 4.2 Graph of hydrodynamic radius *vs* water/TEOS w/w, Samples ES.3.3A-H. Observed (●), Bogush's (—) and Razink's (—) predictions.

Regarding particle size control, it is common to find reports about increasing the diameter of the resulting colloidal silica after the hydrolysis is completed. A subsequent

addition of TEOS can increase the particle size of colloidal silica in a predicted manner. On the contrary, for some applications, it may be necessary to decrease the particle size instead of increasing it. Hydrogen fluoride (HF) has been used to completely etch silica out of other components in particles. The reaction is favored by the formation of the stable silicon fluoride gas molecule.

$$SiO_2 + 4\,HF \longrightarrow SiF_4 + 2\,H_2O$$

Therefore, it is possible to use this reaction in order to decrease the particle size of colloidal silica. The volume of the spheres, and hence their mass, is proportional to the third power of the radius. A radius of ½ of the original was planned. Therefore, the mass of the particles was reduced to $(½)^3$ = ⅛ of its original value. A mass of HF of ⅞ chemical equivalent of the original mass of silica was added. As can be seen in Figure 4.3, the diameter of the silica particles was reduced. The average diameter before etching is 269 nm ± 20 nm and after etching is 160 nm ± 32 nm (both measured form the TEM pictures in Figure 4.3). The size reduction represents 40% of the original size as opposed to the 50% predicted. The polydispersity increased from ± 7.4% to ± 20.0%. The increase in polydispersity is accentuated because smaller particles have larger specific surface area hence can react at a faster rate than larger ones. This size reduction method would be adequate for particles of very low polydispersity values and for small differential reduction values.

4.1.2 Control of Polydispersity

The original Stöber method tends to produce spherical colloidal silica of low polydispersity. It is common to find reports that claim the production of monodisperse silica particles. Although the polydispersity is low in most cases, the resulting particles are not strictly

monodisperse. Nonetheless, the low polydispersity achieved is good enough for a number of applications. It has been a requirement that the TEOS used in the process to be of high purity. Normally it is freshly distilled or purchased with a high purity. Distillation adds one step to a process that is otherwise extremely simple. Purchasing a degree of purity higher than reagent grade for TEOS in laboratory scale translates in a price difference of 2 to 20 times higher.

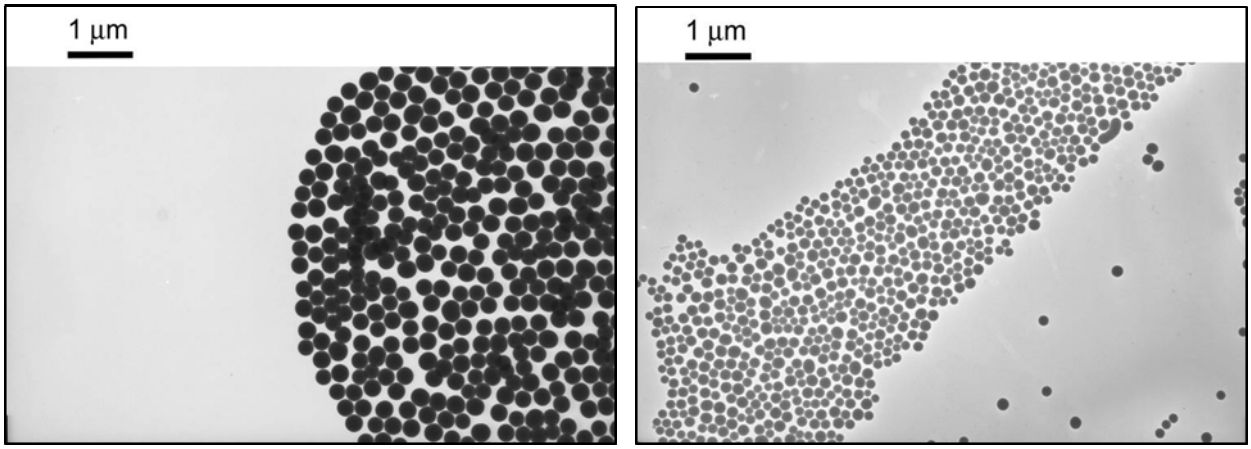

a b

Figure 4.3 TEM images of silica particles. a): Before HF etching, sample ES.4.37A (image 90081). b): After HF etching, sample ES.4.41A (image 90095).

Recently, Zhang *et al.* reported the synthesis of colloidal silica of low polydispersity using reagent grade TEOS.[205] The method is basically a modification of the Stöber method. A key difference is that the TEOS is pre-dissolved in ethanol. The authors claim that, because of the dilution of TEOS, the formation of new nuclei and the aggregation or adhesion of particles can be suppressed. Another difference from the commonly used Stöber synthesis performed in our lab is the total concentration of TEOS. The concentration ranges from ~ 55-60 mg/mL whereas in Zhang's procedure is 15.4 mg/mL. The concentrations of the other components vary accordingly depending on the targeted size. Colloidal silica synthesized using Zhang's procedure has a polydispersity comparable to standard certified silica. Figure 4.4 is a comparison between

the prepared silica particles and a standard from Duke Scientific. From TEM, the size polydispersity of the synthesized particles is 4.9% and the polydispersity of the purchased standard particles is 4.0%. Figure 4.5 is a comparison between the colloidal silica obtained by Zhang's procedure and the traditional Stöber procedure.

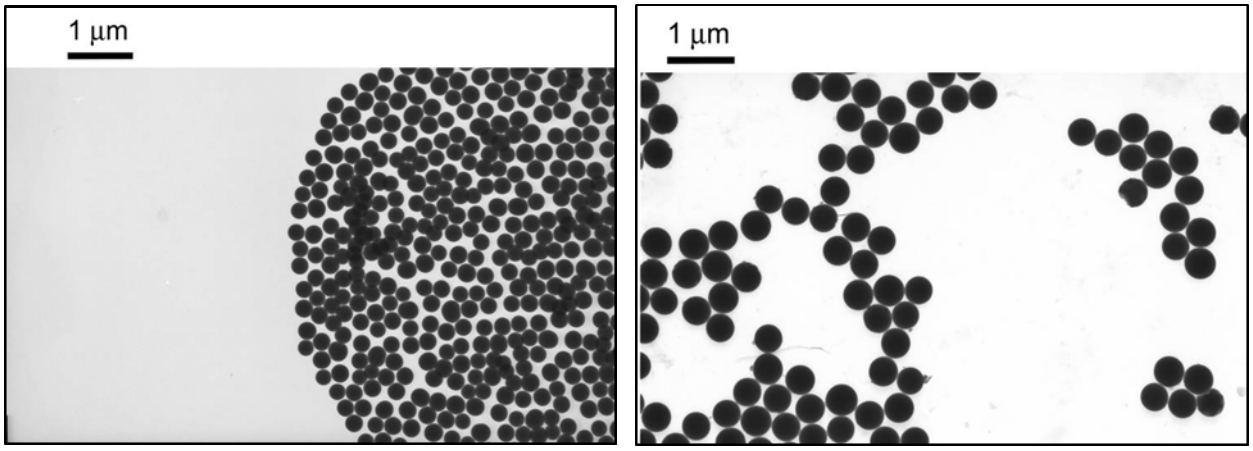

a b

Figure 4.4 TEM images of silica particles. a): Prepared by pre-dissolving reagent grade TEOS in ethanol, sample ES.4.37A (image 90081). b): Certified standard silica, sample ES.3.181A (image 89830).

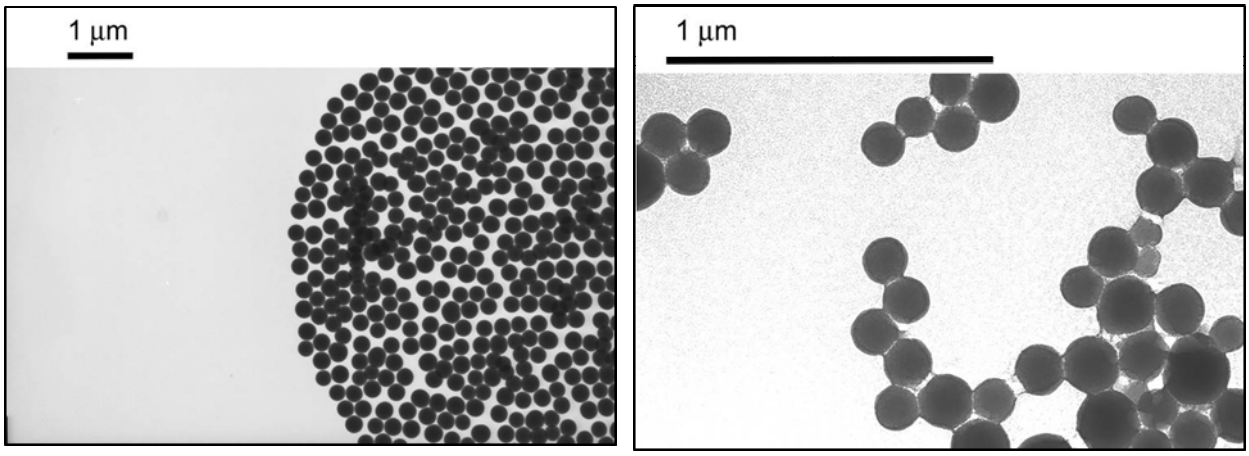

a b

Figure 4.5 TEM images of silica particles. a): Prepared by pre-dissolving reagent grade TEOS in absolute ethanol, sample ES.4.37A (image 90081). b): Prepared using traditional Stöber procedure, sample ES.3.111B (image 89766).

The colloidal silica obtained by Zhang's modified Stöber method has a polydispersity appreciably lower than that made using the original Stöber procedure. The particles obtained by the improved method have such low polydispersity that have hexagonal close packing regions appear.

The synthesized colloidal silica was analyzed by asymmetric flow field-flow fractionation (AF4). A variety of information can be obtained by this technique using the appropriate detectors. The equipment had a UV-vis detector (for concentration), a multi-angle light scattering detector whose signal (if extrapolated to zero angle) is proportional to concentration times mass. The 90° angle detector was connected to an autocorrelator and hence had the ability to perform dynamic light scattering measurements. Therefore it was possible to obtain the hydrodynamic radii of the particles. The collection times for each DLS measurement was 10 seconds. This time is very short considering the size of the particles. Therefore the hydrodynamic radii results are not correct. Figure 4.6 shows the AF4 traces and hydrodynamic radius of the colloidal silica obtained by the modified and the original Stöber methods respectively.

The Astra V software used the multi-angle light scattering information and the form factor of a sphere in order to obtain the geometric radius. For a sphere the geometric radius equals the radius. Figure 4.7 shows the AF4 traces and geometric radius of the colloidal silica obtained by the modified and the original Stöber methods respectively. It can be observed that the average geometric radius for both samples is around 100 nm. The geometric radius is obtained from static light scattering. The quality of the obtained data and the fitting of the sphere form factor were good. The obtained geometric radii are a clearer representation of the colloidal silica particles radii as opposed to the obtained hydrodynamic radii.

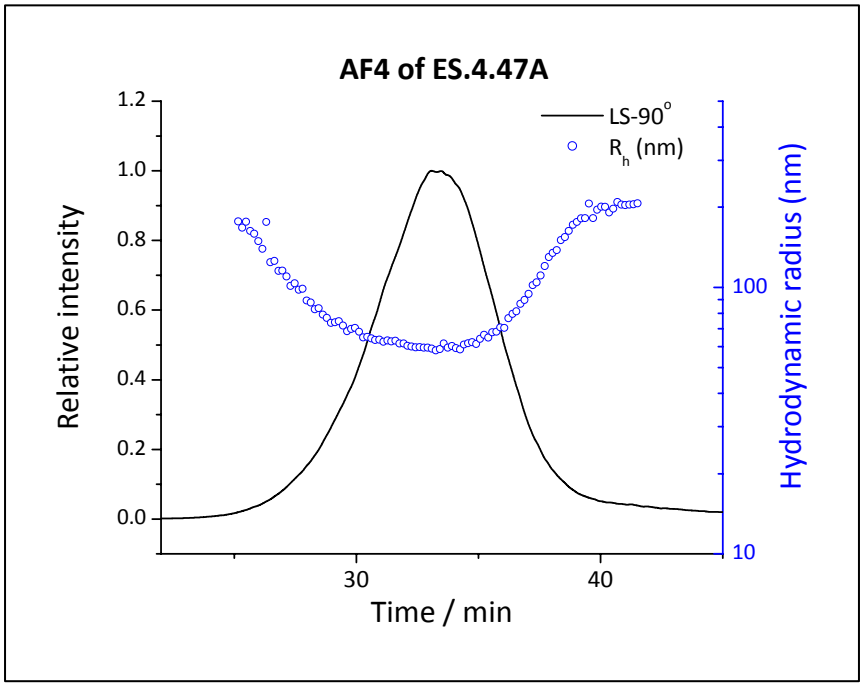

a

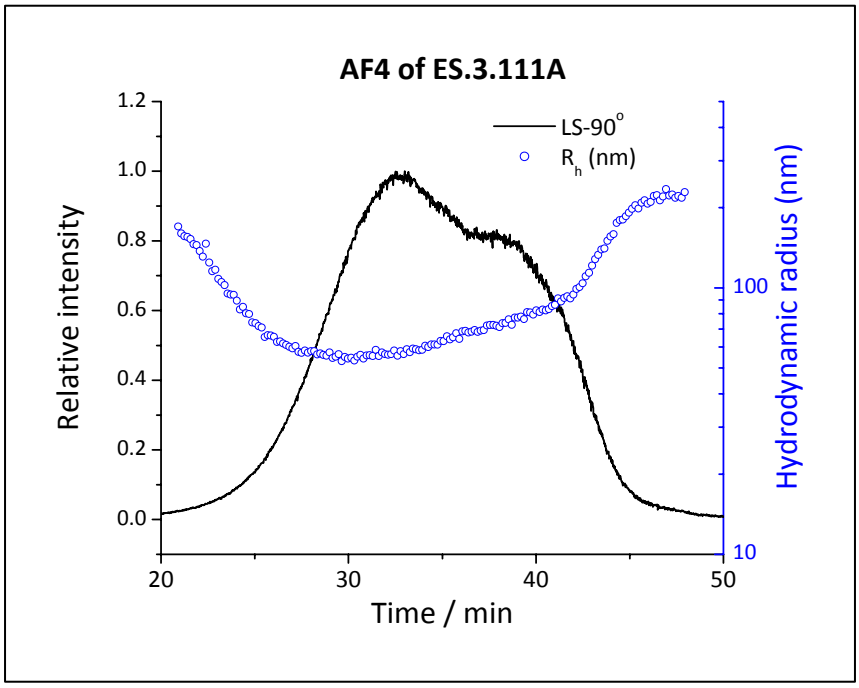

b

Figure 4.6 AF4 trace of colloidal silica, hydrodynamic radius. a): Prepared by pre-dissolving TEOS in ethanol, sample ES.4.47A. b): Prepared using traditional Stöber procedure, sample ES.3.111A. Left axis (black curve), relative intensity of the light scattering detector at 90°. Right axis hydrodynamic radius (blue curve).

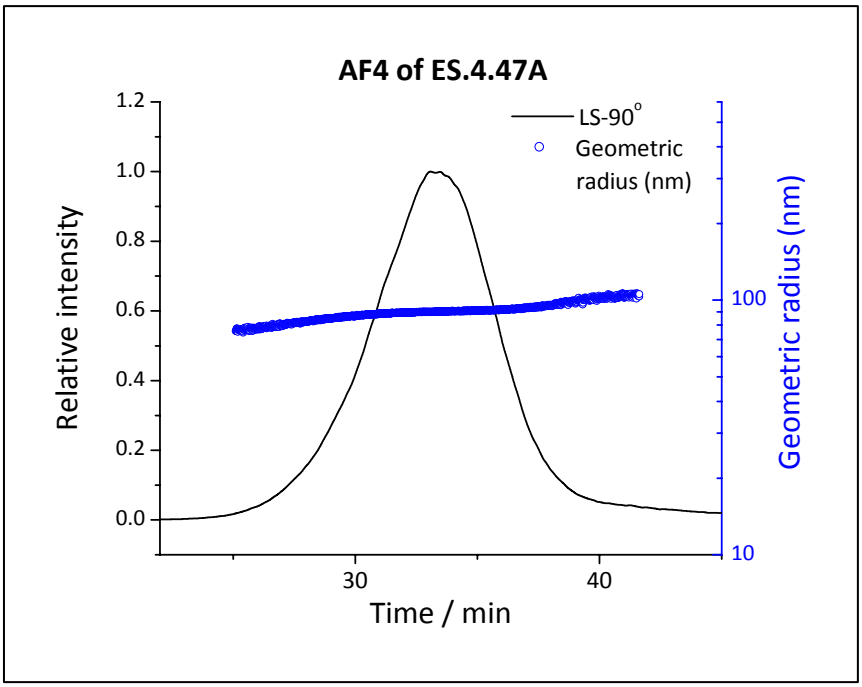

a

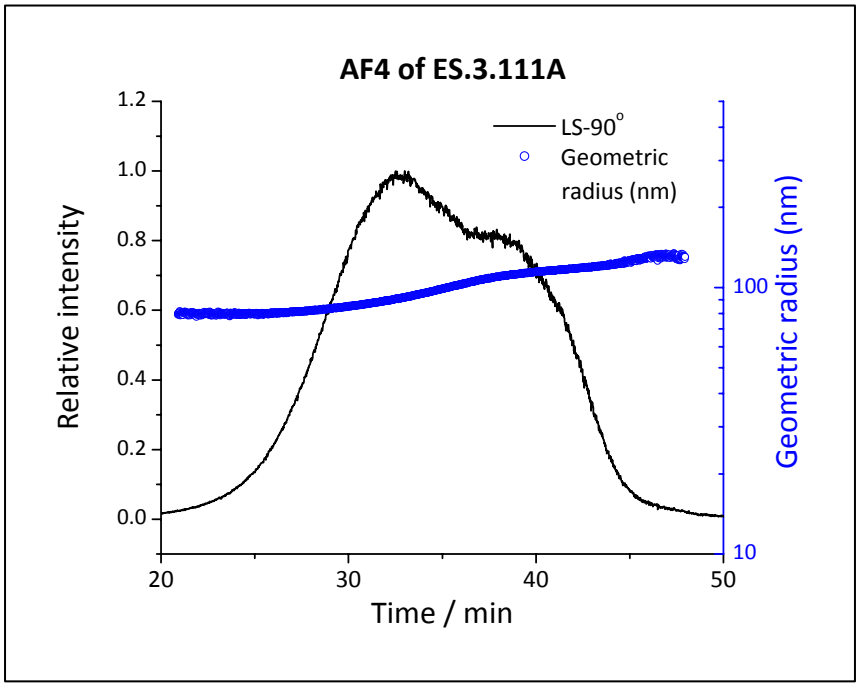

b

Figure 4.7 AF4 trace of colloidal silica, geometric radius. a): Prepared by pre-dissolving TEOS in ethanol, sample ES.4.47A. b): Prepared using traditional Stöber procedure, sample ES.3.111A. Left axis (black curve), relative intensity of the light scattering detector at 90°. Right axis geometric radius (blue curve).

In Figure 4.7 can be observed that the peak from the Stöber method sample is broader than the one from the modified Stöber method sample. The slope of the geometric radius plot in region where most sample is eluted (~18-45 min for sample ES.3.111A and ~28-37 min for sample ES.4.47A) can yield information about the polydispersity of the sample. In the case of the sample obtained by the modified Stöber method the slope is almost flat; this is a good indication of low polydispersity. In the case of the sample obtained by the original Stöber method the slope is clearly positive; the deviation from flatness is an indication of a deviation from monodispersity.

From Figure 4.7 it can be observed that the average geometric radius for both samples is around 100 nm which is close to the value obtained by TEM of 130 nm ± 10 nm.

4.1.3 Quantification of Amino Groups

The surface of the colloidal silica particles was modified. Amino and methyl groups were added. The source of amino groups was (3-aminopropyl) trimethoxysilane (APS). Methyl groups from methyl-trimethoxysilane (MTMS) were introduced in order to act as spacers among the amino groups. The methyl groups in MTMS are unreactive towards NCAs while the amino groups in APS can initiate the polymerization of NCAs. The methoxy groups of APS and MTMS can hydrolyze in solution. The degree of hydrolysis depends on the concentration of water in the solvent. The solvent is absolute ethanol and has a water content of 0.02%, which is relatively low. The hydrolyzed and non-hydrolyzed molecules then hydrogen bond to the silanol groups on the surface. The condensation of water or ethanol produces the Si_s-O-Si_f bonds (subscripts s and f are for surface and functionalization molecule respectively). Figure 4.8 shows the chemical structures of APS and MTMS.

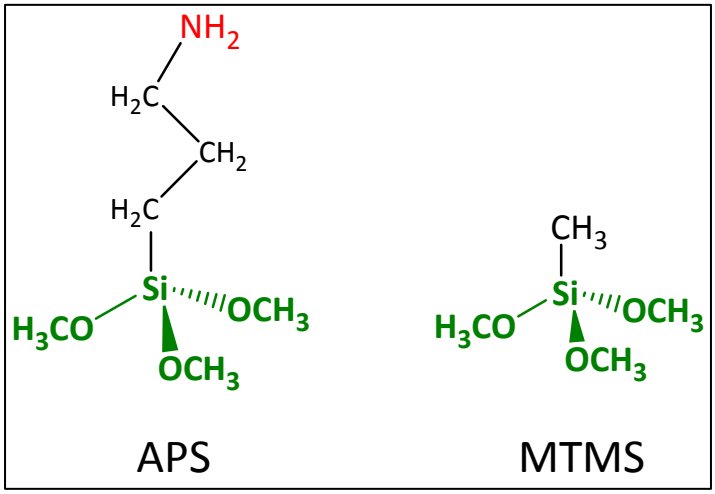

Figure 4.8 Chemical structures of (3-aminopropyl) trimethoxysilane (APS) and methyl-trimethoxysilane (MTMS).

Mixtures of different molar ratios of APS and MTMS were freshly prepared in order to passivate/functionalize the surface of the colloidal silica. It is possible to calculate the surface area of a particle by knowing its radius (the surface roughness was neglected). For this study, spherical colloidal silica particles of R_h = 103.2 nm ± 2 nm were used (sample ES.3.79A). Therefore, the surface area per particle is 4.6 x 10^6 nm^2. By knowing the concentration of the dispersion and the density of colloidal silica of 1.96 g/cm^3, one calculates the total surface area of the sample. Reports on the surface density of APS, dichloromethyl- or chlorodimethyl silanes range in the order of 2-6 groups/nm^2.[84;98] Considering the nature of APS, MTMS and the silica substrate It was assumed that for a monolayer of APS or MTMS the area occupied is 4 groups/nm^2. For the functionalization calculations the number of moles necessary for a monolayer plus an excess of about 10-20% was added. It is possible to estimate the concentration of amino groups on the surface if the composition of the APS/MTMS mixture is known.

The quantification of amino groups on the surface of the passivated-functionalized silica particles (P/F particles) was performed using UV-vis spectrometry after reaction with ninhydrin. Ninhydrin is known for yielding a bright purple complex when reacted with primary or secondary amines. Ninhydrin has been used mostly for qualitative purposes,[103] but it can also be used for quantification.[113;114] One of the arguments against the use of ninhydrin for quantification is that some of the colored product remains on the surface. Sarin *et al.* proposed a mechanism for this observation.[114] The mechanism involves ion exchange of the negatively charged blue product. Unmodified silica has a large negative zeta potential (~ -50 mV) on a wide range of pH. This suggests that a large negative charge exists on the surface probably due to deprotonated silanol groups. While on the passivated/functionalized particles it is possible to have a positive charge at low pH values, it is mostly either negatively charged (–OH) or neutral ($–CH_3$). A slight blue coloration is observed on the colloidal silica particles but it is faint. Because of the ion exchange mechanism proposed in the literature and the observation of only a very faint blue coloration on the particles, it is safe to say that a quantitative amount of the colored product is in solution. Hence the use of ninhydrin is valid for the quantification of amino groups.

The reaction proceeds in a similar fashion for primary and secondary amines. An important feature of the ninhydrin reaction is that the nitrogen in the amine molecule is withdrawn. This is a desired characteristic for the quantification of amino groups on the P/F particles. The blue complex can be separated from the colloidal particles by simple centrifugation hence avoiding the problems that arise from measurements in turbid systems. Figure 4.9 shows a scheme of the reaction of ninhydrin with P/F silica cores.

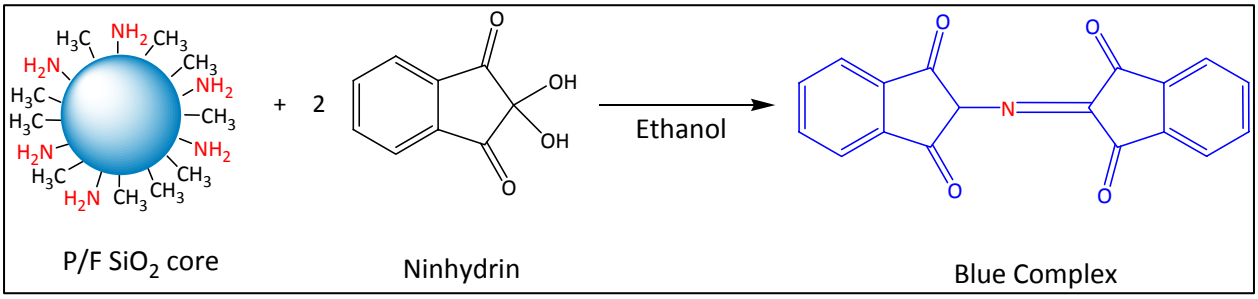

Figure 4.9 Scheme of the reaction of ninhydrin with P/F silica cores.

When using UV-vis spectrometry for quantification purposes, it is necessary to verify that the absorbance *vs* concentration plot is linear for the concentration range of interest. In other words, that that the absorbance *vs* concentration plot follows Beer's law. A calibration plot was built using hexylamine as standard. The linearity of the calibration plot can be seen in Figure 4.10. The error bars for each point are present but they are small and difficult to see.

The concentration results obtained from the calibration curve were in millimol/L (mM). It is possible to convert from mM to number of amino groups per nm^2 by knowing the total volume of ninhydrin complex solution, total mass and R_h of the P/F particles. As detailed above, the surface density of amino groups on the surface was based on the assumptions that only a monolayer was formed and that the parking area for either APS or MTMS is 4 molecules/nm^2. These assumptions are justified by literature values[84;98] and by the fact that only a slight excess of functionalizing mixture was added. Figure 4.11 shows the graph of surface density of amino groups (in # of $–NH_2$ groups/nm^2) *vs* mol fraction of amino groups in APS/MTMS solution used for surface modification (in mol %).

At low amino group concentrations the measured and expected values are close. They actually appear to overlap. However, when zooming into the low concentrations values it is

possible to observe the differences. Figure 4.12 shows a zoom at the 0-30 mol% of the surface density graph.

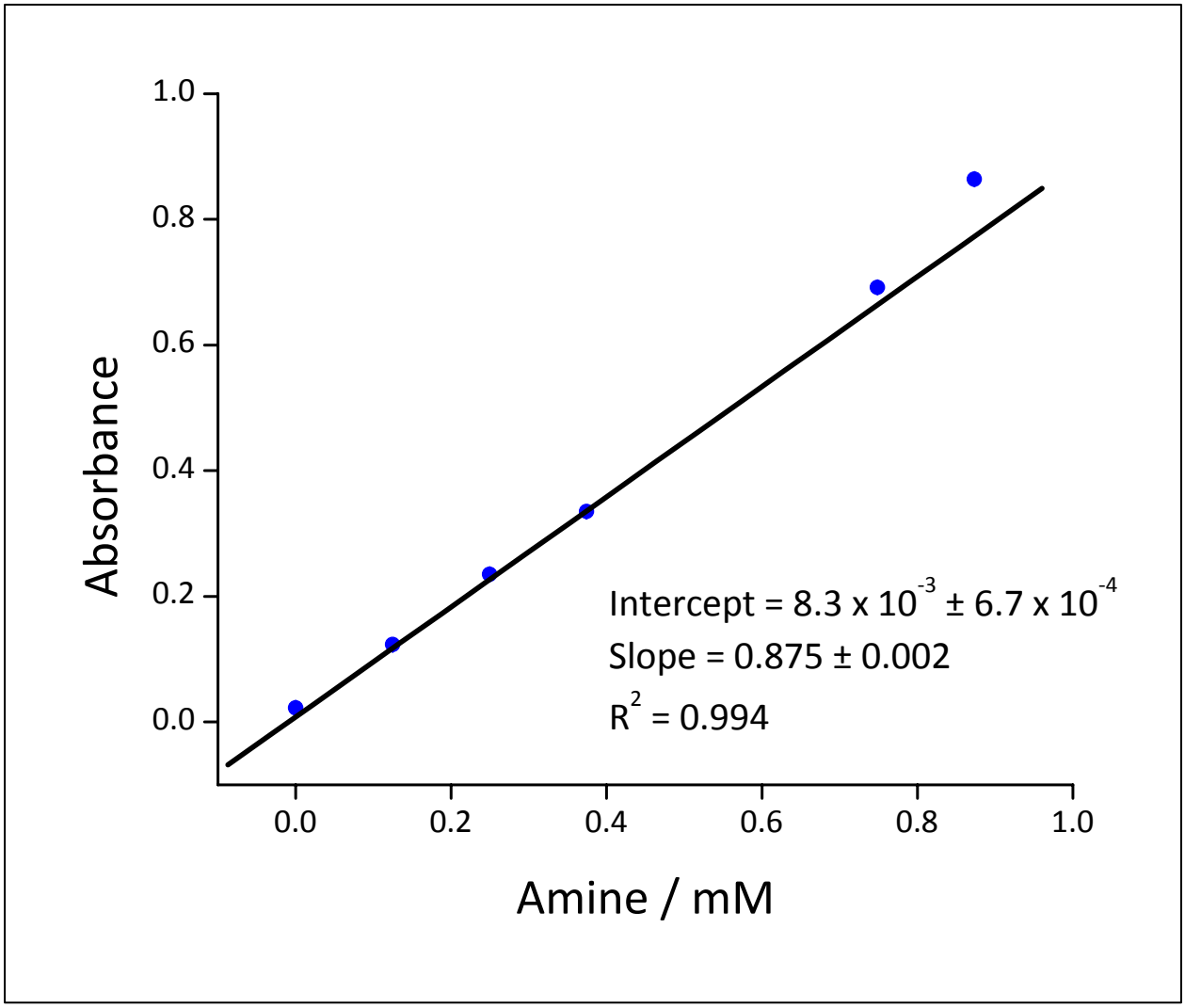

Figure 4.10 Calibration curve for quantification of amino groups.

At low amino group concentrations the expected surface density is within the experimental error of the measurement. At high concentrations the measured value is higher than expected. It is likely that monolayers are being formed at low concentrations. Figure 4.13 shows a representation of what might be the distribution of amino groups on a colloidal silica particle at low concentration.

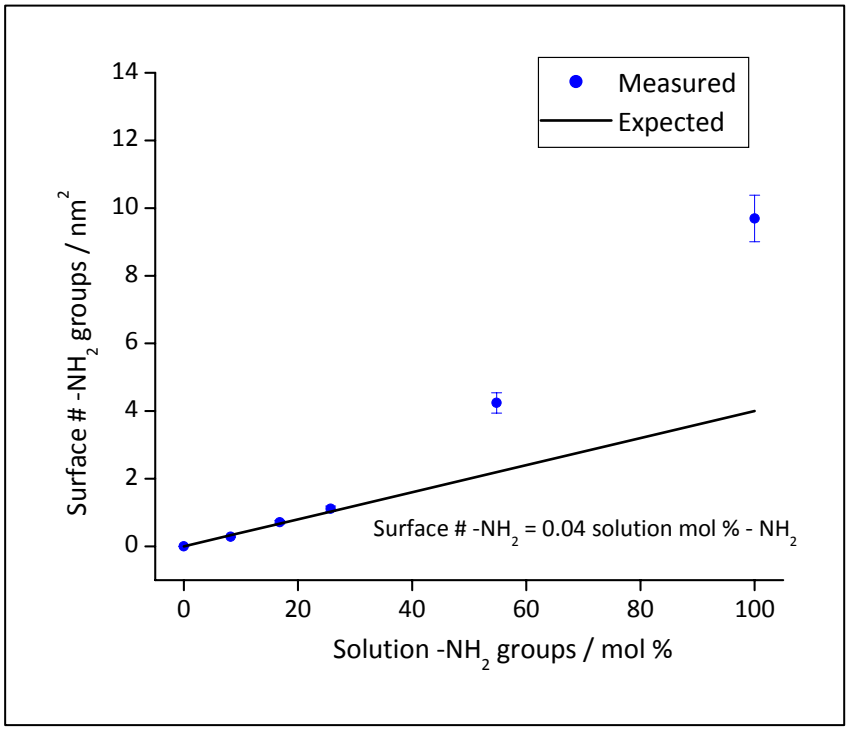

Figure 4.11 Graph of surface density of amino groups measured by the ninhydrin method *vs* mol fraction of APS in the APS/MTMS solution used for surface modification (asumming monolayer formation and that the parking area of APS and MTMS is 4 molecules per nm^2).

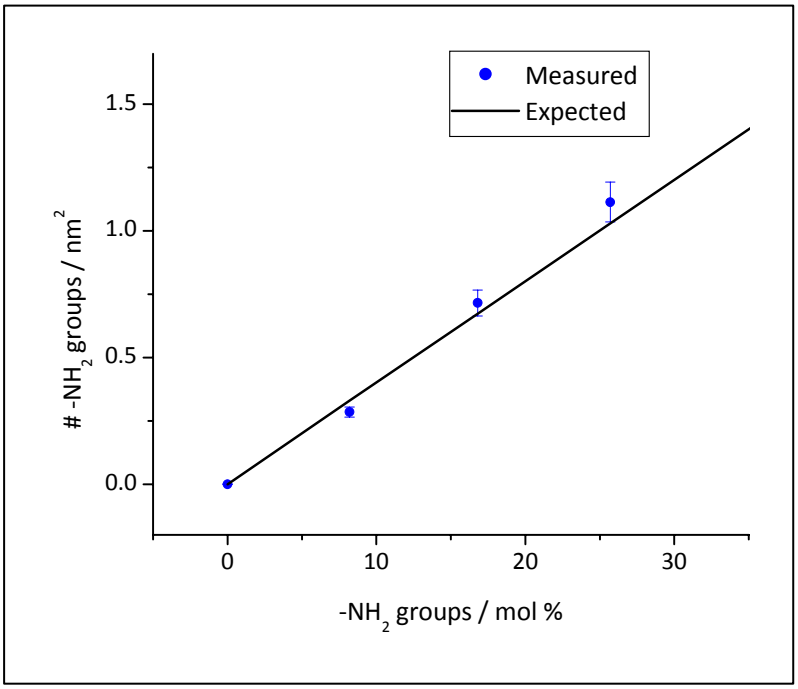

Figure 4.12 Enlarged version of the graph of surface density of amino groups measured by the ninhydrin method *vs* mol fraction of APS in the APS/MTMS solution used for surface modification.

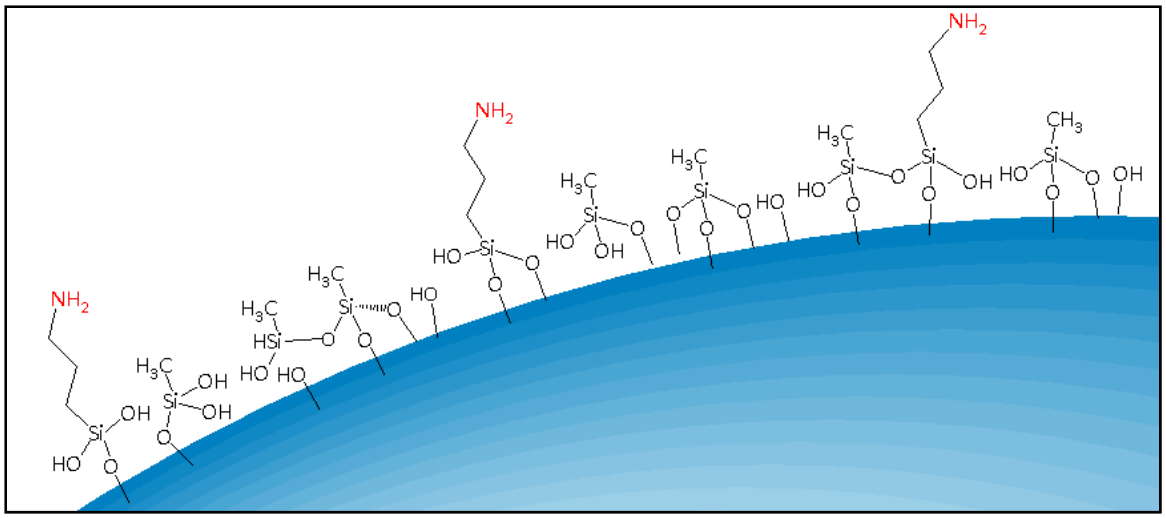

Figure 4.13 Scheme of the distribution of amino groups on the surface of a colloidal silica particle at low concentration.

At high concentrations it is possible that bilayers or multilayers of APS and MTMS are being formed.[78;79;82;87] This would explain the observation that the measured concentration of amino groups is higher than expected for a monolayer. Figure 4.14 shows a representation of what might be the distribution of amino groups on a colloidal silica particle at high concentration.

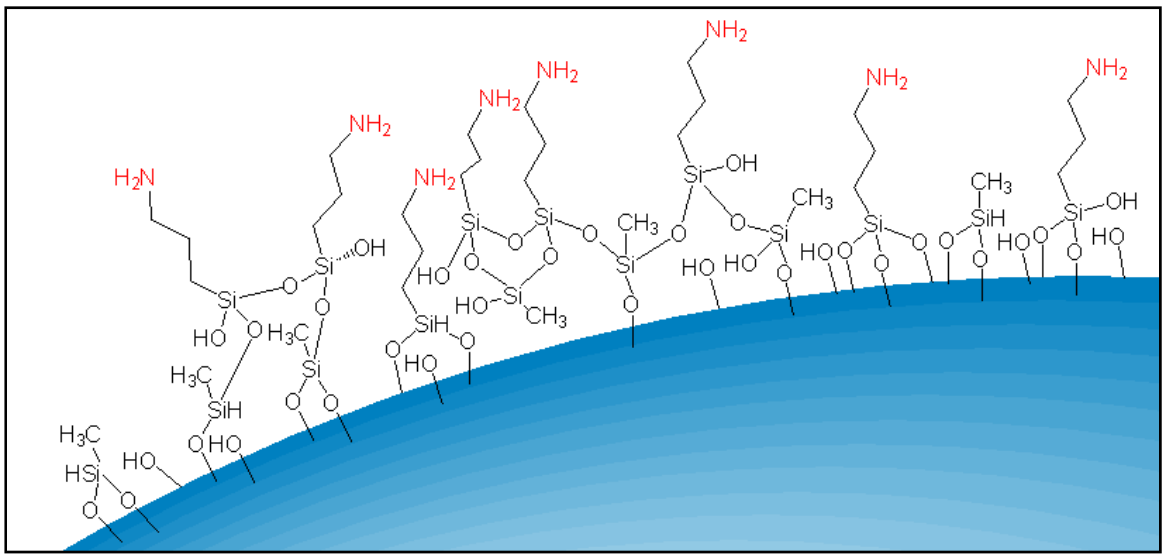

Figure 4.14 Scheme of the distribution of amino groups on the surface of a colloidal silica particle at high concentration.

One of the assumptions made is that the reactivity of APS and MTMS towards the silica surface is the same. This may not be necessarily true. It is possible to argue that MTMS would be more reactive due to its smaller size. However, it is also possible to argue that APS would be more reactive due to inductive effects. The carbon atom next to the silicon has a partial negative charge. On APS the part attached to that carbon is $–CH_2CH_2NH_2$ while in MTMS is –H. Therefore, the mentioned carbon would be more negative on APS than in MTMS making the silicon more positive and hence more reactive.

The low surface concentration regime is of main interest for the purposes of this project. Since the passivated/functionalized particles would serve as the surface for growing rod-like polypeptides such as poly(γ-benzyl-L-glutamate) (PBLG), it is essential to estimate the spatial implications. The cross-sectional diameter, d, of PBLG is 1.6 nm.[189] Therefore the projected area of a rod perpendicular to the surface is $A_p = (\pi d^2)/4$ or 2 nm^2. If an hexagonal close packing of the rod projections on the silica surface is considered (*i.e.* 2 dimensional hexagonal close packing), it can be found that ~ 91% of the total area is occupied by the rod projections. Therefore, the effective area occupied a rod projection is A_p x $(91\%)^{-1}$ = 2.2 nm^2 (considering excluded space).

From the surface density results, it can be seen that for the low concentration regime, the surface density of amino groups is 0.3-1.2 groups/nm^2. This surface density can allow, in principle, all the amino groups to act as initiators. At high surface concentrations the crowding of amino groups makes them inefficient initiators for the polymerization of *N*-carboxyanhydrides.[94] At low amino surface density of amino groups the measured values using the ninhydrin method agree well with the expected ones.

4.1.4 Relationship Between Amino Group Surface Density and Zeta Potential

The ninhydrin method proved to work well in measuring the amino group concentrations of interest on colloidal silica. Even though it is fast and accurate it might be possible to find an even faster method that has the same accuracy. It is known that amino groups are positively charged at low values of pH. The zeta potential (ζ) of a colloidal particle is related, among other factors, to its surface charge. Therefore, in principle, it is possible to obtain a relationship between zeta potential and surface density of amino groups if all other variables (such as particle size, shape, concentration, ionic strength) are kept constant. A zeta potential measurement is easier and considerably faster (~ 1-2 minutes) than the ninhydrin method (> 60 minutes). The zeta potential of samples of different surface density of amino groups was measured at pH = 1 and 1 mM $NaNO_3$. An empirical relationship was obtained. Figure 4.15 shows a graph of the zeta potential (ζ) *vs* surface density of amino groups (# -NH_2/nm^2).

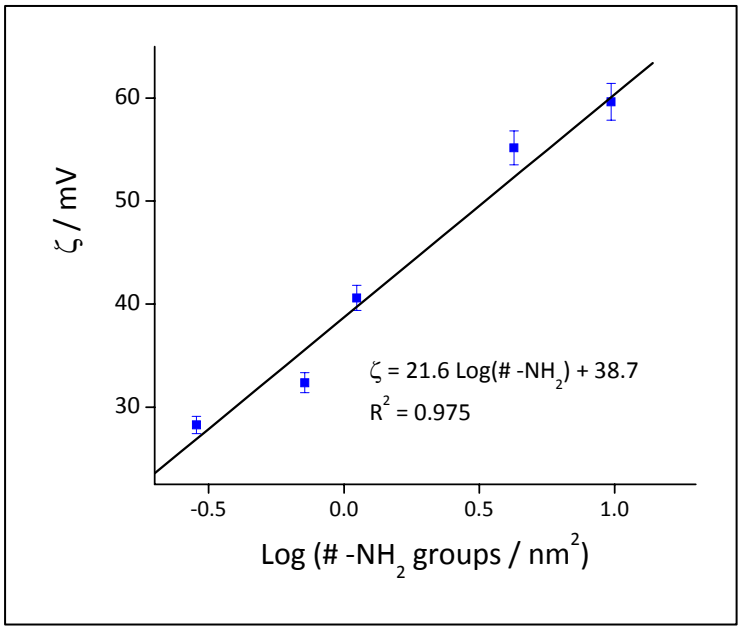

Figure 4.15 Graph of zeta potential (ζ) *vs* the logarithm of the surface density of amino groups as measured using ninhydrin method.

A good correlation between the zeta potential and the logarithm of the surface density can be observed. This is a preliminary result that shows that it is possible to measure the surface density of amino groups by a simple zeta potential measurement. A calibration plot with more points has to be built and particles of other sizes have to be tested.

4.2 Polypeptide Shell

4.2.1 Sequential Growth of Polypeptide

It was demonstrated in Chapter 4.1 that the size of the silica cores as well as the surface density of amino groups can be easily controlled. It is equally important to have control over the polypeptide shell content. The fact that the polymerization of *N*-carboxyanhydrides initiated by primary amines has an *undead* character[93] makes it possible to grow the polypeptide shell by the sequential addition of monomer. It may be tempting to claim that the growth of the polypeptide has a *living* character. A *living* polymerization is *undead* in the sense that after is complete, more monomer can be added and the polymer continues to grow. However; a *living* polymerization has other characteristics as well. For example the molecular weight of the resulting polymer is given by the monomer to initiator ratio $[M_0]/[I_0]$. The growth of molecular weight is linear with respect to $[M_0]/[I_0]$. Hence increasing the size and polypeptide content of the particles' shell is not conclusive evidence to claim that the polypeptide growth has a living character. The molecular weight of the tethered polypeptide would have to be known and its molecular weight would be given by $[M_0]/[I_0]$.

Fong demonstrated earlier that the polypeptide is likely covalently bound to the silica surface.[94] It was observed that after a series of centrifugation-dispersion (washing) steps, the composite particles still had an IR signal characteristic of amides (PBLG) whereas in a mixture of

PBLG and functionalized silica particles that had gone through the same centrifugation-dispersion steps that band was not observed. Figure 4.16 shows the TGA curves of silica-PBLG composite particles obtained by the sequential addition of monomer (BLG-NCA) to amino-functionalized silica cores (described in section 3.1.3.1 under *sequential addition*). The TGA curve of PBLG was added as an insert at the bottom left for re-scaling reasons.

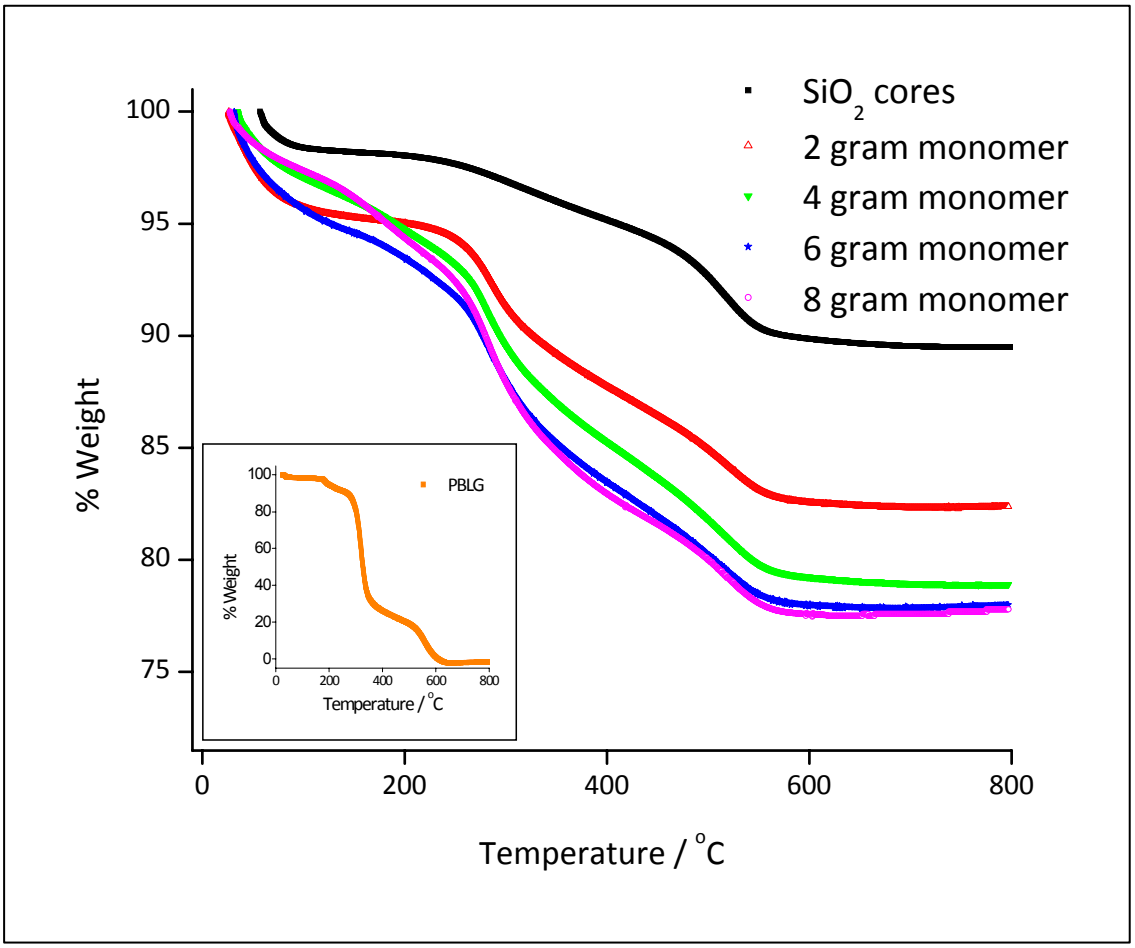

Figure 4.16 TGA curves of silica-PBLG composite particles (ES.3.186B-ES.3.188C) obtained by the sequential addition of monomer (BLG-NCA) to amino-functionalized silica cores (ES.3.186A). Inner figure (bottom left) is the TGA curve of neat PBLG.

The curve of the SiO_2 cores shows three regions of weight loss. The first one is ~ 30-120 °C; this corresponds to the loss of adsorbed water by the silica surface. Silica has a high affinity for water and even though the exposure to the environment is short, silica adsorbs water. The

second region is ~ 150-400 °C; this corresponds to hydration water *i.e.* water that is inside the structure of silica. The third region ~ 400-600 °C corresponds to loss of water due to dehydroxylation of the silica surface.[61]

The curves of the composite particles show a weight loss that increases as more monomer was added. This suggests that more polypeptide is present on the particles' surface. A clear difference can be seen between the SiO_2 cores and the 2 gram monomer added curves. An obvious difference can be seen between the 2 and 4 gram monomer added curves. The differences are more subtle as more monomer was added. From the neat PBLG curve it can be observed that most of the weight loss (~ 94%) occurs in the 200 °C - 600 °C range. Therefore an analysis of the % weight difference between 200 °C and 600 °C may yield more realistic information on the polypeptide content. Figure 4.17 shows a graph of the % weight difference between 200 and 600 °C ($\Delta_{600\text{-}200}$) for silica-PBLG composite particles formed by sequential addition of monomer.

The silica-PBLG composite particles were synthesized using silica cores that were functionalized with a mixture of APS/MTMS 10/90 (v/v). The estimated surface density of amino groups is about 0.28 groups/nm^2 (Chapter 4.1.3). In principle, all the amino groups could act as initiators considering that the projected surface area occupied by a hexagonally packed PBLG molecule in the α-helix conformation is about 2.2 nm^2. In other words, there are (0.28 groups/nm^2)(2.2 nm^2)= 0.62 amino groups in the area occupied by the projection of a hexagonally packed PBLG molecule. The curvature of the silica spheres surface provides freedom for the growth of the polypeptide. Reports of PBLG polymerized from amino-functionalized flat silicon surfaces in solution or by vapor deposition-polymerization show a

plateau in the thickness of the polypeptide of about 25 nm.[167;168] Figure 4.18 shows the hydrodynamic radius ($R_{h,\ app}$) of silica-PBLG composite particles obtained by sequential addition of monomer.

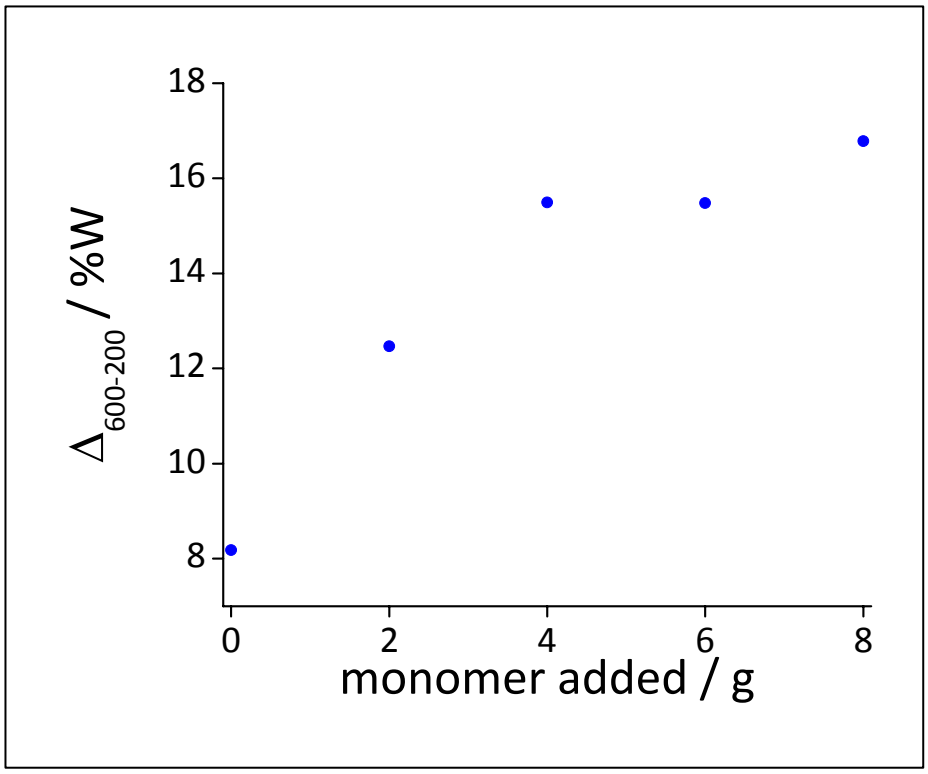

Figure 4.17 Graph of the %weight difference between 200 and 600 °C (Δ600-200) for silica-PBLG composite particles (ES.3.186B-ES.3.188C) obtained by the sequential addition of monomer (BLG-NCA) to amino-functionalized silica cores (ES.3.186A).

The sample obtained after adding 10 gram of monomer was aggregated at several dilute concentrations in pyridine. The sample obtained after adding 2 gram of monomer has a larger hydrodynamic radius than the subsequent samples. The error in the measurement is large (± 18%). A possible explanation for this observation is that in the initial stages of growth, the polypeptide is in an extended conformation. PBLG is believed to be in a α-helical conformation in pyridine at the temperature of the measurements.[93] Another possibility is that, in the initial stages of PBLG growth, the tilt angle is closer to 90° than in later stages. This would yield a

thicker PBLG shell but not necessarily a longer PBLG chain. Wieringa *et al.* were able to measure the average tilt angle of PBLG on a flat silicon surface using Fourier transform infrared spectroscopy (FTIR).[210] This was possible because the transition dipole moment directions of the different amide bands with respect to the helix were known. On a curved surface such as the silica core it might not be possible to obtain a representative average tilt angle because it would be an average over an infinite number of tangents.

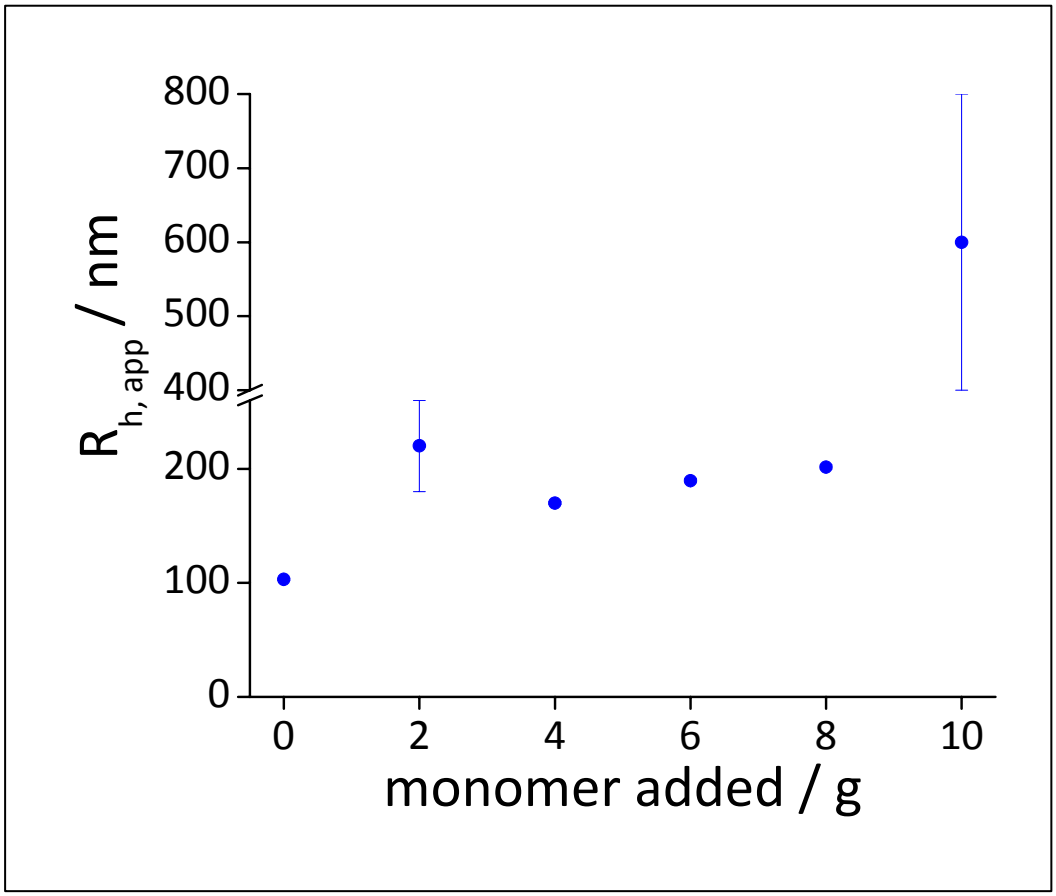

Figure 4.18 Graph of $R_{h,app}$ *vs* monomer added for silica-PBLG composite particles (ES.3.186B-ES.3.188C) obtained by the sequential addition of monomer (BLG-NCA) to amino-functionalized silica cores (ES.3.186A) in THF. DLS measurements were performed in pyridine.

The thickness of the polypeptide shell is obtained by subtracting the hydrodynamic radius of the silica cores from the hydrodynamic radius of the silica-PBLG composite particles.

Figure 4.19 shows the shell thickness of silica-PBLG composite particles obtained by sequential addition of monomer. The upward trend of the plot of shell thickness *vs* monomer added is similar to the trend of the plot of $\Delta_{600\text{-}200}$ *vs* monomer added. This indicates that overall the PBLG content contributes to the shell thickness. Therefore, the average tilt angle of the PBLG chains is different from zero.

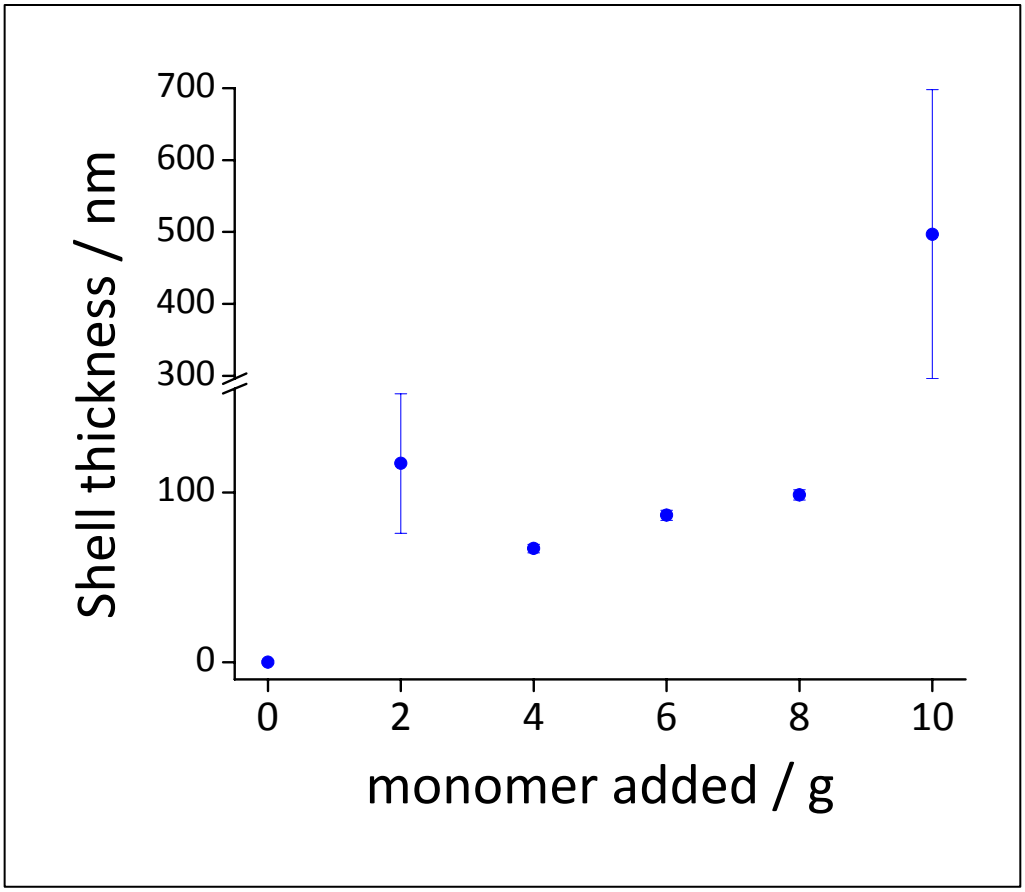

Figure 4.19 Graph of polypeptide shell thickness *vs* monomer added for silica-PBLG composite particles (ES.3.186B-ES.3.188C) obtained by the sequential addition of monomer (BLG-NCA) to amino-functionalized silica cores (ES.3.186A).

It may be tempting to use pyridine as the reaction solvent instead of THF. Pyridine is a good solvent for PBLG;[188] therefore it may not be necessary to wash the composite particles prior to DLS measurements. Pyridine is an aromatic tertiary amine. The fact that pyridine is

aromatic may lead to think that it would not function as initiator for the ring-opening polymerization of NCAs. Nonetheless, Kricheldorf *et al.* reported that pyridine does initiate the polymerization of NCAs[211] yielding cyclic oligomers. This does not necessarily affect the DLS measurement as long as changes in the viscosity and/or refractive index of the solvent are taken into account. Qiu found that PBLG and pyridine are nearly isorefractive.[2] Nevertheless, the viscosity of the solutions increases drastically depending on the monomer concentration and reaction time. For example, for a solution containing 4 mg/mL of BLG-NCA, the measured viscosity at 20 °C after 3 days is 1.70 cP. The measured viscosity of pure pyridine is 0.95 cP which agrees with the reported literature value.[212] A correct diffusion coefficient and subsequently $R_{h,\,app}$ can be obtained if the correct viscosity is used but this is rather a nuisance and presupposes the validity of the Stokes-Einstein equation in this complex fluid. A solvent that does not initiate the polymerization of NCAs such as THF or 1,4-dioxane is more appropriate as the reaction medium. But because the polypeptide aggregates in such solvents, it is necessary to wash the resulting silica-polypeptide composite particles. The washing was done by centrifuging-redispersing cycles in pyridine.

4.2.2 Shell Visualization by Positive Staining Transmission Electron Microscopy

Scattering and microscopy methods complement to yield a better picture of a microscopic system. Both methodologies are powerful from different points of view. Scattering methods give better statistical information because they take in consideration many particles ($\sim 10^6$-10^{12}). Nevertheless one of the weaknesses is that they do not give much detailed information of the microscopic structure (it is possible to obtain such information but a number of scattering methods have to be applied). Some scientists say “seeing is believing” and here is where microscopy methods can complement very well with scattering methods. Scientists

skeptic of microscopy methods argue that "using microscopy you can see whatever you want to see". This is because one microscope field may show an image that is not necessarily representative of the sample. By combining scattering and microscopy methods it is possible to elaborate conclusions that are more resistant to skepticism.

Silica-PBLG composite particles were synthesized by the reaction of amino-functionalized colloidal silica with BLG-NCA. Figure 4.20 shows the dynamic light scattering results ($R_{h,app}$ *vs* q^2) for the silica cores ($R_{h,app}$= 103 nm $\pm$ 1 nm) and for the silica-PBLG composite particles ($R_{h,app}$= 189 nm ± 3 nm). The difference in hydrodynamic radii between the silica cores and the silica-PBLG composite particles is the shell thickness (86 nm ± 4 nm). The apparent hydrodynamic radii are independent of scattering angle, *i.e.* the curve of $R_{h,app}$ *vs* q^2 is almost flat. It is possible that the increase of $R_{h,app}$ of the silica-PBLG composite particles compared to the silica cores may be due to particle aggregation and not polypeptide growth. Qiu found that PBLG and pyridine have almost identical refractive indices. Therefore the scattered light comes almost from the silica cores. The measured radius of gyration (R_g) was the same for the silica cores and for silica-PBLG composite particles. This indicated the absence of aggregation.[2] The polypeptide content can be quantified by TGA. Figure 4.21 shows the TGA curves of the silica cores and silica-PBLG composite particles. The weight loss of the silica cores is about 10.5% and about 33.5% for the silica-PBLG composite particles. Hence the PBLG content is about 23%. The increase in $R_{h,app}$ of the composite particles as compared to the silica cores is probably caused by the polypeptide growth. The magnitude of the increase in $R_{h,\,app}$ as well as on polypeptide content is comparable with the silica-PBLG composite particles obtained by sequential addition of monomer under similar conditions.

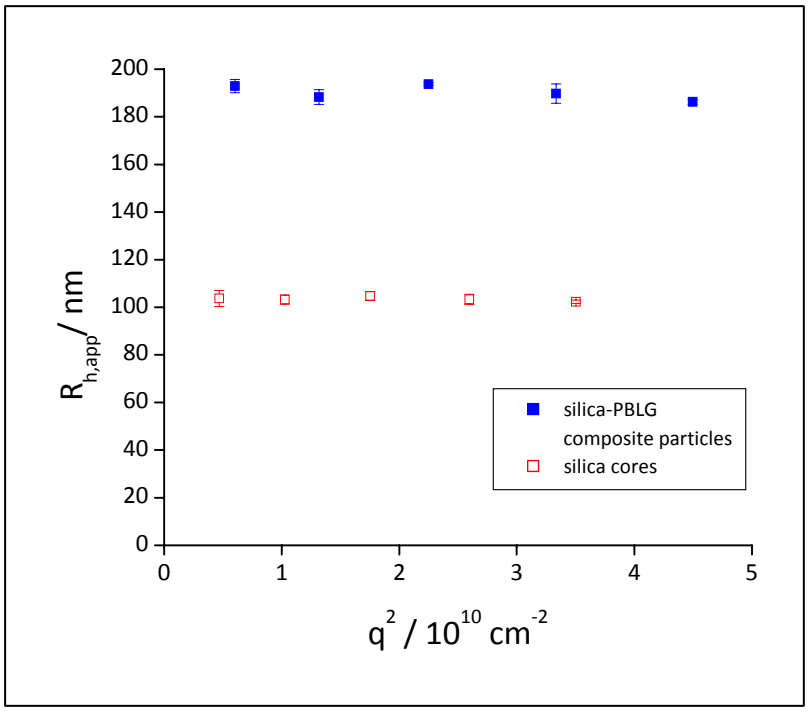

Figure 4.20 Graph of $R_{h,app}$ *vs* q^2 for silica cores (□ ES.3.79A in water) and silica-PBLG composite particles (■ ES.3.128A in pyridine).

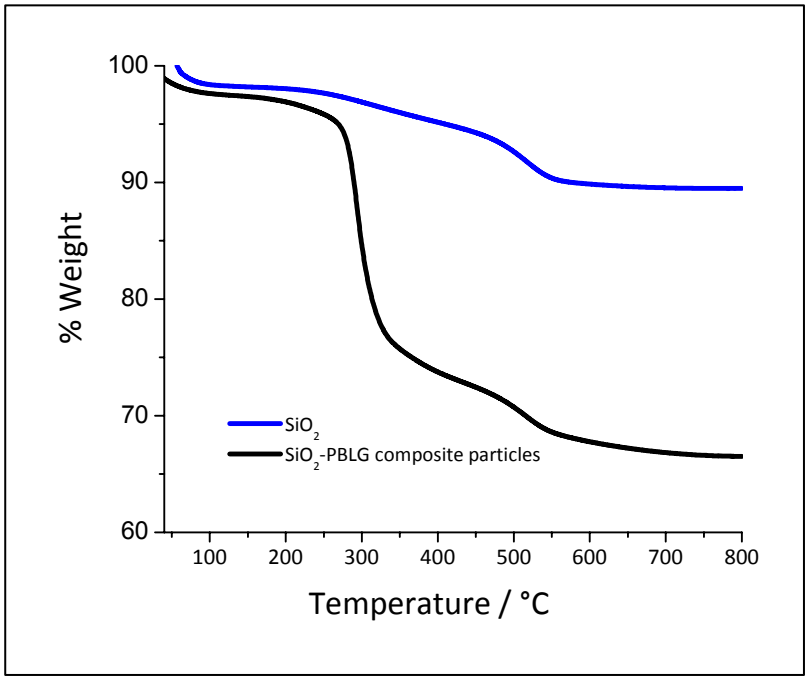

Figure 4.21 TGA curves of silica cores (ES.3.79A) and silica-PBLG composite particles (ES.3.128A).

In the characterization of silica-polypeptide particles, it is important to observe the "wet" sample in order to obtain information about the polypeptide. In regular scanning electron microscopy (SEM), the sample often is dried and sputter coated with a metal.[213] Newer SEM techniques such as environmental SEM have the ability to observe hydrated samples but the achievable resolutions are not as good as in high vacuum SEM.[214] Sheiko *et al.* used atomic force microscopy (AFM) to measure the molecular weight of cylindrical polymer brushes.[215] AFM was used to observe silica-polypeptide composite particles but the results were unsuccessful.

Transmission electron microscopy (TEM) works at higher voltages than conventional SEM and produces images of higher resolution. TEM is more useful when one wants to observe through the sample whereas SEM is better for observing the sample's surface. The incident electrons in TEM are scattered by the sample which has to be relatively thin.

In TEM the scattering of electrons is the result of the Coulomb interaction with the nucleus (positively charged) and with the electron cloud (negatively charged). The atomic scattering factor ($f_e(\theta)$)contains two contributions of opposite sign:

$$f_e(\theta) = \frac{me^2\lambda}{2h^2}\frac{[Z - f_X(\theta)]}{\sin^2\theta} \qquad \text{Equation 4.1}$$

where $f_X(\theta)$ is the atomic scattering factor for X-rays, which are only scattered by the electron cloud. Z is the atomic number, λ is the electron wavelength, m is the electron mass, e is the electron charge, h is Planck's constant, and θ is the scattering angle. The electron wavelength is given by the de Broglie relation $\lambda = h/mv$. It is related to the accelerating potential E by the relativistic relation shown in Equation 4.2.

$$\lambda = h\left[2m_0E\left(1+\frac{eE}{2m_0c^2}\right)\right]^{-\frac{1}{2}}$$ Equation 4.2

where m_0 is the rest mass of the electron. Since *E* is in the range 80-400 kV, the electrons used in electron microscopy can be considered relativistic because they travel at speeds larger than half the speed of light.[216]

Several preparatory techniques are used in TEM for the observation of liquid or "wet" samples. For example, the Ballauff group used cryogenic transmission electron microscopy (cryo-TEM) for the visualization of PS-PNIPAM and PS-poly(styrene sulfonate acid) core-sell particles.[161;217] In cryo-TEM the liquid sample is cooled down very rapidly, often in liquid ethane at its freezing temperature. This very fast freezing (vitrification) prevents the liquid in the sample (normally water) from crystallizing. The sample is kept at a very low temperature using liquid nitrogen and observed in the TEM in the low-dose imaging to minimize electron-beam radiation damage.[218] Another technique is freeze-fracture TEM. Meyer and Richter used freeze-fracture TEM to study lipids and membranes.[219] In brief, the technique consists of cooling down the sample very fast similarly to cryo-TEM. The vitrified sample is then fractured while keeping it at a cold temperature. After that, the fractured sample is coated with carbon and shadowed with platinum. The replica is then observed in a regular TEM. Cryo-TEM and freeze-fracture TEM require the use of cryogenic equipment which is often expensive. A particularly high level of skill is needed in order to obtain representative images.

The organic component of silica-polypeptide composite particles is formed by atoms of low atomic number and low electron density (C, H, O, N). It can be seen from Equation 4.1, the scattering factor increases as the atomic number increases. The beam of electrons passes

through the organic component with relative ease and therefore, only a poor contrast can be achieved. Salts and oxides of transition metals and rare-earth elements such as lead, iron, tungsten, uranium and osmium are often used in order to introduce contrast.[220] This process is known as staining and can be divided into positive and negative. In negative staining the specimen is embedded in the stain. After drying, the electron-dense atoms enclose the specimen. The difference between the specimen and the surrounding electron-dense atoms provides the necessary contrast. The specimen appears light surrounded by a dark background of dried stain. In positive staining, the electron scattering power of the specimen is increased by the introduction of heavy metals. The electron-dense metals bind (sometimes selectively) to the specimen. The difference between the background and the coated specimen provides the necessary contrast.[221] A disadvantage of staining approaches is that sometimes the specimen has to be dried or may suffer changes on contact with the stain hence not representing the sample appearance in the liquid or "wet" state.

Several staining procedures were attempted in order to visualize the polypeptide shell of silica-polypeptide composite particles. The dried particles were put in contact with aqueous solutions of the stains lead citrate, osmium tetroxide and uranyl acetate. Also, a different approach was tried which consisted of fixation in glutaraldehyde, embedding in epoxy resin, curing of the resin, slicing the embedded particles using an ultramicrotome (slices of ~ 20 nm thickness) and putting the slices in contact with the stains. Neither approach produced images that agreed with the DLS results. No shell or a shell considerably thinner (~ 5-10% of the obtained value by DLS) was observed. This is possibly because the hydrophobic polypeptide collapsed in the presence of aqueous solutions.

A different approach was tried which avoided the direct contact of the dispersed silica-polypeptide particles with water yet the sample had a slight contact with the stain. Osmium tetroxide (OsO_4) is a relatively volatile solid. Its melting point is around 40.5 °C and its boiling point is around 133 °C. The August's formula, expressed in Equation 4.3, can predict the vapor pressure of OsO_4 in a range below its melting point:

$$\log P = -\frac{2542.01}{T} + 9.51791 \qquad \text{Equation 4.3}$$

where P is the vapor pressure of OsO_4 in millimeters of mercury (mm Hg) and T is the absolute temperature. At 21.92 °C the calculated vapor pressure (from Equation 3.3) is 7.97 mm Hg which is very close to the observed value of 7.95 mm Hg.[222] The 21.92 °C is approximate to the room temperature value at which the staining was performed. The concentration of the OsO_4 solution was 1%; this corresponds to a mole fraction $\chi_{OsO_4} = 7.14x10^{-4}$. At this low mol fraction, the solution may be considered as ideal and would obey Raoult's law. Therefore the vapor pressure of OsO_4 is P = (7.95 mm Hg)($7.14x10^{-4}$) = $5.7x10^{-3}$ mm Hg. This value may seem low but OsO_4 has a high affinity for nitrogen ligands such as pyridine. OsO_4 complexes with nitrogen ligands bind to bases in DNA.[223;224] It is possible that the complex of OsO_4 with pyridine would bind to one of the components of a PBLG molecule such as the amide nitrogen. The ability of an amide nitrogen to donate electrons is considerably lower than an amine nitrogen. Therefore, the binding of the OsO_4 complex with pyridine to PBLG would be weaker than it is for DNA. Figure 4.22 shows a picture and a depiction (not to scale) of the staining setup. It consisted of a small Petri dish (~ 2 inch diameter) in which a filter paper was taped on the bottom and another one at the top. a. About 1 μL of liquid sample (~ 1% silica-polypeptide composite particles in pyridine) was placed on top of a carbon-coated TEM copper grid which was inside

the chamber. Also a small lid containing 1 mL of 1% osmium tetroxide aqueous solution was placed inside. The top filter paper was slightly soaked with ~ 200 µL of the same osmium tetroxide solution. The chamber was closed for 15 or 30 minutes. After that, the TEM grid was taken out of the chamber and allowed to air dry for ~ 20 minutes. The dry, sample-containing TEM grid was then observed in the TEM.

a

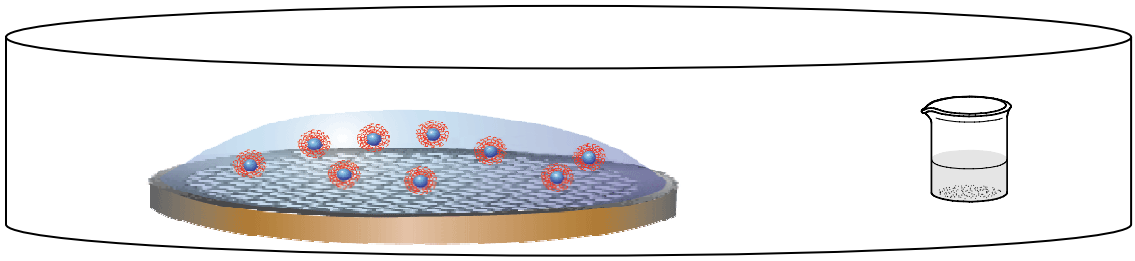

b

Figure 4.22 a): Picture of the staining setup, b): depiction of the staining setup (not drawn to scale).

Figure 4.23 shows TEM images of silica-PBLG composite particle stained with osmium tetroxide vapors after 15 and 30 minutes of exposure to the vapors in the setup described above.

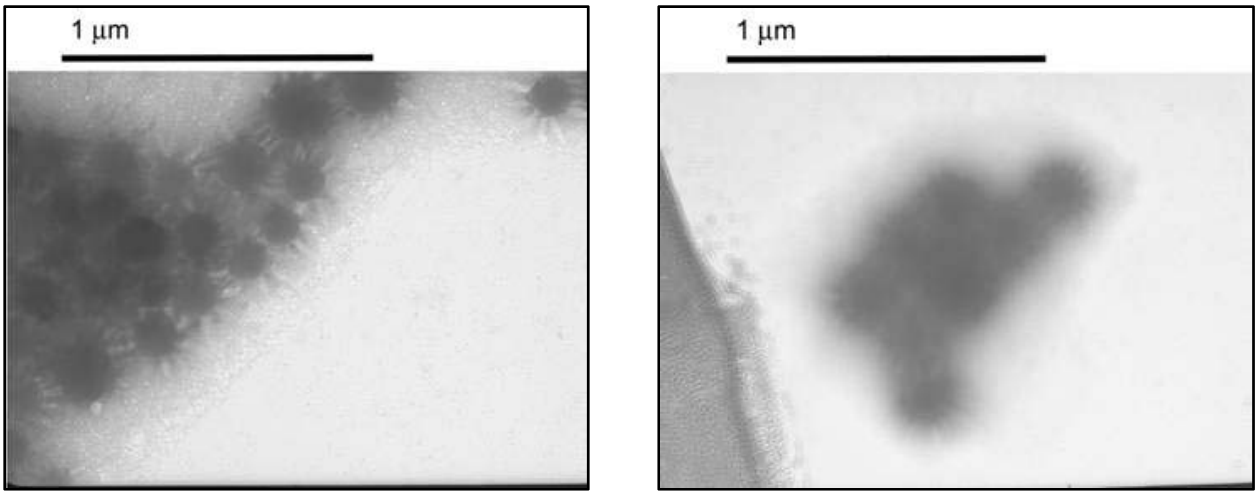

a b

Figure 4.23 TEM images of silica-PBLG composite particles (ES.3.128A) stained with osmium tetroxide vapors. a): 15 minutes of exposure (image 89734), b): 30 minutes of exposure (image 89736).

It appears from the images shown in Figure 4.23 that 15 minutes of exposure is an adequate time since the silica core and the polypeptide shell (light corona around the cores) can be differentiated visually. The image of 30 minutes of exposure does not offer a good contrast between core and shell. In both images the background looks very similar; this indicates that the difference in brightness of the silica-PBLG particles is not an artifact or an issue with time of electron beam exposure or accelerating voltage. This also indicates that the staining process is time dependent and is not instantaneous.

The possibility of an artifact cannot be ruled out exclusively by observing the images of the stained silica-PBLG particles. It is essential to conduct a negative control experiment in which P/F silica cores are treated as the stained silica-PBLG composite particles. It is also

important to rule out an accelerating voltage effect. This is because lower accelerating voltages produce images of less contrast. Also, from Equations 4.1 and 4.2 it is possible to observe that if the accelerating voltage approached infinite, the wavelength of the incident electrons (λ) would approach zero making the scattering factor ($f_e(\theta)$) approach zero. As a result, a very bright image would be observed. On the contrary, if the accelerating voltage approached zero, the wavelength of the incident electrons (λ) would approach infinity making the scattering factor ($f_e(\theta)$) approach infinity. As a result, a very dark image would be observed.

Figure 4.24 shows TEM images of P/F silica cores at different accelerating voltages. It can be observed that the background appears brighter as the accelerating voltage increases. The contrast between the background and the particles' edges appears to be higher in the 80 kV image (3.15.d) but in all images it is visually well-defined. Although the accelerating voltage does not seem to be a factor in the appearance of the particles' size, a more rigorous image analysis is imperative. The software for image analysis ImageJ from the National Institutes of Health was used. Figure 4.25 shows the TEM image of P/F silica cores chosen for image analysis. Two particles were arbitrarily selected for analysis. The yellow line in Figure 4.25 goes approximately through the diameters of the particles. The small grainy dots observed in Figure 4.25 around some of the particles are an artifact that sometimes is observed when the threshold of the image is adjusted inside ImageJ. Threshold adjustment is not always needed for analysis. Figure 4.26 shows the plot profiles of TEM images of P/F silica cores at different accelerating voltages. The variation in size as function of accelerating is not obvious in the images or in the plot profiles. The size of the particles was measured from the plot profiles at about the mid height of the respective gray value. The size results are shown in Table 4.1.

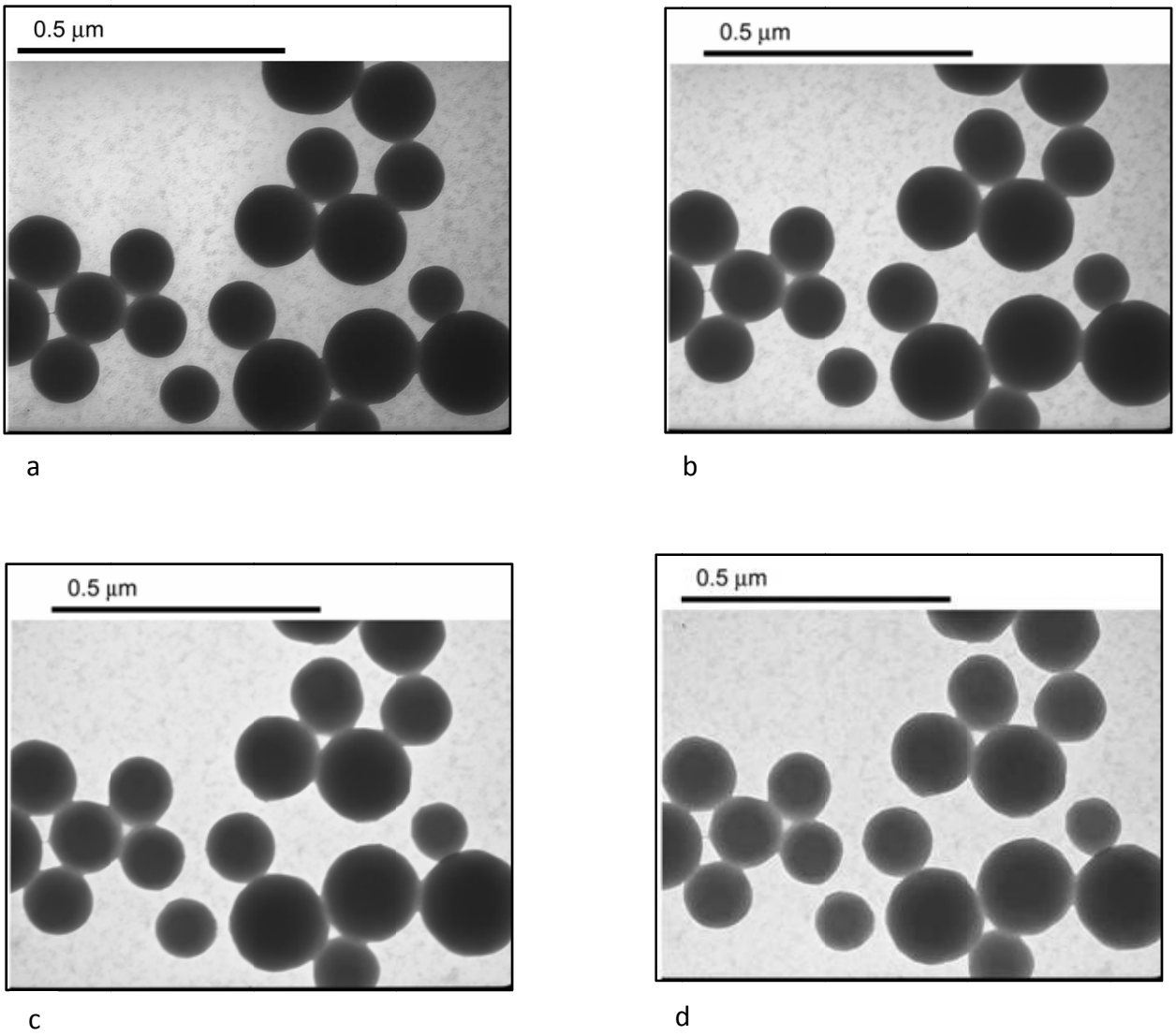

Figure 4.24 TEM images of P/F silica cores (ES.3.111B) at different accelerating voltages. a): 40 kV, b): 60 kV, c): 80 kV, d): 100 kV (images 89385-88).

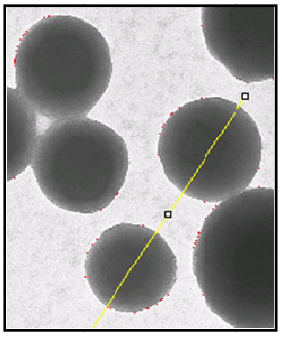

Figure 4.25 TEM image of P/F silica cores (ES.3.111B) chosen for image analysis (from Figure 4.24). The yellow line is the straight line selection over which the plot profile was analyzed.

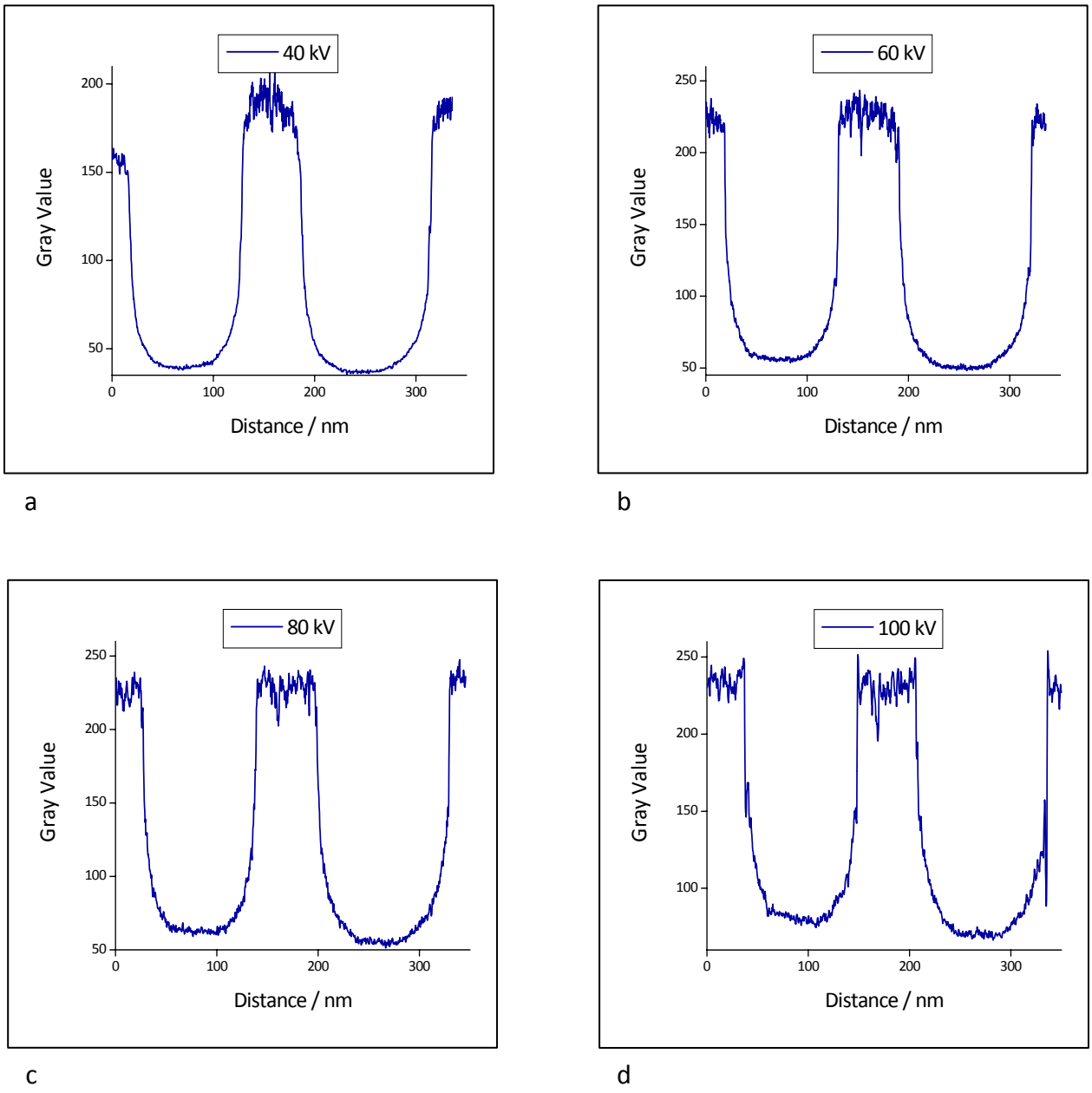

Figure 4.26 Plot profiles of TEM images of P/F silica cores (ES.3.111B) at different accelerating voltages. a): 40 kV, b): 60 kV, c): 80 kV, d): 100 kV.

The average size is 109 nm ± 2 nm (± 1.8%) and 127 nm ± 2 nm (± 1.6%) respectively. The variations in size are small and within the experimental error. Therefore, there is no evidence that the accelerating voltage in the work range (40-100 kV) has an effect on the observed size of P/F silica cores by TEM.

Table 4.1 Size of P/F silica particles measured by TEM at different accelerating voltages

Accelerating voltage / kV	Size / nm	
40	109	126
60	111	129
80	109	128
100	107	125

The same analysis was performed on silica-PBLG composite particles. Figure 4.27 shows TEM images of silica-PBLG composite particles at different accelerating voltages. The silica cores appear to have a corona around which is likely the polypeptide shell. The osmium in OsO_4 has a larger atomic number than silicon. It is possible to argue that the shell should appear lighter than the core. Nonetheless, the amount of scattered and absorbed electrons is also proportional to the thickness of the sample. The electrons that go through the silica core have to go through the polypeptide shell twice.

The images appear lighter, and the contrast between the cores and the shells appears to be higher, as the accelerating voltage increases. The accelerating voltage does not seem to be a factor in the particles' size or in the presence or absence of the shell around the core. The images are visually very similar. Nonetheless, they were also analyzed using ImageJ. Figure 4.28 shows the image of a silica-PBLG composite particle chosen for analysis. One particle was chosen for image analysis because of convenience. A clear diameter can be drawn in the chosen particle that has the background-shell-core-shell-background sequence and goes through the

diameter of the particle. Figure 4.29 shows the plot profiles of TEM images of silica-PBLG composite particles at different accelerating voltages.

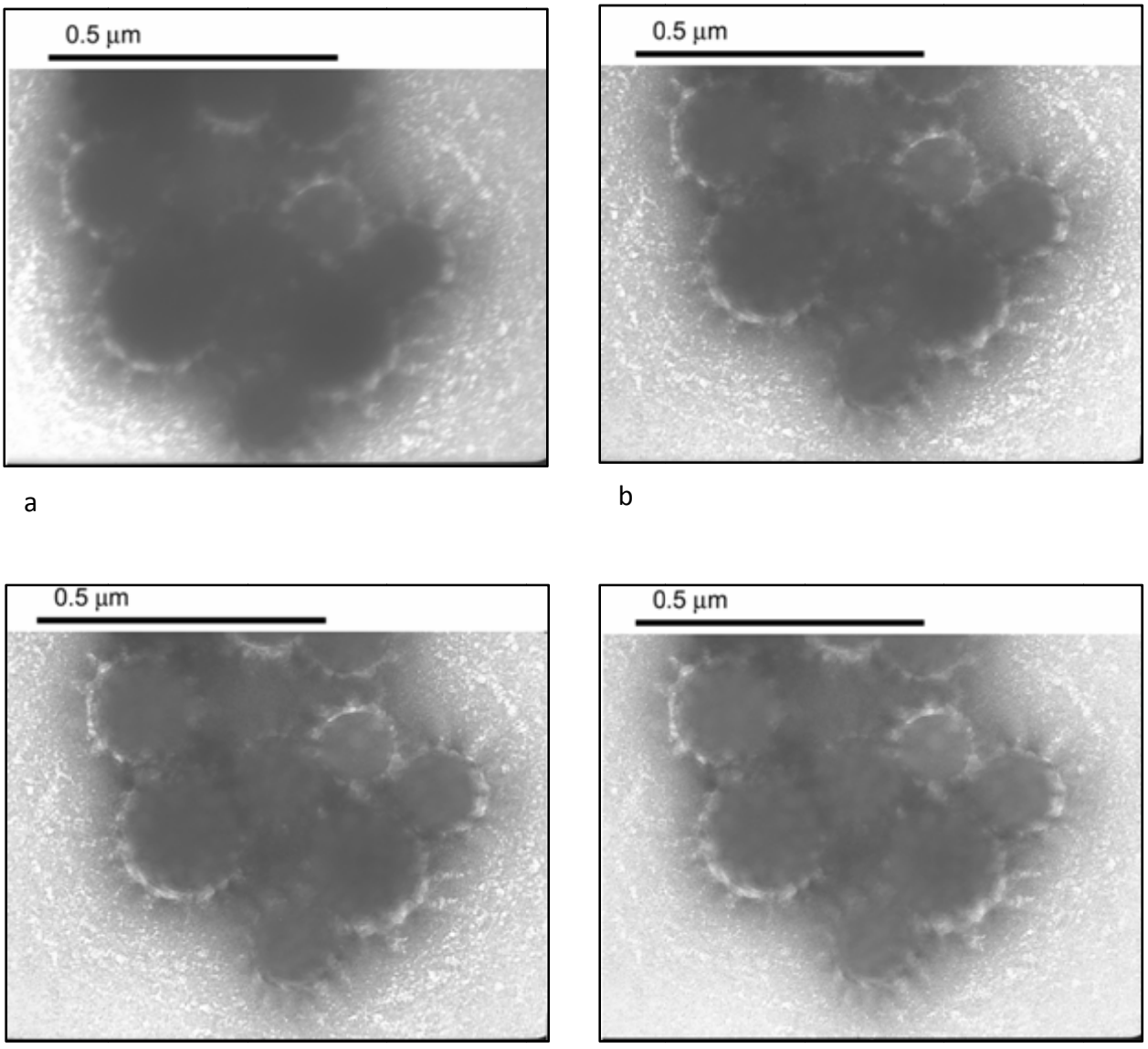

Figure 4.27 TEM images of silica-PBLG composite particles (ES.3.128A) at different accelerating voltages. a): 40 kV, b): 60 kV, c): 80 kV, d): 100 kV (images 89389-92).

Like in the P/F silica cores images, the variations in size are not visually obvious. The accelerating voltage does not appear to have an effect on the observed sizes. The size results are shown in Table 4.2.

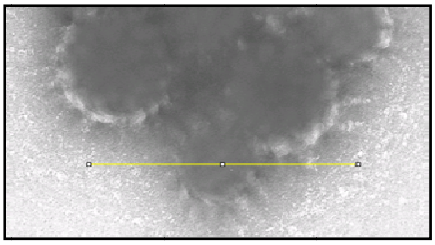

Figure 4.28 TEM images of silica-PBLG composite particle (ES.3.128A) chosen for image analysis (from Figure 4.27). The yellow line is the straight line selection over which the plot profile was analyzed.

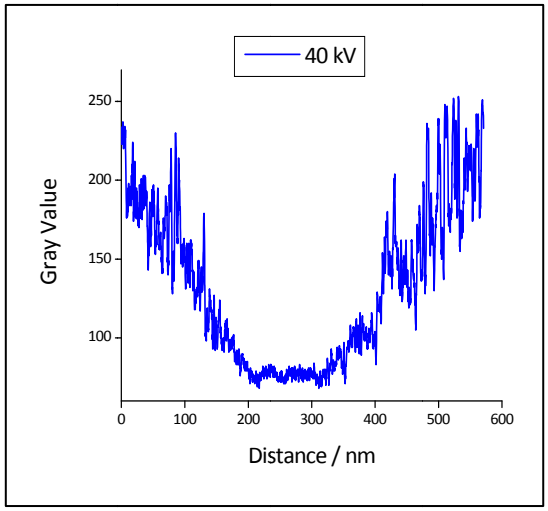

a

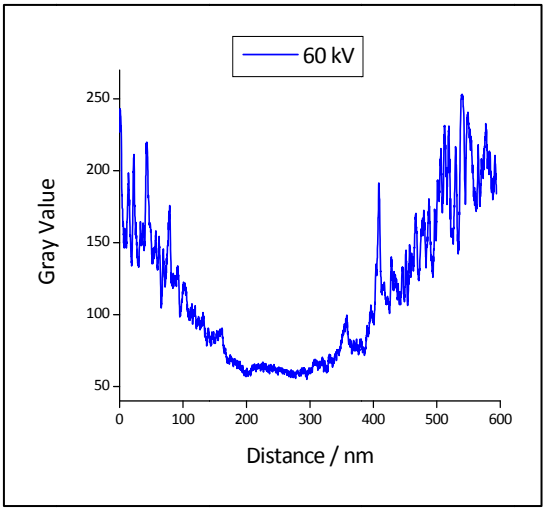

b

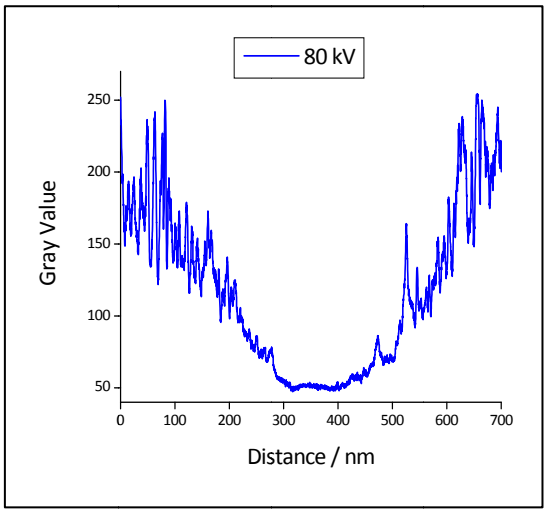

c

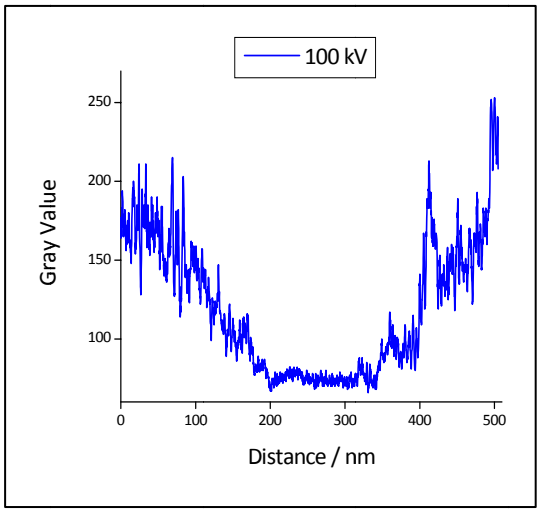

d

Figure 4.29 Plot profiles of TEM images of silica-PBLG (ES.3.128A) at different accelerating voltages. a): 40 kV, b): 60 kV, c): 80 kV, d): 100 kV.

Table 4.2 Size of silica-PBLG composite particles measured by TEM at different accelerating voltages.

Accelerating voltage / kV	Size / nm
40	343
60	366
80	366
100	345

The average size of the analyzed silica-PBLG composite particles is 355 nm ± 12 nm (3.3 %). The variations in size are small and within the experimental error. As in the case of P/F silica cores, there is no evidence that the accelerating voltage in the work range (40-100 kV) has an effect on the observed size of silica-PBLG composite particles by TEM.

The corona around the core in the silica-PBLG composite particles is presumably the PBLG shell. The corona is not observed in the P/F silica cores used also as negative control. The evidence may be compelling; although, it is possible to argue that because of the sample preparation or some contamination in the TEM grid, the corona observed on the silica-PBLG particles may be an artifact. An internal negative control would be useful because it can have all the exact same treatment as the sample of interest to the point of being on the same TEM grid. In 2003, Kobayashi of the Liz-Marzan group reported the synthesis of silica-coated cobalt nanoparticles (Co@silica).[118] The surface chemistry of such particles is the same as of silica. Silica-coated cobalt nanoparticles were prepared and passivated/functionalized in the same fashion as the P/F silica cores. Figure 4.30 show a TEM image of P/F silica-coated cobalt nanoparticles.

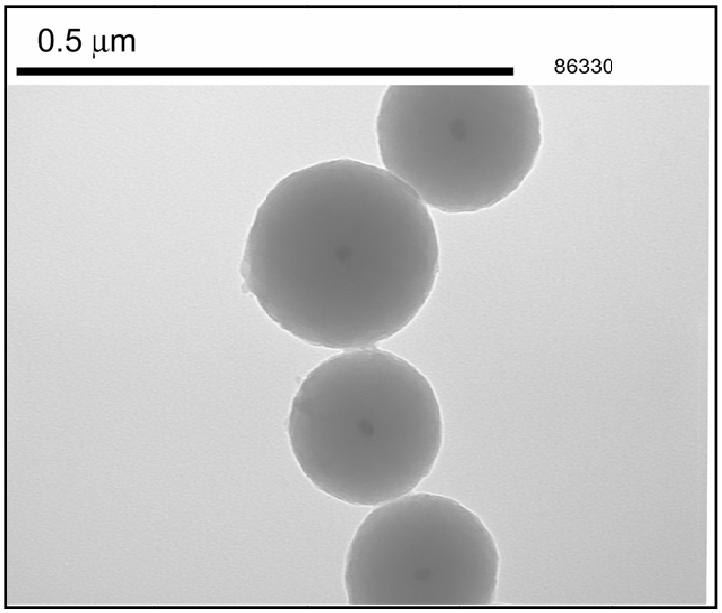

Figure 4.30 TEM image of P/F silica-coated cobalt nanoparticles to be used as internal negative control (image 86330).

The darker core is the cobalt and the lighter shell is the silica. The appearance and size of the P/F silica-coated cobalt nanoparticles resembles the one of P/F silica cores. Figure 4.31 shows images of silica-PBLG composite particles mixed with P/F silica-coated cobalt nanoparticles at different magnifications. It can be observed that the silica-PBLG composite particles present the corona around the silica core. The P/F silica-coated cobalt nanoparticles are distinct because they have a darker, smaller core (cobalt) and they do not have a polypeptide shell. The images of the corona present in the silica-PBLG composite particles and absent in the P/F silica-coated cobalt nanoparticles (internal negative control) make a compelling argument that the corona is in fact the polypeptide shell. Since the polypeptide is likely stained by OsO_4, it appears darker compared to the background. It is probable that the polypeptide aggregates during drying therefore yielding some polypeptide-rich and polypeptide-poor areas. The polypeptide-rich areas appear darker in the images. Individual

polypeptide molecules are not observed in the images. The corona appears considerably smaller in the particles whose interface is in contact with other particles. These interfaces appear darker. This is probably due to polypeptide shrinkage after drying.

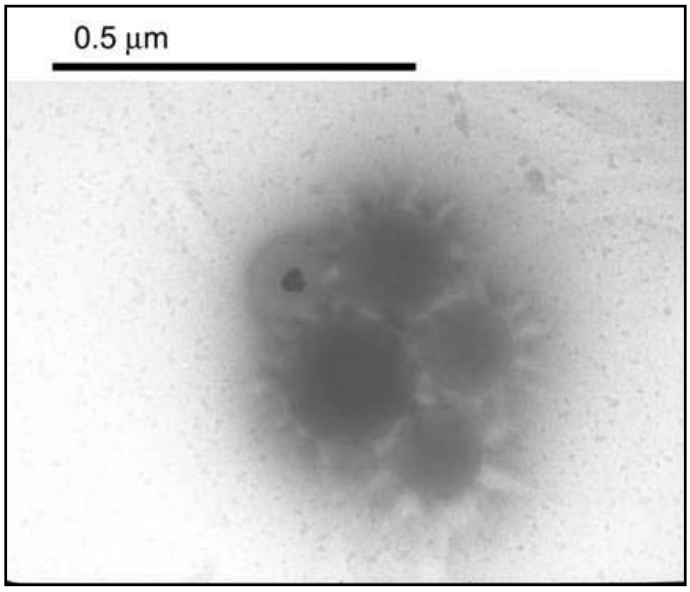

a

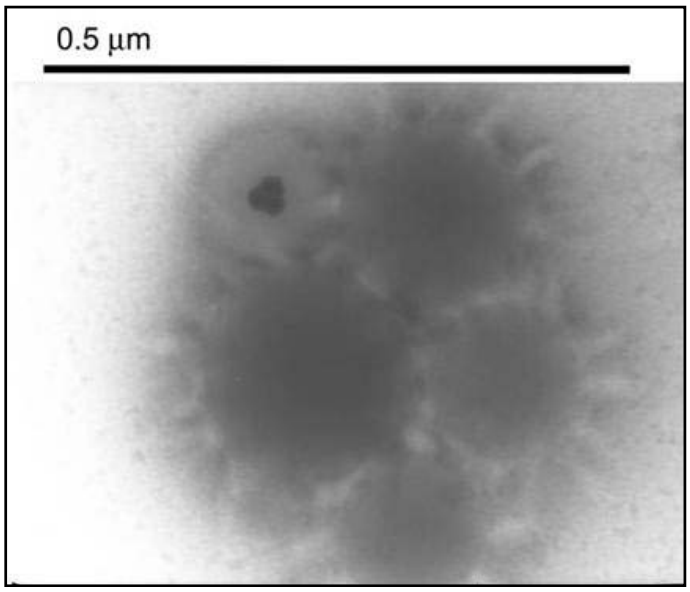

b

Figure 4.31 TEM images of silica-PBLG composite particles (ES.3.128B) with Co@silica particles (ES.3.114A) as internal negative control. a): 100 kX, b): 160 kX (images 89761-62).

Figure 4.32 shows a digitally-colored image of silica-PBLG composite particles mixed with silica-coated cobalt nanoparticles. The corona was colored for visual enhancement.

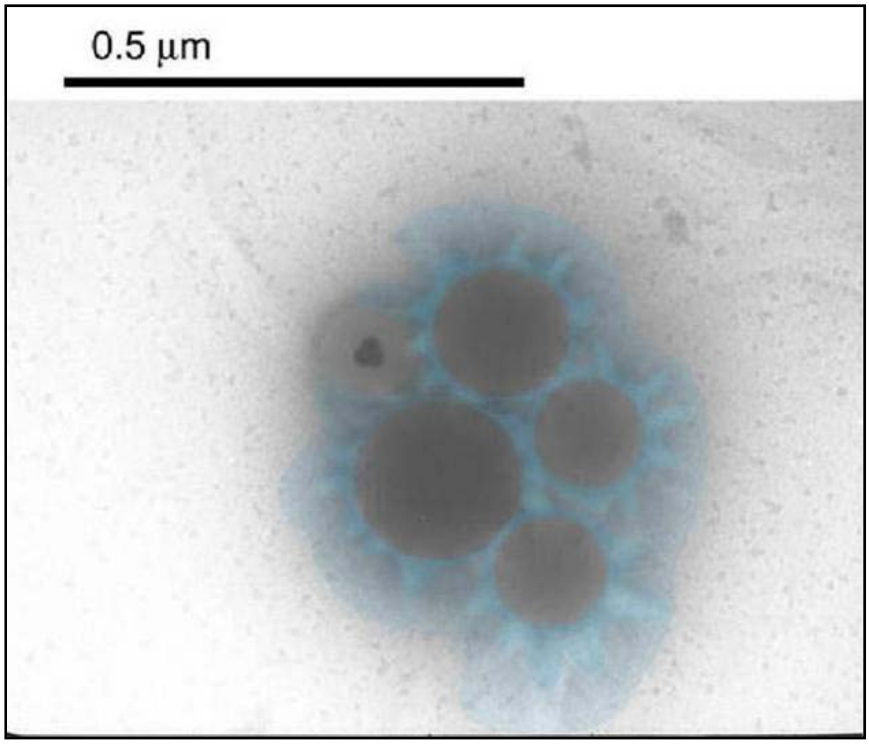

Figure 4.32 TEM image of silica-PBLG composite particles (ES.3.128B) with Co@silica particles (ES.3.114A) as internal negative control. The corona was digitally colored for visual enhancement (image 89761).

The thickness of the polypeptide shell ($R_{core\text{-}shell} - R_{core}$) obtained by DLS and TEM is comparable. Around 100 particles were measured by TEM. The results are shown in Table 4.3.

Table 4.3 Comparison of the core hydrodynamic radius and shell thickness of silica-PBLG composite particles measured by dynamic light scattering and TEM.

Dynamic light scattering		Transmission electron microscopy	
R_{core} / nm	$R_{core\text{-}shell} - R_{shell}$ / nm	R_{core} / nm	$R_{core\text{-}shell} - R_{shell}$ / nm
103 ± 1	86 ± 4	81 ± 8	75 ± 14

The radius of the core is about 20% larger by DLS. This is probably due to the weight that DLS gives to larger particles. Nevertheless, the radius of the composite particles by DLS is 189 nm ± 3 nm and by TEM is 156 nm ± 22 nm. Hence, the lower limit by DLS is 186 nm and the higher limit by TEM is 178 nm. Because the size of the polypeptide shell obtained by DLS and TEM is statistically similar, it is possible that the length of the polypeptide in solution and, dried after staining, is the same. The staining procedure may fix the polypeptide while in solution and remains unchanged after drying.

4.2.3 pH Behavior of PLGA-SiPCPs

Silica-PLGA composite particles were prepared by the debenzylation of the PBLG shell in silica-PBLG composite particles. Hydrogen bromide can quantitatively remove the benzyl groups in PBLG. [195;196] The removal of benzyl groups was confirmed by ^{1}H-NMR (nuclear magnetic resonance of proton) in D_2O. Aromatic proton signals (~ 7.2 ppm) were observed in silica-PBLG composite particles but no aromatic signals were observed in silica-PLGA composite particles. Because PLGA is neutral at low pH and negatively charged at high pH when deprotonated, it is expected to have a similar behavior when tethered to colloidal silica. When PLGA is grafted on a flat silicon surface it is in a compact α-helical conformation at low pH and in an extended random-coil conformation at high pH.[171] A similar conformational and charge behavior is expected for PLGA grafted on colloidal silica. Figure 4.32 shows the combined graph of hydrodynamic radius and zeta potential as function of pH for silica-PLGA composite particles. At high pH the particles are negatively charged and almost uncharged at low pH. This is indicated by a zeta potential of about -30 mV and about 0 mV respectively. In Figure 4.33 the zeta potential is slightly negative at the last point (pH = 4.84) after being neutral at the second to last point (pH = 5.81). This may be due to the damage that the electrode suffers after several

measurements. At high pH the hydrodynamic radius of the particles is around 135 nm and around 85 nm at low pH. The combination of hydrodynamic radii and zeta potential results suggests that the tethered PLGA is charged and extended at high pH. Likewise, these results suggest that the tethered PLGA is uncharged and compact at low pH.

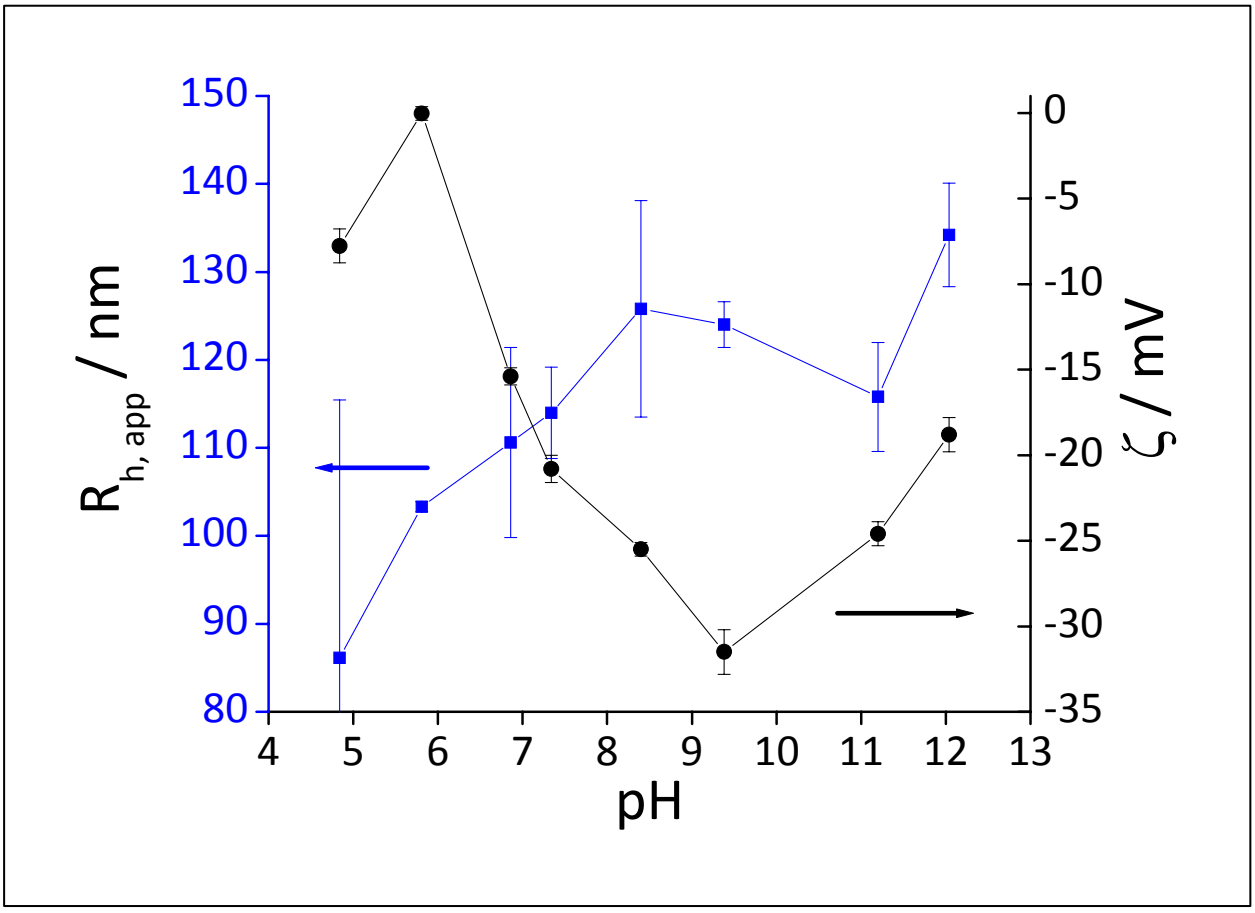

Figure 4.33 Combined graph of hydrodynamic radius (■) on left axis and zeta potential (●) on right axis *vs* pH for silica-PLGA composite particles (ES.4.59A). [NaCl] ~ 0.1. Hydrodynamic radii data obtained from Malvern Zetasizer instrument.

The P/F silica cores do not exhibit a change in size as a function of pH. They are positively charged at low pH and neutral at high pH. Therefore, the changes in hydrodynamic radius of the silica-PLGA composite particles can be attributed to the changes in the PLGA shell. At low pH, amino groups that did not initiate the polymerization of BLG-NCA (monomer) may

contribute to the overall charge of the silica-PLGA composite particles. Consequently they can neutralize some of the negative charge on PLGA. Figure 4.34 shows a similar graph as 4.33 for silica-PLGA composite particles of smaller hydrodynamic radius.

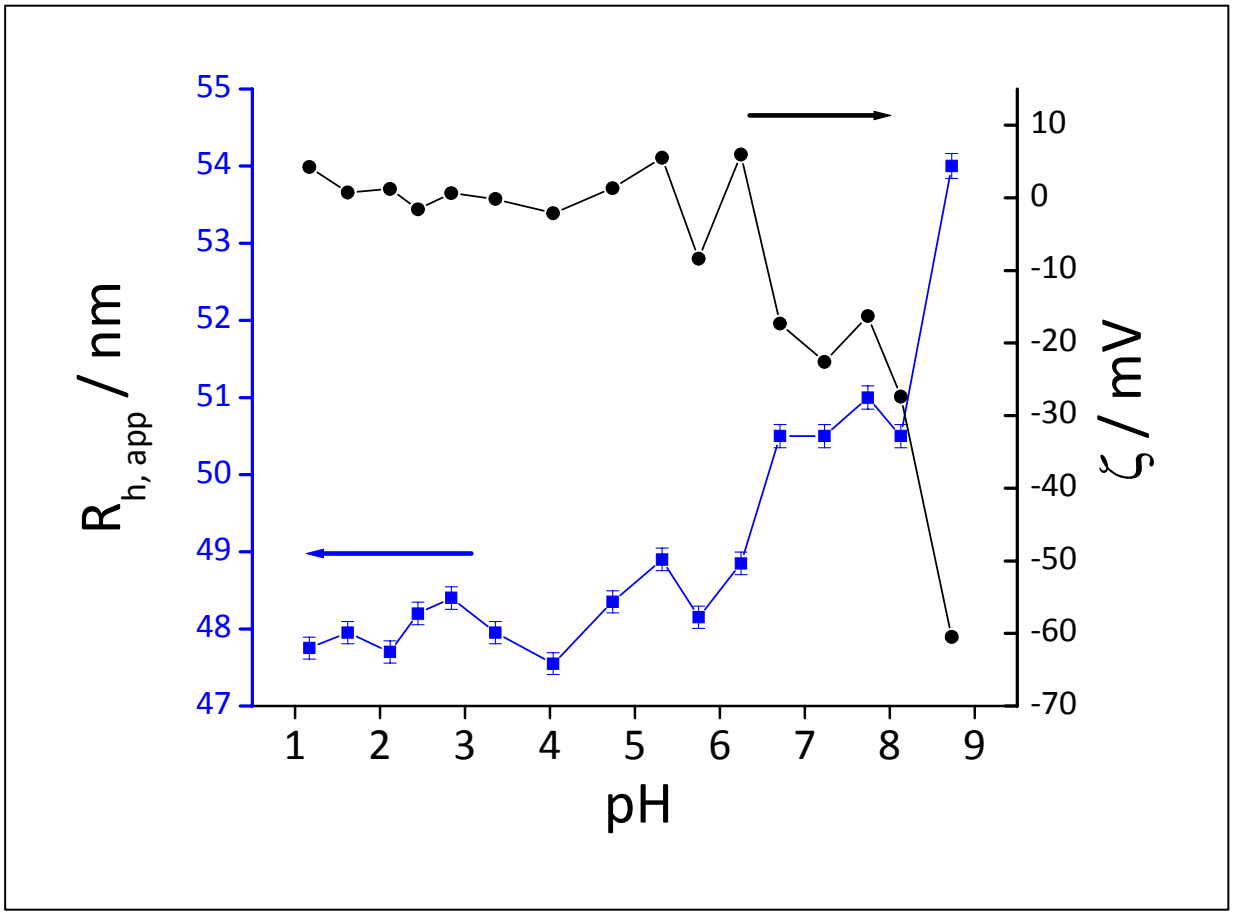

Figure 4.34 Combined graph of hydrodynamic radius (■) on left axis and zeta potential (●) on right axis *vs* pH for silica-PLGA composite particles (ES.3.105B). [NaCl] ~ 0.1. Hydrodynamic radii data obtained from Malvern Zetasizer instrument.

In spite of having a lower PLGA content, the zeta potential of the smaller silica-PLGA composite particles is larger in magnitude. The unreacted (and negatively charged at high pH) silanol groups on the silica surface may be contributing to the double layer charge. In both examples the silica-PLGA composite particles have a larger hydrodynamic radius and are more negatively charged at high pH. They exhibit a smaller hydrodynamic radius and are almost

uncharged at low pH. A transition occurs between pH = 5-8. The pK_a of the side chain of glutamic acid is 4.3.[104] Wang and Chang observed a conformation transition of PLGA grafted on a flat silica substrate at pH 5.75-7.[171]

The measurements were done in dilute dispersions at ~ 0.1 M ionic strength and went from high pH to low pH. The final concentration of silica-PLGA particles was about 0.3 to 0.5 of the initial concentration. As the titrant HCl was added the total volume of dispersion increased throughout the titration. Hence concentration effects on the DLS measurements may be neglected.

4.2.4 NMR Study of PCBL-SiPCPs

PCBL exhibits a temperature-induced coil→helix transition in *m*-cresol at around 27 °C.[199-203] Turksen studied the change in hydrodynamic radius of Co@silica-PCBL composite particles in *m*-cresol as a function of temperature. The hydrodynamic radius suffers a transition at around 27 °C. This is probably due to the coil→helix transition of the PCBL shell.[1] Figure 4.35 shows a graph of hydrodynamic radius of Co@silica-PCBL composite particles *vs* temperature in *m*-cresol.

In order to investigate if the changes in hydrodynamic radius are due to a coil→helix transition of the PCBL shell, it is necessary to use a method that yields more direct information about the polypeptide itself. Circular dichroism cannot be used because *m*-cresol has a large molar absorptivity in the UV range. *m*-cresol also absorbs strongly in the 1200-1650 cm^{-1} wavenumber; therefore, infrared spectroscopy (IR) may not discern the change in amide peaks of PCBL. Optical rotatory dispersion (ORD) has been successfully used to explore the coil→helix transition of untethered PCBL.[202] In order to obtain information about the coil→helix transition from ORD, the data is taken in the 300 to 600 nm range. Scattering may be a problem because

of the hydrodynamic radius of the particles. Nuclear magnetic resonance (NMR) has been used to study coil→helix transitions several polymers and biopolymers.[225-229] NMR does not have the drawbacks of the other methods. Nevertheless, NMR does not work with magnetic samples; it also presents other experimental challenges and data analysis when the analyte is a large polymer. Since the magnetic core of Co@silica-PCBL composite particles cannot be removed without altering the integrity of the particles, similar particles without the magnetic core are required for NMR studies.

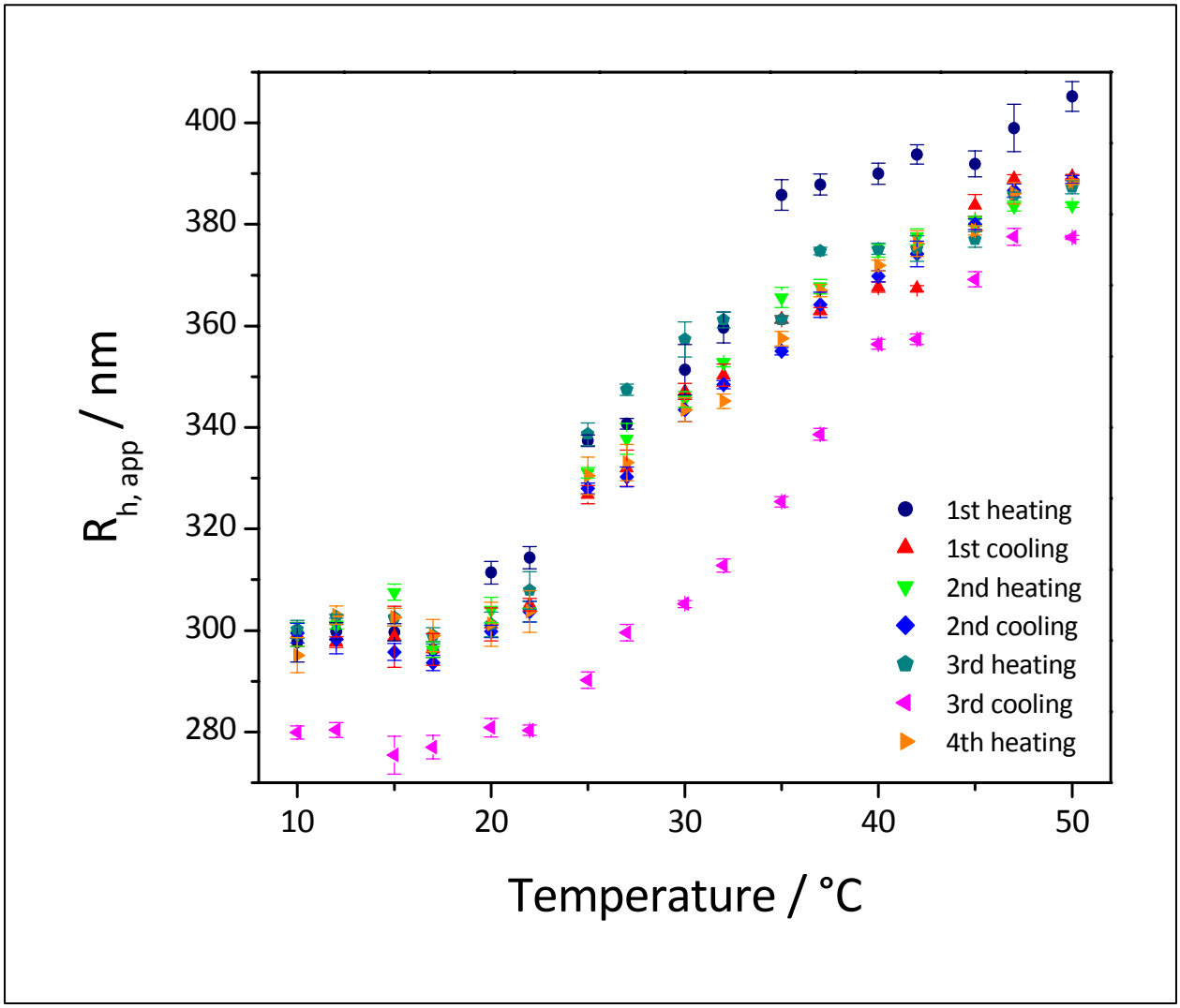

Figure 4.35 Graph of hydrodynamic radius of Co@silica-PCBL composite particles *vs* temperature in *m*-cresol. (Copied with permission from reference 1)

In order to simplify the study PCBL on of silica-PCBL composite particles, untethered PCBL was studied first. PCBL of a low polydispersity (1.083) and molecular weight 202,000 g/mol was synthesized. The estimated length of the PCBL (considering an α-helical conformation – see equation A2) is around 120 nm which is in the range of the estimated length of the PCBL in silica-PCBL composite particles. Figure 4.36 shows the gel permeation chromatography (GPC) trace of the synthesized PCBL.

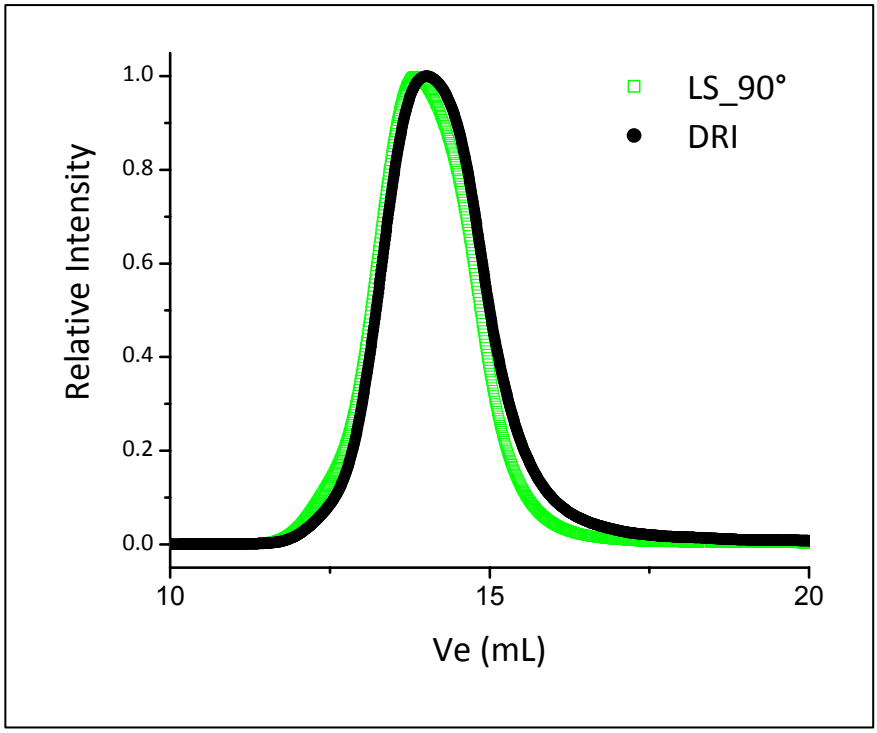

Figure 4.36 GPC trace of PCBL for conformational studies (ES.4.33A). Mobile phase 0.1 M LiBr in DMF. Differential refractive index (DRI) signal (□) and light scattering at θ = 90° (LS_90°) (●) signal.

Figure 4.37 shows the conformation plot (log(R_g) *vs* log(molar mass)) of the synthesized PCBL. This conformation plot does not provide information about the conformation of the polypeptide *per se*. In other words it is not possible to determine the α-helix or random coil content of the polypeptide from the conformation plot. From the slope of the conformation

plot it is possible to determine if the polypeptide is in an extended rod conformation (slope = 1) or in a compact coil conformation (slope = 0.5 or 0.6 depending on solvent quality).

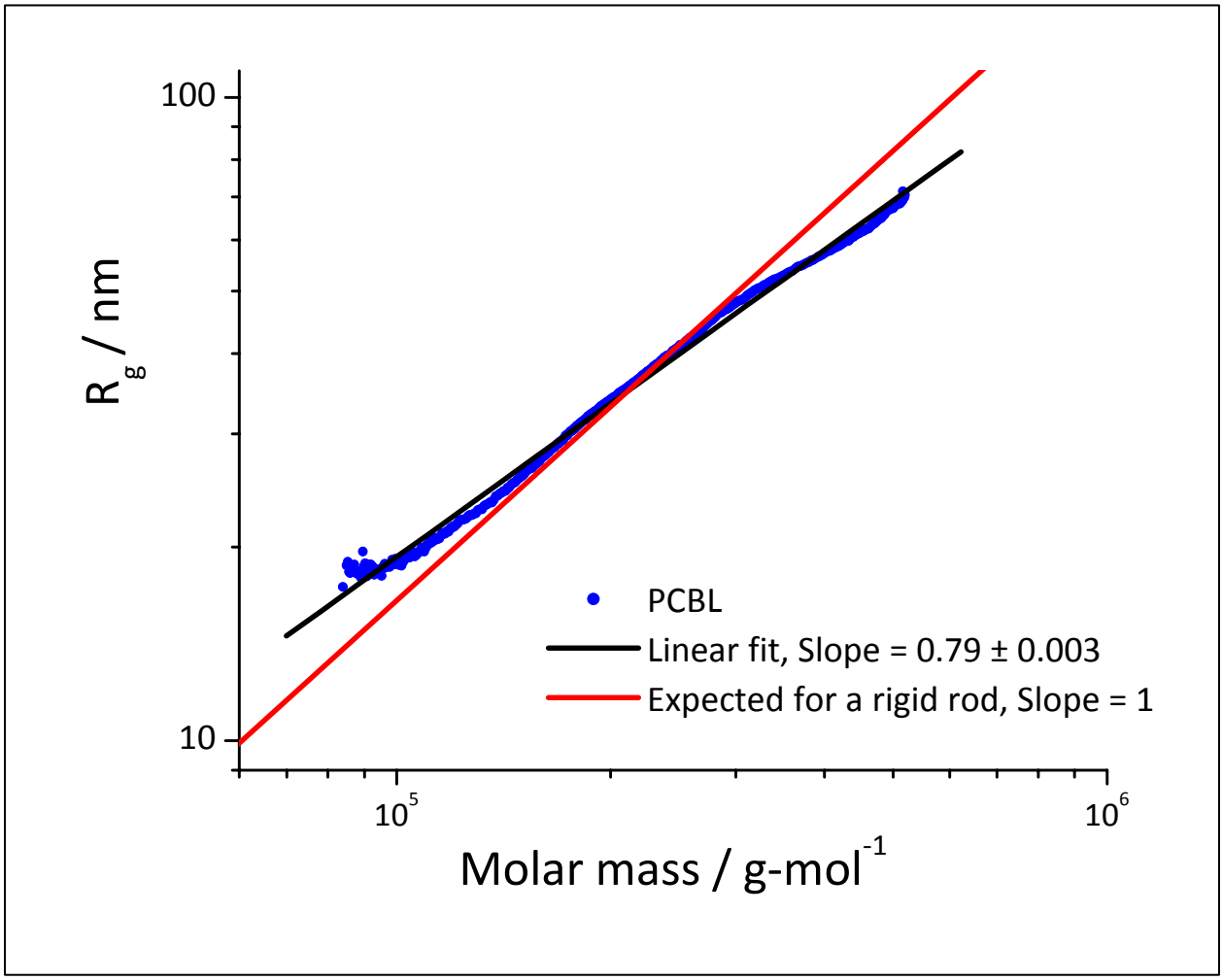

Figure 4.37 Conformation plot (log(R_g) *vs* log(molar mass)) of PCBL for conformational studies (ES.4.33A). Mobile phase 0.1 M LiBr in DMF.

The slope of the conformation plot is about 0.8; it indicates that the PCBL in 0.1 M LiBr in DMF is in an extended conformation. The slope for a rigid rod would be expected to be 1. The value of 0.8 may indicate some branching or some bending.

NMR spectra of PCBL in *m*-cresol-d_8 were recorded at different temperatures below and above the reported coil→helix transition temperature. ppm. Figure 4.38 shows the full NMR

spectra of PCBL at temperatures below and above the reported transition temperature (15 °C and 50 °C respectively). The assignment of the chemical shifts of large molecules is not trivial. The proposed assignments shown in Figure 4.38 are based on the prediction of ^{1}H-NMR spectra from ChemDraw® Ultra and literature reports of PCBL and other polypeptides under similar conditions.[225;227;230;231] The largest changes are in the amide, α and ε protons.

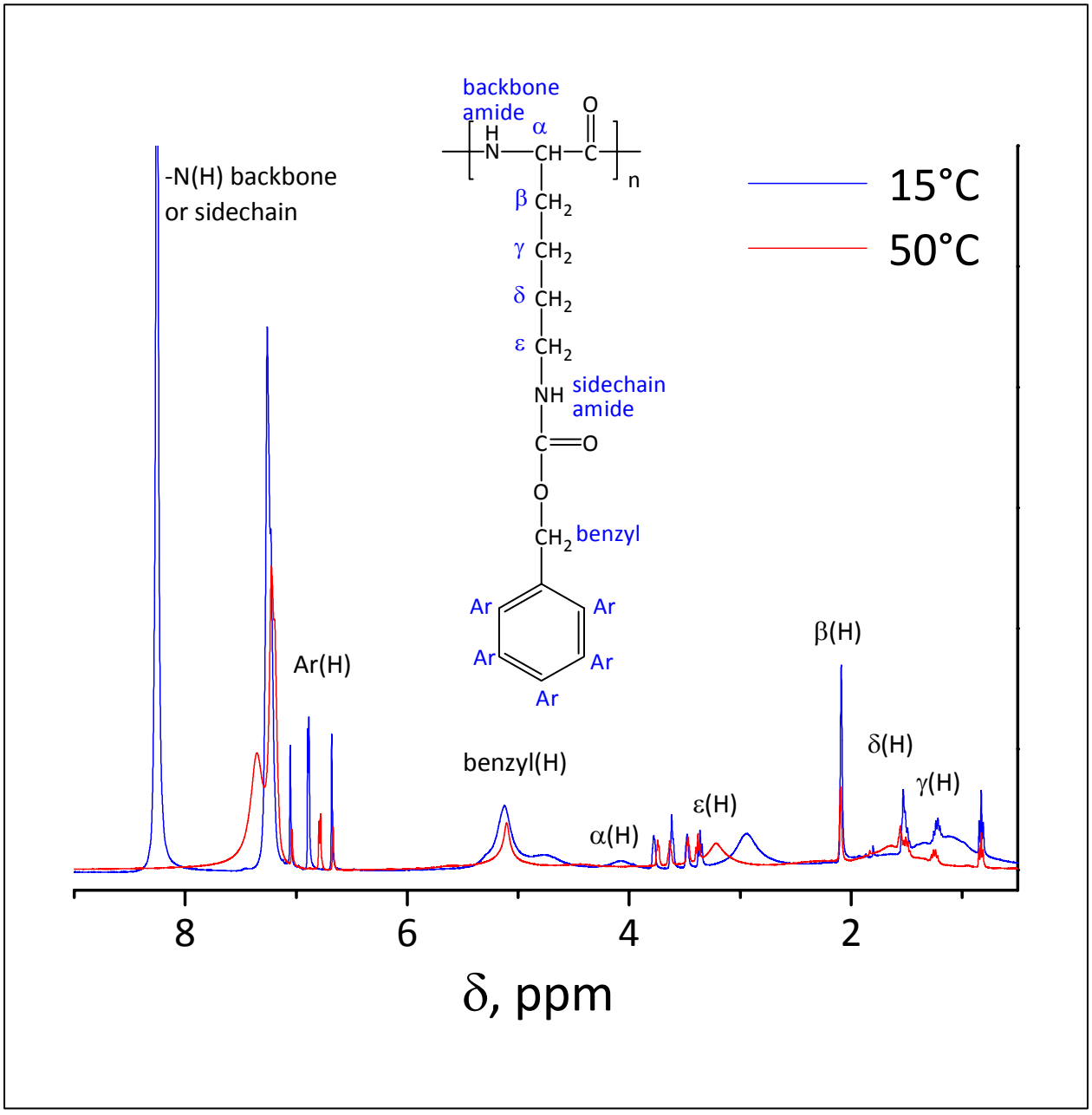

Figure 4.38 NMR spectra of PCBL at temperatures below and above the reported transition temperature (15 °C and 50 °C respectively).

Figure 4.39 a shows a rescaling of Figure 4.38 focusing on the α and ε protons. 4.39 b shows a plot of the chemical shift, δ, of the ε protons atoms at different temperatures.

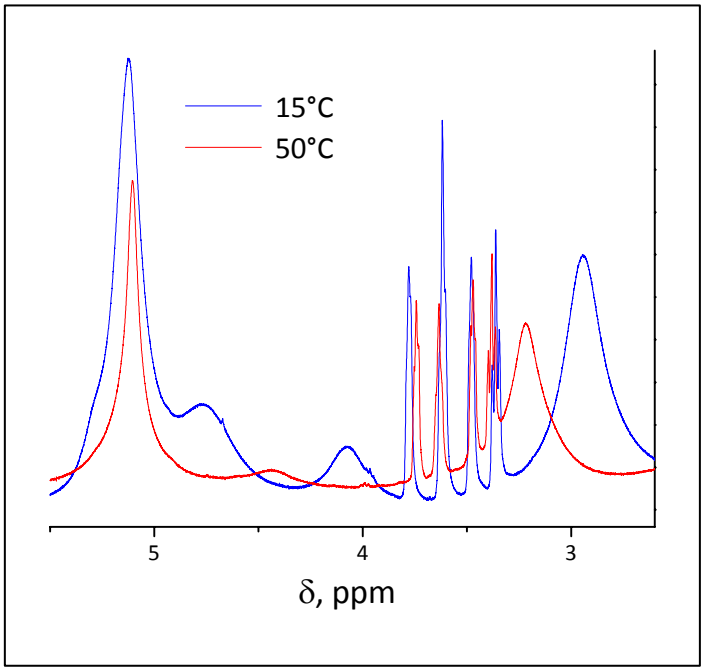

a

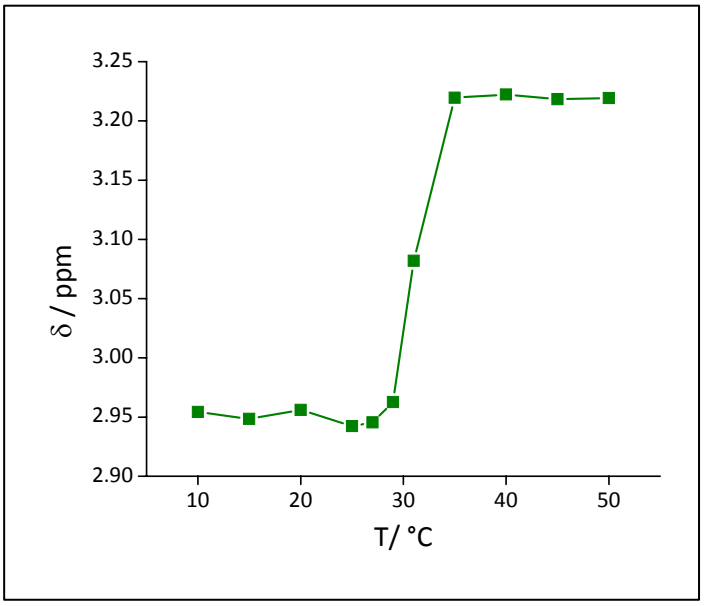

b

Figure 4.39 a): ^{1}H-NMR spectra of PCBL in *m*-cresol-d_8 at 15 (—) and 50 °C (—) (rescaling of Figure 4.38 focusing on the α and ε protons), b): graph of chemical shift, δ, *vs* temperature for the ε-CH_2 of PCBL.

The change in chemical shift of the ε hydrogen atoms is probably due to the temperature-induced coil→helix transition. From Figure 4.39 b can be observed that a sharp change occurs at around 30 °C which is close to the reported transition temperature of 27 °C.

The observed transition in the chemical shifts of the ε protons probably associated to the coil→helix transition of PCBL suggests the possibility of detecting that transition on silica-PCBL composite particles. Figure 4.40 shows the dynamic light scattering results ($R_{h,app}$ *vs* q^2) for the silica cores ($R_{h,app}$= 104 nm ± 1 nm) and for the silica-PCBL composite particles ($R_{h,app}$= 244 nm ± 3 nm). The difference in hydrodynamic radii between the silica cores and the silica-PCBL composite particles is the shell thickness (140 nm ± 4 nm). The apparent hydrodynamic radii are independent of scattering angle, *i.e.* the curve of $R_{h,app}$ *vs* q^2 is almost flat.

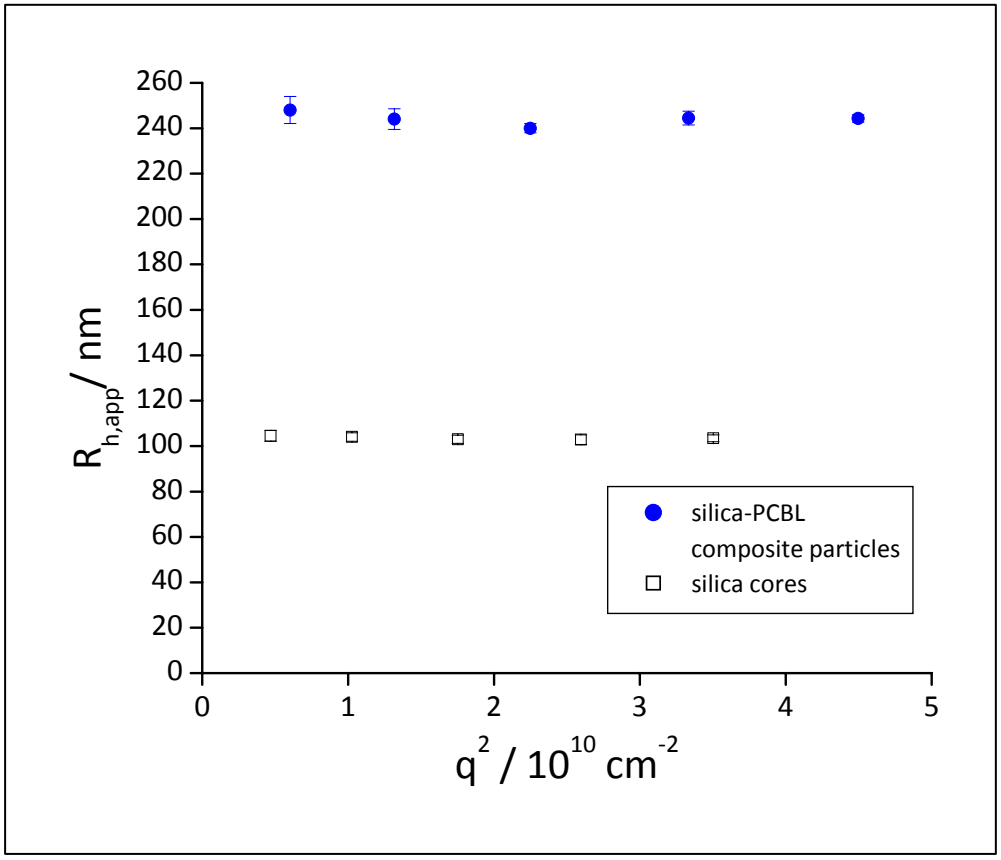

Figure 4.40 Graphs of $R_{h,\ app}$ vs q^2. a): silica cores (ES.4.47A), b): silica-PCBL composite particles (ES.4.53A in *m*-cresol at 20 °C).

The Co@silica cores synthesized by Turksen had an estimated surface density of amino groups of around 0.7 $-NH_2$ groups / nm^2. In order to allow the PCBL molecules to have a better spacing, the synthesized silica cores for the present study had a smaller surface density of amino groups. The estimated surface density was 0.3 $-NH_2$ groups / nm^2. Figure 4.41 shows the TGA curves of the silica cores and the silica-PCBL composite particles.

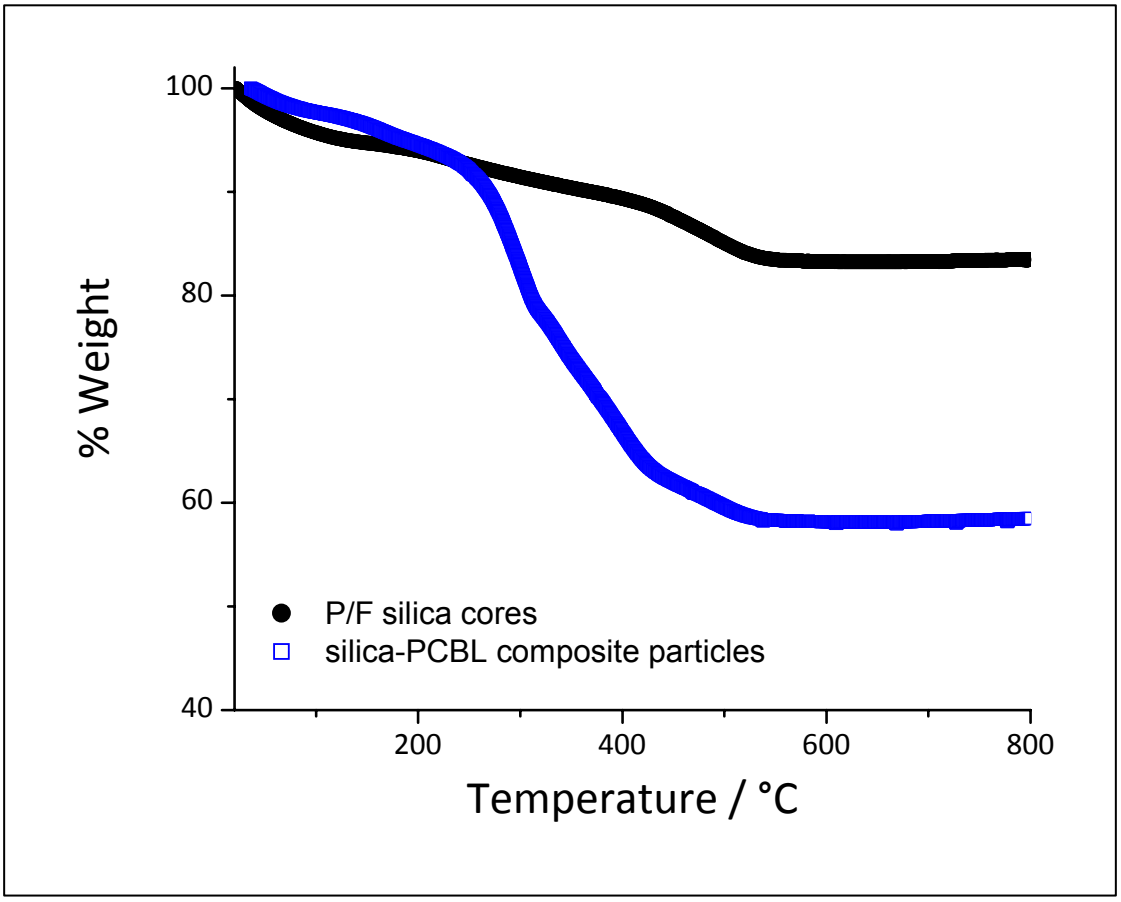

Figure 4.41 TGA curves of silica cores (ES.4.47A)(●) and silica-PCBL composite particles (ES.4.53A)(□).

The silica-PCBL composite particles were also observed by TEM using the OsO_4 staining technique (detailed in Chapter 4.2.2). Figure 4.41 shows TEM images of the silica cores and the silica-PCBL composite particles. The stained polypeptide shell can be observed around the silica cores in Figure 4.42 b.

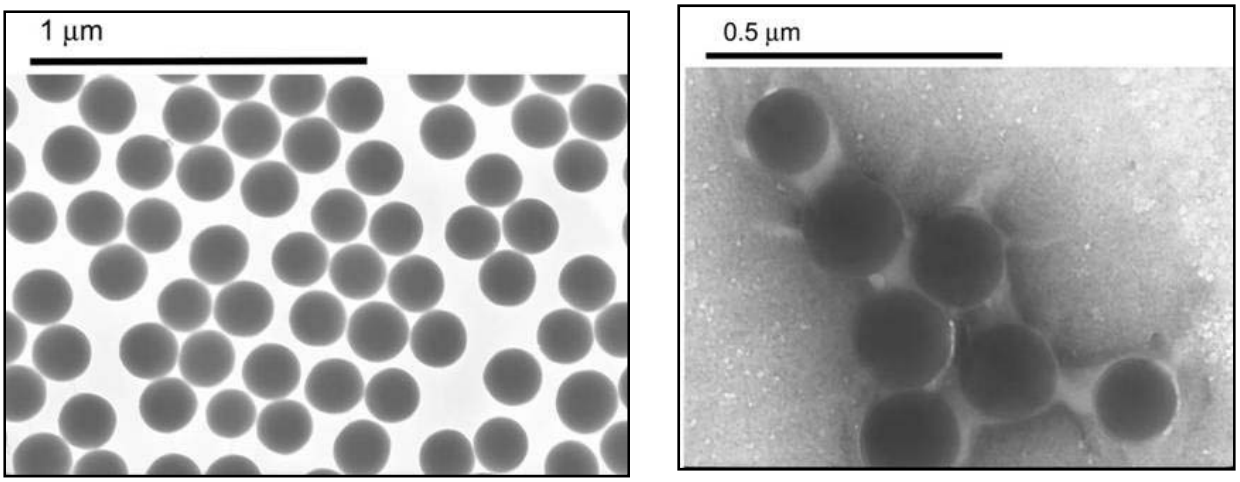

a b

Figure 4.42 TEM images. a): silica cores (ES.4.47A), b): silica-PCBL composite particles (ES.4.53A in pyridine).

^{1}H NMR spectra of the silica-PCBL composite particles were recorded at different temperatures below and above the reported transition temperature of untethered PCBL. Figure 4.43 shows the ^{1}H-NMR spectra of silica-PCBL composite particles in *m*-cresol-d_8 at 15 °C and 40 °C. Several chemical shifts change from 15 to 40 °C. NMR was also collected in the 40 °C to 15 °C direction. The final spectrum at 15 °C was identical as the starting at 15 °C. The assignment of the chemical shifts is more even complex when the polypeptide is attached to a relatively large colloidal particle. More sophisticated NMR techniques are needed for a proper assignment of the chemical shifts. The signal attributed to the ε proton that appeared at around 3 ppm on the ^{1}H-NMR spectra of untethered PCBL is not observed in the ^{1}H-NMR spectra of silica-PCBL. The signal assigned to the α proton at around 4 ppm does not appear to change. The signal at around 8 ppm believed to correspond to the amide protons is relatively more intense than the amide proton signals from untethered PCBL. Figure 4.44 shows a graph of chemical shift, δ, *vs* temperature for the amide proton of silica-PCBL composite particle in *m*-cresol-d_8.

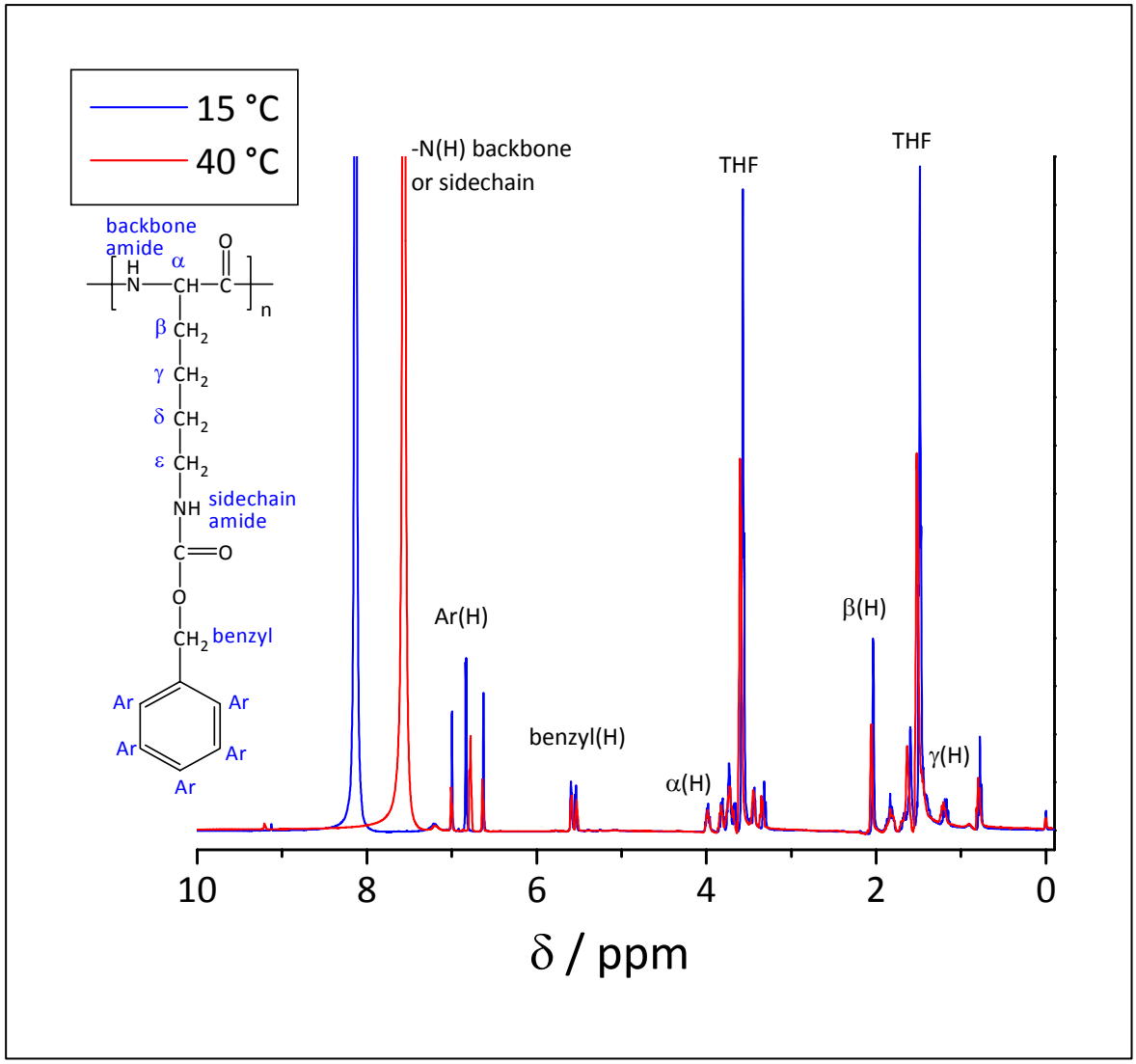

Figure 4.43 ^{1}H-NMR spectra of silica-PCBL in *m*-cresol-d_8 at 15 (—) and 40 °C (—).

Unlike the chemical shift of the ε-CH_2 hydrogen atoms in untethered PCBL, a clear transition cannot be observed. It is possible to observe small changes around the transition temperature. In order to enhance the changes of chemical shift with temperature, the approximate derivative $\Delta\delta / \Delta T = (\delta_{final} - \delta_{initial}) / (T_{final} - T_{initial})$ was computed for each step. Figure 4.45 shows graphs of the approximate derivative $\Delta\delta / \Delta T$, *vs* temperature for the amide protons of silica-PCBL composite particles in *m*-cresol-d_8.

A change in the approximate derivative $\Delta\delta$ / ΔT for the amide protons of PCBL on silica-PCBL composite particles can be observed at 25 °C in the heating direction and at 28 °C in the cooling direction. These values are close to the reported coil→helix transition of PCBL. Although this sole evidence is not conclusive of a coil→helix transition, it suggests it.

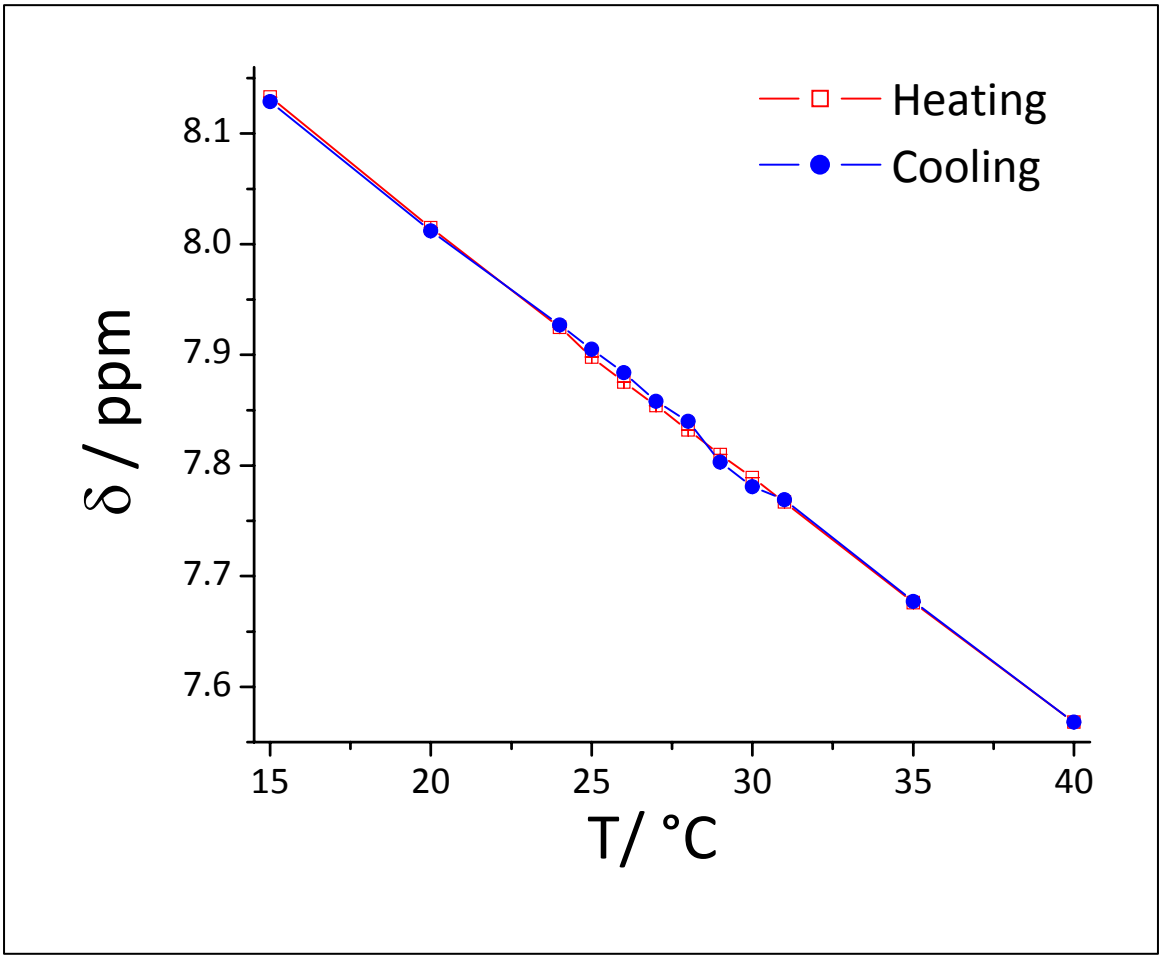

Figure 4.44 Graph of chemical shift, δ, *vs* temperature for the amide of silica-PCBL composite particle in *m*-cresol-d_8.

The silica-PCBL composite particles were studied by DLS in order to observe if they behave as the Co@silica-PCBL composite particles synthesized by Turksen. The viscosity values were obtained from the literature.[232] Table 4.4 shows the hydrodynamic radius at temperatures below and above the reported transition temperature of PCBL.

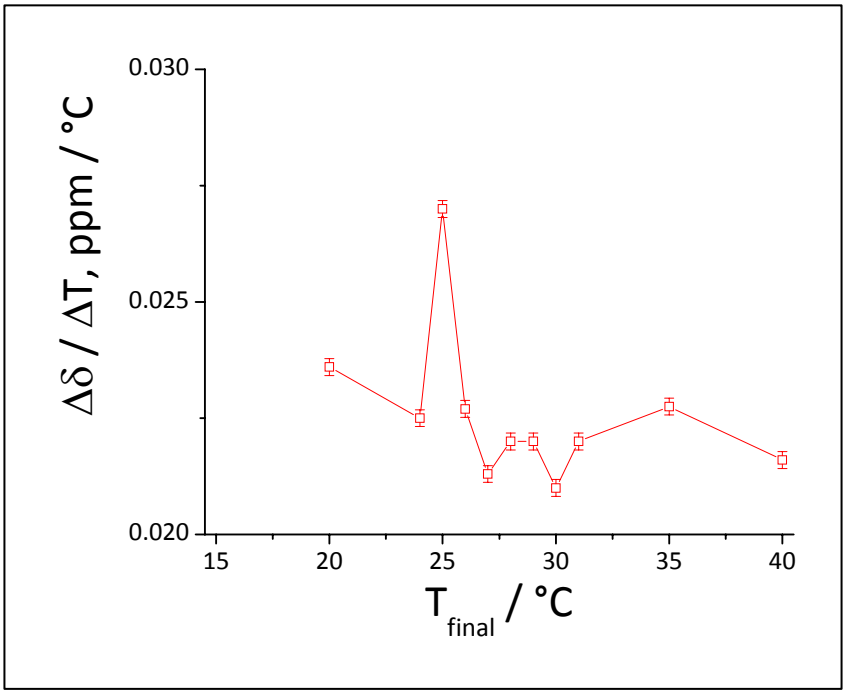

a

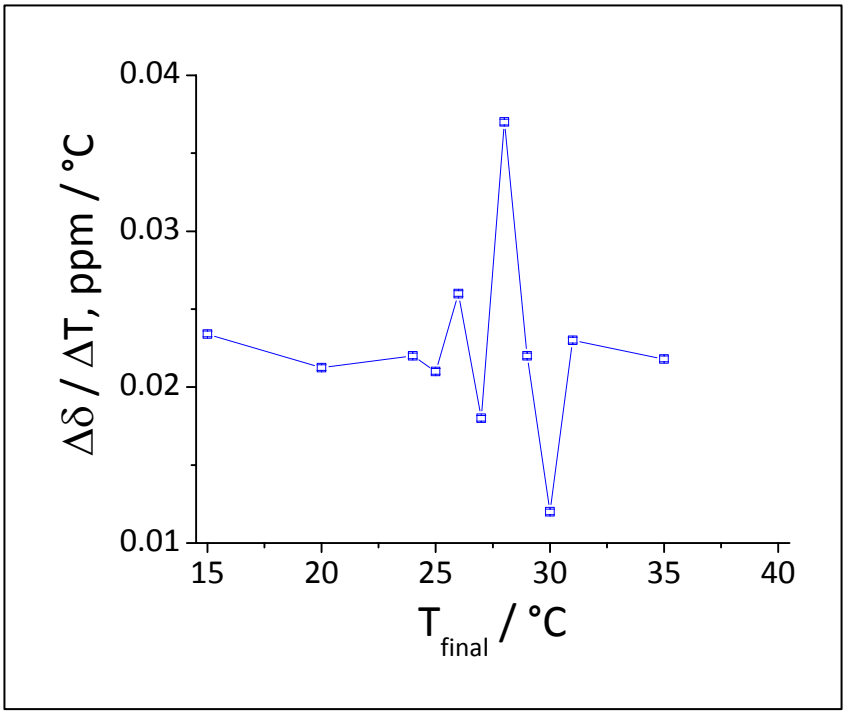

b

Figure 4.45 Graphs of the approximate derivative $\Delta\delta$ / ΔT *vs* temperature for the amide protons of silica-PCBL composite particles in *m*-cresol-d_8 (with data from Figure 4.44). a): heating direction, b): cooling direction.

Table 4.4 Comparison of the hydrodynamic radius and shell thickness of silica-PCBL composite particles of low initiator surface density (ES.4.53A) at 15 °C and 40 °C in *m*-cresol measured by dynamic light scattering.

T / °C	$R_{h\ silica\text{-}PCBL}$ / nm	$R_{h\ silica\text{-}PCBL} - R_{h\ silica}$ / nm
15	219 ± 9	116 ± 11
40	224 ± 2	121 ± 4

The hydrodynamic radius is statistically the same at both temperatures. Despite that the NMR results suggest a transition at 25-28 °C, the hydrodynamic behavior of the particles is statistically the same at temperatures below and above that range. The P/F silica cores had an estimated lower surface density of amino groups compared to the P/F Co@silica cores used by Turksen. This was done in an attempt to give more freedom to the PCBL chains grown from the silica surface. It is possible that the lower surface density of amino groups yielded a lower surface density of PCBL. A lower surface density of polypeptide chains can make them less susceptible to changes in the shell, like a conformation transition. The polypeptide has also more freedom to collapse and get adsorbed onto the silica surface.

A new batch of silica cores of about the same hydrodynamic radius was synthesized. The functionalization was done so that the surface density of amino groups would be similar to the Co@silica cores synthesized by Turksen (~ 0.7 $-NH_2$ groups / nm^2). Silica-PCBL composite particles were synthesized using the P/F silica cores. Table 4.5 shows the DLS results at 15 and 40 °C.

An increase in the surface density of amino groups on the P/F silica cores from ~ 0.3 to 0.7 $-NH_2$ groups / nm^2 did not have an apparent effect on the shell thickness of silica-PCBL

composite particles (116 nm ± 11 nm to 117 nm ± 10 nm respectively). The increase, on the other hand, caused a change in the hydrodynamic behavior of the silica-PCBL composite particles at temperatures below and above the reported coil→helix transition of PCBL. A high density of surface initiators (amino groups) yielded composite particles that did not exhibit a temperature-induced change in hydrodynamic radius.[1] This is possibly due to the overcrowding and lack of mobility of the polypeptide chains. Similarly, a low density of surface initiators yielded composite particles that did not exhibit a temperature-induced change in hydrodynamic radius but that had changes in the NMR spectra that suggested a change possibly due to the coil→helix transition of the PCBL shell.

Table 4.5 Comparison of the hydrodynamic radius and shell thickness of silica-PCBL composite particles of high initiator surface density (ES.4.53A) at 15 °C and 40 °C in *m*-cresol measured by dynamic light scattering.

T / °C	$R_{h\ silica\text{-}PCBL}$ / nm	$R_{h\ silica\text{-}PCBL} - R_{h\ silica}$ / nm
15	207 ± 8	117 ± 10
40	257 ± 14	147 ± 16

CHAPTER 5 CONCLUSIONS AND FUTURE WORK

5.1 Conclusions

Monodisperse colloidal silica particles bearing a controlled amount of amino groups have been synthesized. The hydrodynamic radius of the particles can be easily controlled in the 20-140 nm range by adjusting the water/TEOS ratio in the synthesis. The colloidal silica particles were passivated/functionalized using a mixture of APS and MTMS. APS is the source of amino groups and MTMS provides non-reactive methyl groups that act as spacers among the amino groups. The surface density of amino groups was measured by UV-Vis spectroscopy after the amino groups were reacted with ninhydrin. A good correlation between the measured and the expected values for a monolayer were obtained at low amino group surface densities. However, at high concentrations, the measured values are higher than expected. This is probably due to the formation of multilayers of APS. An empirical correlation between the surface density of amino groups and zeta potential at low pH was established. Amino groups are positively charged at low pH therefore giving surface charge to the particles. The synthesized particles of low surface density of amino groups are good candidates for serving as initiators for the polymerization of *N*-carboxyanhydrides.

Silica-PBLG composite particles of controlled polypeptide content were synthesized by sequential addition of monomer. The thickness of the shell increased as the content of PBLG increased. This simple procedure allows, in principle, the synthesis of silica-PBLG composite particles of a predetermined polypeptide content or shell thickness.

A positive staining procedure was developed for the visualization of silica-PBLG composite particles in the “wet” state by transmission electron microscopy. A corona, which

was presumably the polypeptide shell, was observed around the silica cores. The sizes obtained by dynamic light scattering and transmission electron microscopy are comparable. The polypeptide shell was probably stained by the complex of osmium tetroxide and pyridine. The accelerating voltage used in the transmission electron microscope did not have an apparent effect in the observed size of the silica cores or the silica-PBLG composite particles. The incorporation of silica-coated cobalt nanoparticles as an internal negative control strengthened the hypothesis that the corona observed around the silica particles was the PBLG shell.

pH-responsive silica-PLGA composite particles were synthesized by reaction of silica-PBLG composite particles with anhydrous hydrogen bromide. The responsiveness of the particles was probably due to the responsiveness of the PLGA shell. The particles were charged and extended at high pH, this was evidenced by a high negative zeta potential and a large hydrodynamic radius. At low pH the particles were uncharged and compact.

Silica-PCBL composite particles were synthesized. Dynamic light scattering and nuclear magnetic resonance suggest a temperature-induced coil→helix transition of the PCBL shell. The surface density of initiator moieties on the silica cores plays an important role in the resulting silica-PCBL composite particles. At low surface density, the polypeptide suffers a temperature-induced change that is observable by NMR and attributable to the coil→helix transition of the PCBL shell. The apparent hydrodynamic radius of the particles does not change. At higher surface density, the resulting silica-PCBL composite particles exhibit a temperature-induced change in the apparent hydrodynamic radius. This suggests that the surface density of initiators on the silica surface and probably the surface density of PCBL have an important effect in the hydrodynamic behavior of the particles. At higher surface density, changes in the polypeptide shell are more *apparent* as observed by dynamic light scattering which measures diffusion.

5.2 Future Work

5.2.1 Measurement of the Molecular Weight of PBLG

Knowing the molecular weight of macromolecules is a key in understanding their behavior and properties. The molecular weight of polymers is intimately related to their size and sometimes shape. The molecular weight of homopolypeptides can be related to their length. For example, if PBLG is in the α-helical conformation, each repeating unit contributes 1.5 Å to the axial length.[93] Ellipsometry has been used to measure the thickness of PBLG and PCBL films.[171;172] Dynamic light scattering has been used to measure the thickness of the polymer shell in core-shell particles.[94;130;133;144;145;233] However, in order to know the molecular weight of the polymer, it is necessary to know not only the thickness but the tilt angle as well and the relationship between length and molecular weight. Therefore it is more convenient and accurate to measure the molecular weight of untethered polymers in solution.

A strategy for knowing the molecular weight of PBLG on silica-PBLG composite particles consists of cleaving the PBLG off the silica surface without degrading the polymer. Etching the silica cores with 50 % HF aqueus solution was tried but the PBLG showed signs of degradation and debenzylation. As part of future work the reaction with an almost stoichiometric amount of anhydrous HF is proposed. The stoichiometric amount of HF should be based on the amount of silicon atoms on the silica surface and not on the total weight of silica. An excess of anhydrous HF has the potential of debenzylating the PBLG.[234] Once the PBLG is cleaved from the silica surface it can be separated from the dispersion by centrifugation. The colloidal silica is expected to sediment first and the PBLG would remain in solution. After that it can be easily transferred to another solvent. In order to open the venue for this analysis, commercial PBLG was studied

by gel permeation chromatography (GPC). This study will allow the characterization of cleaved PBLG from the silica-PBLG composite particles. The results are shown in Appendix A.

REFERENCES

1) Turksen,S. Synthesis and Characterization of Superparamagnetic Silica-homopolypeptide Composite Particles. *Louisiana State University, Ph.D.Dissertation* **2004**,

2) Qiu,J. Properties of Silica-Polypeptide Composite Particles. *Louisiana State University, Ph.D.Dissertation* **2007**,

3) Sounderya,N.; Zhang,Y. Use of core/shell structured nanoparticles for biomedical applications. *Recent Pat.Biomed.Eng.* **2008**, *1*, 34-42.

4) Zhong,C.J.; Maye,M.M. Core-shell assembled nanoparticles as catalysts. *Adv.Mater.(Weinheim, Ger.)* **2001**, *13*, 1507-1511.

5) Kuykendall,D.W.; Zimmerman,S.C. Nanoparticles: A very versatile nanocapsule. *Nat.Nanotechnol.* **2007**, *2*, 201-202.

6) Yow,H.N.; Routh,A.F. Formation of liquid core-polymer shell microcapsules. *Soft Matter* **2006**, *2*, 940-949.

7) Sameti,M.; Bohr,G.; Ravi Kumar,M.N.V.; Kneuer,C.; Bakowsky,U.; Nacken,M.; Schmidt,H.; Lehr,C.M. Stabilisation by freeze-drying of cationically modified silica nanoparticles for gene delivery. *Int.J.Pharm.* **2003**, *266*, 51-60.

8) Csogor; Nacken,M.; Sameti,M.; Lehr,C.M.; Schmidt,H. Modified silica particles for gene delivery. *Mater.Sci.Eng., C* **2003**, *C23*, 93-97.

9) Kneuer,C.; Sameti,M.; Haltner,E.G.; Schiestel,T.; Schirra,H.; Schmidt,H.; Lehr,C.M. Silica nanoparticles modified with aminosilanes as carriers for plasmid DNA. *Int.J.Pharm.* **2000**, *196*, 257-261.

10) Yang,Y.Y.; Wang,Y.; Powell,R.; Chan,P. Polymeric core-shell nanoparticles for therapeutics. *Clin.Exp.Pharmacol.Physiol.* **2006**, *33*, 557-562.

11) Haag,R. Supramolecular drug-delivery systems based on polymeric core-shell architectures. *Angew.Chem., Int.Ed.* **2004**, *43*, 278-282.

12) Gemeinhart,R.A.; Luo,D.; Saltzman,W.M. Cellular Fate of a Modular DNA Delivery System Mediated by Silica Nanoparticles. *Biotechnol.Prog.* **2005**, *21*, 532-537.

13) Oishi,M.; Nagasaki,Y. Synthesis, characterization, and biomedical applications of core-shell-type stimuli-responsive nanogels - Nanogel composed of poly[2-(N,N-diethylamino)ethyl methacrylate] core and PEG tethered chains. *React.Funct.Polym.* **2007**, *67*, 1311-1329.

14) Chen,Z.; Hsu,F.C.; Battigelli,D.; Chang,H.C. Capture and release of viruses using amino-functionalized silica particles. *Anal.Chim.Acta* **2006**, *569*, 76-82.

15) Geho,D.H.; Jones,C.D.; Petricoin,E.F.; Liotta,L.A. Nanoparticles: potential biomarker harvesters. *Curr.Opin.Chem.Biol.* **2006**, *10*, 56-61.

16) Georganopoulou,D.G.; Chang,L.; Nam,J.M.; Thaxton,C.S.; Mufson,E.J.; Klein,W.L.; Mirkin,C.A. Nanoparticle-based detection in cerebral spinal fluid of a soluble pathogenic biomarker for Alzheimer's disease. *Proc.Natl.Acad.Sci.U.S.A.* **2005**, *102*, 2273-2276.

17) Smith,J.E.; Wang,L.; Tan,W. Bioconjugated silica-coated nanoparticles for bioseparation and bioanalysis. *TrAC, Trends Anal.Chem.* **2006**, *25*, 848-855.

18) Nam,J.M.; Thaxton,C.S.; Mirkin,C.A. Nanoparticle-based bio-bar codes for the ultrasensitive detection of proteins. *Science (Washington, DC, U.S.)* **2003**, *301*, 1884-1886.

19) Burns,A.; Ow,H.; Wiesner,U. Fluorescent core-shell silica nanoparticles: towards "Lab on a Particle" architectures for nanobiotechnology. *Chem.Soc.Rev.* **2006**, *35*, 1028-1042.

20) Shipway,A.N.; Willner,I. Nanoparticles as structural and functional units in surface-confined architectures. *Chem.Commun.(Cambridge, U.K.)* **2001**, 2035-2045.

21) Reiss,P. ZnSe based colloidal nanocrystals: synthesis, shape control, core/shell, alloy and doped systems. *New J.Chem.* **2007**, *31*, 1843-1852.

22) Leventis,N. Three-Dimensional Core-Shell Superstructures: Mechanically Strong Aerogels. *Acc.Chem.Res.* **2007**, *40*, 874-884.

23) Salgueirino-Maceira,V.; Correa-Duarte,M.A. Increasing the complexity of magnetic core/shell structured nanocomposites for biological applications. *Adv.Mater.(Weinheim, Ger.)* **2007**, *19*, 4131-4144.

24) Martel,S.; Tremblay,C.C.; Ngakeng,S.; Langlois,G. Controlled manipulation and actuation of micro-objects with magnetotactic bacteria. *Appl.Phys.Lett.* **2006**, *89*, 233904-1-233904/3.

25) Martel,S.; Mathieu,J.B.; Felfoul,O.; Chanu,A.; Aboussouan,E.; Tamaz,S.; Pouponneau,P.; Yahia,L.'H.; Beaudoin,G.; Soulez,G.; Mankiewicz,M. Automatic navigation of an untethered device in the artery of a living animal using a conventional clinical magnetic resonance imaging system. *Appl.Phys.Lett.* **2007**, *90*, 114105-1-114105/3.

26) Velev,O.D. Self-Assembly of Unusual Nanoparticle Crystals. *Science (Washington, DC, U.S.)* **2006**, *312*, 376-377.

27) Velev,O.D.; Lenhoff,A.M.; Kaler,E.W. A class of microstructured particles through colloidal crystallization. *Science (Washington, D.C.)* **2000**, *287*, 2240-2243.

28) Adams,M.; Dogic,Z.; Keller,S.L.; Fraden,S. Entropically driven microphase transitions in mixtures of colloidal rods and spheres. *Nature (London)* **1998**, *393*, 349-352.

29) Koenderink,G.H.; Philipse,A.P. Rotational and Translational Self-Diffusion in Colloidal Sphere Suspensions and the Applicability of Generalized Stokes-Einstein Relations. *Langmuir* **2000**, *16*, 5631-5638.

30) Lettinga,M.P.; van Kats,C.M.; Philipse,A.P. Rotational Diffusion of Tracer Spheres in Packings and Dispersions of Colloidal Spheres Studied with Time-Resolved Phosphorescence Anisotropy. *Langmuir* **2000**, *16*, 6166-6172.

31) Koenderink,G.H.; Philipse,A.P.; Kluijtmans,S.G.J.M. Sphere dynamics in isotropic colloidal rod fluids. *J.Phys.: Condens.Matter* **2000**, *12*, A339-A343

32) Lettinga,M.P.; van Zandvoort,M.A.M.J.; van Kats,C.M.; Philipse,A.P. Phosphorescent Colloidal Silica Spheres as Tracers for Rotational Diffusion Studies. *Langmuir* **2000**, *16*, 6156-6165.

33) Schartl,W. Crosslinked spherical nanoparticles with core-shell topology. *Adv.Mater.(Weinheim, Ger.)* **2000**, *12*, 1899-1908.

34) Anonymous DEFINITION AND CLASSIFICATION OF COLLOIDS. *http://www.iupac.org/reports/2001/colloid_2001/manual_of_s_and_t/node33.html* **2005**,

35) Stoeber,W.; Fink,A.; Bohn,E. Controlled growth of monodisperse silica spheres in the micron size range. *Journal of Colloid and Interface Science* **1968**, *26*, 62-69.

36) Coenen,S.; De Kruif,C.G. Synthesis and growth of colloidal silica particles. *Journal of Colloid and Interface Science* **1988**, *124*, 104-110.

37) Van Blaaderen,A.; Van Geest,J.; Vrij,A. Monodisperse colloidal silica spheres from tetraalkoxysilanes: particle formation and growth mechanism. *Journal of Colloid and Interface Science* **1992**, *154*, 481-501.

38) Mou,C.Y.; Lin,H.P. Control of morphology in synthesizing mesoporous silica. *Pure Appl.Chem.* **2000**, *72*, 137-146.

39) Johnson,P.M.; van Kats,C.M.; Van Blaaderen,A. Synthesis of Colloidal Silica Dumbbells. *Langmuir* **2005**, *21*, 11510-11517.

40) Khan,S.A.; Guenther,A.; Schmidt,M.A.; Jensen,K.F. Microfluidic Synthesis of Colloidal Silica. *Langmuir* **2004**, *20*, 8604-8611.

41) Howard,A.G.; Khdary,N.H. Spray synthesis of monodisperse sub-micron spherical silica particles. *Mater.Lett.* **2007**, *61*, 1951-1954.

42) Costa,C.A.R.; Leite,C.A.P.; Galembeck,F. Size Dependence of Stober Silica Nanoparticle Microchemistry. *J.Phys.Chem.B* **2003**, *107*, 4747-4755.

43) Bogush,G.H.; Tracy,M.A.; Zukoski,C.F., IV Preparation of monodisperse silica particles: control of size and mass fraction. *J.Non-Cryst.Solids* **1988**, *104*, 95-106.

44) Tan,C.G.; Bowen,B.D.; Epstein,N. Production of monodisperse colloidal silica spheres: effect of temperature. *J.Colloid Interface Sci.* **1987**, *118*, 290-293.

45) Bailey,J.K.; Mecartney,M.L. Formation of colloidal silica particles from alkoxides. *Colloids Surf.* **1992**, *63*, 151-161.

46) Esquena,J.; Pons,R.; Azemar,N.; Caelles,J.; Solans,C. Preparation of monodisperse silica particles in emulsion media. *Colloids Surf., A* **1997**, *123-124*, 575-586.

47) Rao,K.S.; El Hami,K.; Kodaki,T.; Matsushige,K.; Makino,K. A novel method for synthesis of silica nanoparticles. *J.Colloid Interface Sci.* **2005**, *289*, 125-131.

48) Gan,L.M.; Zhang,K.; Chew,C.H. Preparation of silica nanoparticles from sodium orthosilicate in inverse microemulsions. *Colloids Surf., A* **1996**, *110*, 199-206.

49) Corradi,A.B.; Bondioli,F.; Ferrari,A.M.; Focher,B.; Leonelli,C. Synthesis of silica nanoparticles in a continuous-flow microwave reactor. *Powder Technol.* **2006**, *167*, 45-48.

50) Lindberg,R.; Sundholm,G.; Pettersen,B.; Sjoeblom,J.; Friberg,S.E. Multivariate analysis of the size dependence of monodisperse silica particles prepared according to the sol-gel technique. *Colloids Surf., A* **1997**, *123-124*, 549-560.

51) Lieftink,D.J.; Geus,J.W. The preparation of silica from the olivine process and its possible use as a catalyst support. *J.Geochem.Explor.* **1998**, *62*, 347-350.

52) Kim,S.S.; Kim,H.S.; Kim,S.G.; Kim,W.S. Effect of electrolyte additives on sol-precipitated nano silica particles. *Ceram.Int.* **2004**, *30*, 171-175.

53) Jal,P.K.; Sudarshan,M.; Saha,A.; Patel,S.; Mishra,B.K. Synthesis and characterization of nanosilica prepared by precipitation method. *Colloids Surf., A* **2004**, *240*, 173-178.

54) Zhang,X.d.; Sun,Y.y.; Zhuang,J.q.; Yang,W.s. Oligo-lysine induced formation of silica particles in neutral silicate solution. *Chem.Res.Chin.Univ.* **2006**, *22*, 368-370.

55) Van Helden,A.K.; Jansen,J.W.; Vrij,A. Preparation and characterization of spherical monodisperse silica dispersions in nonaqueous solvents. *J.Colloid Interface Sci.* **1981**, *81*, 354-368.

56) Wang,W.; Gu,B.; Liang,L. Effect of anionic surfactants on synthesis and self-assembly of silica colloidal nanoparticles. *J.Colloid Interface Sci.* **2007**, *313*, 169-173.

57) Sadasivan,S.; Rasmussen,D.H.; Chen,F.P.; Kannabiran,R.K. Preparation and characterization of ultrafine silica. *Colloids Surf., A* **1998**, *132*, 45-52.

58) Lee,K.; Sathyagal,A.N.; McCormick,A.V. A closer look at an aggregation model of the Stober process. *Colloids Surf., A* **1998**, *144*, 115-125.

59) Green,D.L.; Lin,J.S.; Lam,Y.F.; Hu,M.Z.C.; Schaefer,D.W.; Harris,M.T. Size, volume fraction, and nucleation of Stober silica nanoparticles. *J.Colloid Interface Sci.* **2003**, *266*, 346-358.

60) Bogush,G.H.; Zukoski,C.F., IV Studies of the kinetics of the precipitation of uniform silica particles through the hydrolysis and condensation of silicon alkoxides. *J.Colloid Interface Sci.* **1991**, *142*, 1-18.

61) Zhuravlev,L.T. Surface characterization of amorphous silica-a review of work from the former USSR. *Colloids Surf., A* **1993**, *74*, 71-90.

62) Brinker,J.; Scherer,G.*Sol-gel science : the physics and chemistry of sol-gel processing*; Academic Press: Boston, 2004;

63) Denkov,N.; Velev,O.; Kralchevski,P.; Ivanov,I.; Yoshimura,H.; Nagayama,K. Mechanism of formation of two-dimensional crystals from latex particles on substrates. *Langmuir* **1992**, *8*, 3183-3190.

64) Kobayashi,Y.; Miyauchi,H.; Gu,S.; Nagao,D.; Konno,M. Fabrication of mono- and multi-layers of submicron-sized spheres by a dip-coating technique and their transmittance property. *J.Chem.Eng.Jpn.* **2004**, *37*, 614-621.

65) Micheletto,R.; Fukuda,H.; Ohtsu,M. A Simple Method for the Production of a Two-Dimensional, Ordered Array of Small Latex Particles. *Langmuir* **1995**, *11*, 3333-3336.

66) Nostell,P.; Roos,A.; Karlsson,B. Optical and mechanical properties of sol-gel antireflective films for solar energy applications. *Thin Solid Films* **1999**, *351*, 170-175.

67) Hsu,W.P.; Yu,R.; Matijevic,E. Paper whiteners. I. Titania coated silica. *J.Colloid Interface Sci.* **1993**, *156*, 56-65.

68) Claesson,E.M.; Philipse,A.P. Thiol-functionalized silica colloids, grains, and membranes for irreversible adsorption of metal(oxide) nanoparticles. *Colloids Surf., A* **2007**, *297*, 46-54.

69) Bagwe,R.P.; Hilliard,L.R.; Tan,W. Surface Modification of Silica Nanoparticles to Reduce Aggregation and Nonspecific Binding. *Langmuir* **2006**, *22*, 4357-4362.

70) Matoussevitch,N.; Gorschinski,A.; Habicht,W.; Bolle,J.; Dinjus,E.; Boennemann,H.; Behrens,S. Surface modification of metallic Co nanoparticles. *J.Magn.Magn.Mater.* **2007**, *311*, 92-96.

71) Kurth,D.G.; Bein,T. Surface reactions on thin layers of silane coupling agents. *Langmuir* **1993**, *9*, 2965-2973.

72) Kulkarni,S.A.; Ogale,S.B.; Vijayamohanan,K.P. Tuning the hydrophobic properties of silica particles by surface silanization using mixed self-assembled monolayers. *J.Colloid Interface Sci.* **2008**, *318*, 372-379.

73) Pham,K.N.; Fullston,D.; Sagoe-Crentsil,K. Surface modification for stability of nano-sized silica colloids. *J.Colloid Interface Sci.* **2007**, *315*, 123-127.

74) Brunner,H.; Vallant,T.; Mayer,U.; Hoffmann,H.; Basnar,B.; Vallant,M.; Friedbacher,G. Substrate Effects on the Formation of Alkylsiloxane Monolayers. *Langmuir* **1999**, *15*, 1899-1901.

75) Moon,J.H.; Shin,J.W.; Kim,S.Y.; Park,J.W. Formation of Uniform Aminosilane Thin Layers: An Imine Formation To Measure Relative Surface Density of the Amine Group. *Langmuir* **1996**, *12*, 4621-4624.

76) Sagiv,J. Organized monolayers by adsorption. 1. Formation and structure of oleophobic mixed monolayers on solid surfaces. *J.Am.Chem.Soc.* **1980**, *102*, 92-98.

77) Balachander,N.; Sukenik,C.N. Functionalized siloxy-anchored monolayers with exposed amino, azido, bromo, or cyano groups. *Tetrahedron Lett.* **1988**, *29*, 5593-5594.

78) Bierbaum,K.; Kinzler,M.; Woell,C.; Grunze,M.; Haehner,G.; Heid,S.; Effenberger,F. A Near Edge X-ray Absorption Fine Structure Spectroscopy and X-ray Photoelectron Spectroscopy Study of the Film Properties of Self-Assembled Monolayers of Organosilanes on Oxidized Si(100). *Langmuir* **1995**, *11*, 512-518.

79) Bierbaum,K.; Grunze,M.; Baski,A.A.; Chi,L.F.; Schrepp,W.; Fuchs,H. Growth of Self-Assembled n-Alkyltrichlorosilane Films on Si(100) Investigated by Atomic Force Microscopy. *Langmuir* **1995**, *11*, 2143-2150.

80) Wasserman,S.R.; Tao,Y.T.; Whitesides,G.M. Structure and reactivity of alkylsiloxane monolayers formed by reaction of alkyltrichlorosilanes on silicon substrates. *Langmuir* **1989**, *5*, 1074-1087.

81) Humbert,B. Estimation of hydroxyl density at the surface of pyrogenic silicas by complementary NMR and Raman experiments. *J.Non-Cryst.Solids* **1995**, *191*, 29-37.

82) Fadeev,A.Y.; McCarthy,T.J. Self-Assembly Is Not the Only Reaction Possible between Alkyltrichlorosilanes and Surfaces: Monomolecular and Oligomeric Covalently Attached Layers of Dichloro- and Trichloroalkylsilanes on Silicon. *Langmuir* **2000**, *16*, 7268-7274.

83) Haller,I. Covalently attached organic monolayers on semiconductor surfaces. *Journal of the American Chemical Society* **1978**, *100*, 8050-8055.

84) Kallury,K.M.R.; Macdonald,P.M.; Thompson,M. Effect of Surface Water and Base Catalysis on the Silanization of Silica by (Aminopropyl)alkoxysilanes Studied by X-ray Photoelectron Spectroscopy and 13C Cross-Polarization/Magic Angle Spinning Nuclear Magnetic Resonance. *Langmuir* **1994**, *10*, 492-499.

85) Kanan,S.M.; Tze,W.T.Y.; Tripp,C.P. Method to Double the Surface Concentration and Control the Orientation of Adsorbed (3-Aminopropyl)dimethylethoxysilane on Silica Powders and Glass Slides. *Langmuir* **2002**, *18*, 6623-6627.

86) Krasnoslobodtsev,A.V.; Smirnov,S.N. Effect of Water on Silanization of Silica by Trimethoxysilanes. *Langmuir* **2002**, *18*, 3181-3184.

87) McGovern,M.E.; Kallury,K.M.R.; Thompson,M. Role of Solvent on the Silanization of Glass with Octadecyltrichlorosilane. *Langmuir* **1994**, *10*, 3607-3614.

88) Cao,C.; Fadeev,A.Y.; McCarthy,T.J. Reactions of Organosilanes with Silica Surfaces in Carbon Dioxide. *Langmuir* **2001**, *17*, 757-761.

89) Heise,A.; Menzel,H.; Yim,H.; Foster,M.D.; Wieringa,R.H.; Schouten,A.J.; Erb,V.; Stamm,M. Grafting of Polypeptides on Solid Substrates by Initiation of N-Carboxyanhydride Polymerization by Amino-Terminated Self-Assembled Monolayers. *Langmuir* **1997**, *13*, 723-728.

90) Heiney,P.A.; Grueneberg,K.; Fang,J.; Dulcey,C.; Shashidhar,R. Structure and Growth of Chromophore-Functionalized (3-Aminopropyl)triethoxysilane Self-Assembled on Silicon. *Langmuir* **2000**, *16*, 2651-2657.

91) Boerio,F.J.; Armogan,L.; Cheng,S.Y. The structure of gamma - aminopropyltriethoxysilane films on iron mirrors. *J.Colloid Interface Sci.* **1980**, *73*, 416-424.

92) Ishida,H.; Naviroj,S.; Tripathy,S.K.; Fitzgerald,J.F.; Koenig,J.L. The structure of an aminosilane coupling agent in aqueous solutions and partially cured solids. *J.Polym.Sci., Polym.Phys.Ed.* **1982**, *20*, 701-718.

93) Block,H.*Poly(γ-benzyl-L-glutamate) and other glutamic acid containing polymers*; Gordon and Breach Science Publishers: New York, 1983;

94) Fong,B.; Russo,P.S. Organophilic Colloidal Particles with a Synthetic Polypeptide Coating. *Langmuir* **1999**, *15*, 4421-4426.

95) Fong,B.; Turksen,S.; Russo,P.S.; Stryjewski,W. Colloidal Crystals of Silica-Homopolypeptide Composite Particles. *Langmuir* **2004**, *20*, 266-269.

96) Sugimoto,H.; Daimatsu,K.; Nakanishi,E.; Ogasawara,Y.; Yasumura,T.; Inomata,K. Preparation and properties of poly(methylmethacrylate)-silica hybrid materials incorporating reactive silica nanoparticles. *Polymer* **2006**, *47*, 3754-3759.

97) Hozumi,A.; Yokogawa,Y.; Kameyama,T.; Sugimura,H.; Hayashi,K.; Shirayama,H.; Takai,O. Amino-terminated self-assembled monolayer on a SiO2 surface formed by chemical vapor deposition. *Journal of Vacuum Science & Technology, A: Vacuum, Surfaces, and Films* **2001**, *19*, 1812-1816.

98) Fadeev,A.Y.; McCarthy,T.J. Trialkylsilane monolayers covalently attached to silicon surfaces: wettability studies indicating that molecular topography contributes to contact angle hysteresis. *Langmuir* **1999**, *15*, 3759-3766.

99) Britt,D.W.; Hlady,V. An AFM study of the effects of silanization temperature, hydration, and annealing on the nucleation and aggregation of condensed OTS domains on mica. *J.Colloid Interface Sci.* **1996**, *178*, 775-784.

100) Vallant,T.; Brunner,H.; Mayer,U.; Hoffmann,H.; Leitner,T.; Resch,R.; Friedbacher,G. Formation of Self-Assembled Octadecylsiloxane Monolayers on Mica and Silicon Surfaces Studied by Atomic Force Microscopy and Infrared Spectroscopy. *J.Phys.Chem.B* **1998**, *102*, 7190-7197.

101) Lambert,A.G.; Neivandt,D.J.; Maloney,R.A.; Davies,P.B. A Protocol for the Reproducible Silanization of Mica Validated by Sum Frequency Spectroscopy and Atomic Force Microscopy. *Langmuir* **2000**, *16*, 8377-8382.

102) Brzoska,J.B.; Azouz,I.B.; Rondelez,F. Silanization of Solid Substrates: A Step Toward Reproducibility. *Langmuir* **1994**, *10*, 4367-4373.

103) Kaiser,E.; Colescott,R.L.; Bossinger,C.D.; Cook,P.I. Color test for detection of free terminal amino groups in the solid-phase synthesis of peptides. *Anal.Biochem.* **1970**, *34*, 595-598.

104) Bruice,P.Y.*Organic Chemistry*; Prentice Hall: 2004;

105) Felix,A.M.; Jimenez,M.H. Rapid fluorometric detection for completeness in solid phase coupling reactions. *Anal.Biochem.* **1973**, *52*, 377-381.

106) Hancock,W.S.; Battersby,J.E. A new micro-test for the detection of incomplete coupling reactions in solid-phase peptide synthesis using 2,4,6-trinitrobenzenesulfonic acid. *Anal.Biochem.* **1976**, *71*, 260-264.

107) Flegel,M.; Sheppard,R.C. A sensitive, general method for quantitative monitoring of continuous flow solid phase peptide synthesis. *J.Chem.Soc., Chem.Commun.* **1990**, 536-538.

108) Kay,C.; Lorthioir,O.E.; Parr,N.J.; Congreve,M.; McKeown,S.C.; Scicinski,J.J.; Ley,S.V. Solid-phase reaction monitoring - chemical derivatization and off-bead analysis. *Biotechnol.Bioeng.* **2001**, *71*, 110-118.

109) Kurth,D.G.; Bein,T. Quantification of the reactivity of (3-aminopropyl)triethoxysilane monolayers with the quartz microbalance. *Angew.Chem.* **1992**, *104*, 323-325.

110) Ganachaud,F.; Mouterde,G.; Delair,T.; Elaissari,A.; Pichot,C. Preparation and characterization of cationic polystyrene latex particles of different aminated surface charges. *Polym.Adv.Technol.* **1995**, *6*, 480-488.

111) Saitoh,T.; Nakagaki,N.; Uchida,Y.; Hiraide,M.; Matsubara,C. Spectrophotometric determination of some functional groups on Chlorella for the evaluation of their contribution to metal uptake. *Anal.Sci.* **2001**, *17*, 793-795.

112) Locascio-Brown,L.; Plant,A.L.; Durst,R.A.; Brizgys,M.V. Radiometric and fluorometric determination of aminosilanes and protein covalently bound to thermally pretreated glass substrates. *Anal.Chim.Acta* **1990**, *228*, 107-116.

113) Henry,A.C.; Tutt,T.J.; Galloway,M.; Davidson,Y.Y.; McWhorter,C.S.; Soper,S.A.; McCarley,R.L. Surface Modification of Poly(methyl methacrylate) Used in the Fabrication of Microanalytical Devices. *Anal.Chem.* **2000**, *72*, 5331-5337.

114) Sarin,V.K.; Kent,S.B.H.; Tam,J.P.; Merrifield,R.B. Quantitative monitoring of solid-phase peptide synthesis by the ninhydrin reaction. *Anal.Biochem.* **1981**, *117*, 147-157.

115) Grasset,F.; Marchand,R.; Marie,A.M.; Fauchadour,D.; Fajardie,F. Synthesis of CeO2@SiO2 core-shell nanoparticles by water-in-oil microemulsion. Preparation of functional thin film. *J.Colloid Interface Sci.* **2006**, *299*, 726-732.

116) Kobayashi,Y.; Imai,J.; Nagao,D.; Takeda,M.; Ohuchi,N.; Kasuya,A.; Konno,M. Preparation of multilayered silica-Gd-silica core-shell particles and their magnetic resonance images. *Colloids Surf., A* **2007**, *308*, 14-19.

117) Kobayashi,Y.; Sakuraba,T. Silica-coating of metallic copper nanoparticles in aqueous solution. *Colloids Surf., A* **2008**, *317*, 756-759.

118) Kobayashi,Y.; Horie,M.; Konno,M.; Rodriguez-Gonzalez,B.; Liz-Marzan,L.M. Preparation and Properties of Silica-Coated Cobalt Nanoparticles. *Journal of Physical Chemistry B* **2003**, *107*, 7420-7425.

119) Eggeman,A.S.; Petford-Long,A.K.; Dobson,P.J.; Wiggins,J.; Bromwich,T.; Dunin-Borkowski,R.; Kasama,T. Synthesis and characterisation of silica encapsulated cobalt nanoparticles and nanoparticle chains. *J.Magn.Magn.Mater.* **2006**, *301*, 336-342.

120) Liz-Marzan,L.M.; Giersig,M.; Mulvaney,P. Synthesis of Nanosized Gold-Silica Core-Shell Particles. *Langmuir* **1996**, *12*, 4329-4335.

121) Kim,T.H.; Kim,D.W.; Lee,J.M.; Lee,Y.G.; Oh,S.G. Preparation of gold-silica heterogeneous nanocomposite particles by alcohol-reduction method. *Mater.Res.Bull.* **2008**, *43*, 1126-1134.

122) Lee,J.M.; Kim,D.W.; Jun,Y.D.; Oh,S.G. Preparation of silica-silver heterogeneous nanocomposite particles by one-pot preparation strategy using polyol process: size-controlled immobilization of silver nanoparticles. *Mater.Res.Bull.* **2006**, *41*, 1407-1416.

123) Chou,K.S.; Chen,C.C. Fabrication and characterization of silver core and porous silica shell nanocomposite particles. *Microporous Mesoporous Mater.* **2007**, *98*, 208-213.

124) Kalele,S.A.; Ashtaputre,S.S.; Hebalkar,N.Y.; Gosavi,S.W.; Deobagkar,D.N.; Deobagkar,D.D.; Kulkarni,S.K. Optical detection of antibody using silica-silver core-shell particles. *Chem.Phys.Lett.* **2005**, *404*, 136-141.

125) Lee,J.W.; Kong,S.; Kim,W.S.; Kim,J. Preparation and characterization of SiO2/TiO2 core-shell particles with controlled shell thickness. *Mater.Chem.Phys.* **2007**, *106*, 39-44.

126) van Bruggen,M.P.B. Preparation and Properties of Colloidal Core-Shell Rods with Adjustable Aspect Ratios. *Langmuir* **1998**, *14*, 2245-2255.

127) Giani,E.; Sparnacci,K.; Laus,M.; Palamone,G.; Kapeliouchko,V.; Arcella,V. PTFE-Polystyrene Core-Shell Nanospheres and Nanocomposites. *Macromolecules* **2003**, *36*, 4360-4367.

128) Liu,S.; Weaver,J.V.M.; Tang,Y.; Billingham,N.C.; Armes,S.P.; Tribe,K. Synthesis of Shell Cross-Linked Micelles with pH-Responsive Cores Using ABC Triblock Copolymers. *Macromolecules* **2002**, *35*, 6121-6131.

129) Zhang,Y.; Jiang,M.; Zhao,J.; Wang,Z.; Dou,H.; Chen,D. pH-Responsive Core-Shell Particles and Hollow Spheres Attained by Macromolecular Self-Assembly. *Langmuir* **2005**, 1531-1538.

130) Li,X.; Zuo,J.; Guo,Y.; Yuan,X. Preparation and Characterization of Narrowly Distributed Nanogels with Temperature-Responsive Core and pH-Responsive Shell. *Macromolecules* **2004**, *37*, 10042-10046.

131) Xiao,X.C.; Chu,L.Y.; Chen,W.M.; Wang,S.; Xie,R. Preparation of Submicrometer-Sized Monodispersed Thermoresponsive Core-Shell Hydrogel Microspheres. *Langmuir* **2004**, *20*, 5247-5253.

132) Jones,C.D.; Lyon,L.A. Shell-Restricted Swelling and Core Compression in Poly(N-isopropylacrylamide) Core-Shell Microgels. *Macromolecules* **2003**, *36*, 1988-1993.

133) Qiu,X.; Wu,C. Study of the Core-Shell Nanoparticle Formed through the \"Coil-to-Globule\" Transition of Poly(N-isopropylacrylamide) Grafted with Poly(ethylene oxide). *Macromolecules* **1997**, *30*, 7921-7926.

134) Chu,L.Y.; Park,S.H.; Yamaguchi,T.; Nakao,S.i. Preparation of Micron-Sized Monodispersed Thermoresponsive Core-Shell Microcapsules. *Langmuir* **2002**, *18*, 1856-1864.

135) Kuckling,D.; Vo,C.D.; Wohlrab,S.E. Preparation of Nanogels with Temperature-Responsive Core and pH-Responsive Arms by Photo-Cross-Linking. *Langmuir* **2002**, *18*, 4263-4269.

136) Marinakos,S.M.; Novak,J.P.; Brousseau,L.C., III; House,A.B.; Edeki,E.M.; Feldhaus,J.C.; Feldheim,D.L. Gold Particles as Templates for the Synthesis of Hollow Polymer Capsules. Control of Capsule Dimensions and Guest Encapsulation. *Journal of the American Chemical Society* **1999**, *121*, 8518-8522.

137) Marinakos,S.M.; Shultz,D.A.; Feldheim,D.L. Gold nanoparticles as templates for the synthesis of hollow nanometer-sized conductive polymer capsules. *Advanced Materials (Weinheim, Germany)* **1999**, *11*, 34-37.

138) Shan,J.; Nuopponen,M.; Jiang,H.; Viitala,T.; Kauppinen,E.; Kontturi,K.; Tenhu,H. Amphiphilic Gold Nanoparticles Grafted with Poly(N-isopropylacrylamide) and Polystyrene. *Macromolecules* **2005**, *38*, 2918-2926.

139) Kamata,K.; Lu,Y.; Xia,Y. Synthesis and Characterization of Monodispersed Core-Shell Spherical Colloids with Movable Cores. *Journal of the American Chemical Society* **2003**, *125*, 2384-2385.

140) Gu,S.; Onishi,J.; Mine,E.; Kobayashi,Y.; Konno,M. Preparation of multilayered gold-silica-polystyrene core-shell particles by seeded polymerization. *J.Colloid Interface Sci.* **2004**, *279*, 284-287.

141) Yang,F.; Chu,Y.; Ma,S.; Zhang,Y.; Liu,J. Preparation of uniform silica/polypyrrole core/shell microspheres and polypyrrole hollow microspheres by the template of modified silica particles using different modified agents. *J.Colloid Interface Sci.* **2006**, *301*, 470-478.

142) Luo,X.; Killard,A.J.; Morrin,A.; Smyth,M.R. In situ electropolymerised silica-polyaniline core-shell structures: Electrode modification and enzyme biosensor enhancement. *Electrochim.Acta* **2006**, *52*, 1865-1870.

143) Gu,S.; Kondo,T.; Konno,M. Preparation of silica-polystyrene core-shell particles up to micron sizes. *J.Colloid Interface Sci.* **2004**, *272*, 314-320.

144) Wu,T.; Ke,Y. Preparation of silica-PS composite particles and their application in PET. *Eur.Polym.J.* **2006**, *42*, 274-285.

145) Pathmamanoharan,C. Preparation of monodisperse polyisobutene grafted silica dispersion. *Colloids Surf.* **1988**, *34*, 81-88.

146) Qi,D.m.; Bao,Y.z.; Weng,Z.x.; Huang,Z.m. Preparation of acrylate polymer/silica nanocomposite particles with high silica encapsulation efficiency via miniemulsion polymerization. *Polymer* **2006**, *47*, 4622-4629.

147) Lee,M.H.; Beyer,F.L.; Furst,E.M. Synthesis of monodisperse fluorescent core-shell silica particles using a modified Stober method for imaging individual particles in dense colloidal suspensions. *J.Colloid Interface Sci.* **2005**, *288*, 114-123.

148) Ethiraj,A.S.; Hebalkar,N.; Kharrazi,S.; Urban,J.; Sainkar,S.R.; Kulkarni,S.K. Photoluminescent core-shell particles of organic dye in silica. *J.Lumin.* **2005**, *114*, 15-23.

149) Pacard,E.; Brook,M.A.; Ragheb,A.M.; Pichot,C.; Chaix,C. Elaboration of silica colloid/polymer hybrid support for oligonucleotide synthesis. *Colloids Surf., B* **2006**, *47*, 176-188.

150) Zhang,Z.; Berns,A.E.; Willbold,S.; Buitenhuis,J. Synthesis of poly(ethylene glycol) (PEG)-grafted colloidal silica particles with improved stability in aqueous solvents. *J.Colloid Interface Sci.* **2007**, *310*, 446-455.

151) Yaguee,C.; Moros,M.; Grazu,V.; Arruebo,M.; Santamaria,J. Synthesis and stealthing study of bare and PEGylated silica micro- and nanoparticles as potential drug-delivery vectors. *Chem.Eng.J.(Amsterdam, Neth.)* **2008**, *137*, 45-53.

152) Dietz,E.; Fery,N.; Hamann,K. Polyreactions and pigment surfaces. IV. Polymerization of N-carboxy-alpha -amino acid anhydrides on a silicon dioxide surface. *Angew.Makromol.Chem.* **1974**, *35*, 115-129.

153) Tsubokawa,N.; Kobayashi,K.; Sone,Y. Grafting of polypeptide from carbon black by the ring-opening polymerization of γ-methyl L-glutamate N-carboxyanhydride initiated by amino groups on carbon black surface. *Polymer Journal (Tokyo, Japan)* **1987**, *19*, 1147-1155.

154) Soto-Cantu,E.; Turksen,S.; Qiu,J.; Russo,P.S. Silica-polypeptide composite microparticles. *Polym.Prepr.(Am.Chem.Soc., Div.Polym.Chem.)* **2006**, *47*, 930

155) Bridger,K.; Fairhurst,D.; Vincent,B. Nonaqueous silica dispersions stabilized by terminally grafted polystyrene chains. *J.Colloid Interface Sci.* **1979**, *68*, 190-198.

156) Mei,Y.; Sharma,G.; Lu,Y.; Ballauff,M.; Drechsler,M.; Irrgang,T.; Kempe,R. High Catalytic Activity of Platinum Nanoparticles Immobilized on Spherical Polyelectrolyte Brushes. *Langmuir* **2005**, *21*, 12229-12234.

157) Lu,Y.; Mei,Y.; Walker,R.; Ballauff,M.; Drechsler,M. Nano-tree'-type spherical polymer brush particles as templates for metallic nanoparticles. *Polymer* **2006**, *47*, 4985-4995.

158) Alcantar,N.A.; Aydil,E.S.; Israelachvili,J.N. Polyethylene glycol-coated biocompatible surfaces. *J.Biomed.Mater.Res.* **2000**, *51*, 343-351.

159) Bridger,K.; Vincent,B. The terminal grafting of poly(ethylene oxide) chains to silica surfaces. *Eur.Polym.J.* **1980**, *16*, 1017-1021.

160) Tokareva,I.; Minko,S.; Fendler,J.H.; Hutter,E. Nanosensors Based on Responsive Polymer Brushes and Gold Nanoparticle Enhanced Transmission Surface Plasmon Resonance Spectroscopy. *Journal of the American Chemical Society* **2004**, *126*, 15950-15951.

161) Lu,Y.; Wittemann,A.; Ballauff,M.; Drechsler,M. Preparation of polystyrene-poly(N-isopropylacrylamide) (PS-PNIPA) core-shell particles by photoemulsion polymerization. *Macromol.Rapid Commun.* **2006**, *27*, 1137-1141.

162) Fan,X.; Zhou,Q.; Xia,C.; Cristofoli,W.; Mays,J.; Advincula,R. Living Anionic Surface-Initiated Polymerization (LASIP) of Styrene from Clay Nanoparticles Using Surface Bound 1,1-Diphenylethylene (DPE) Initiators. *Langmuir* **2002**, *18*, 4511-4518.

163) Fan,X.; Xia,C.; Fulghum,T.; Park,M.K.; Locklin,J.; Advincula,R.C. Polymer Brushes Grafted from Clay Nanoparticles Adsorbed on a Planar Substrate by Free Radical Surface-Initiated Polymerization. *Langmuir* **2003**, *19*, 916-923.

164) Zhang,M.; Liu,L.; Zhao,H.; Yang,Y.; Fu,G.; He,B. Double-responsive polymer brushes on the surface of colloid particles. *J.Colloid Interface Sci.* **2006**, *301*, 85-91.

165) Miura,Y.; Kimura,S.; Imanishi,Y.; Umemura,J. Formation of Oriented Helical Peptide Layers on a Gold Surface Due to the Self-Assembling Properties of Peptides. *Langmuir* **1998**, *14*, 6935-6940.

166) Chang,Y.C.; Frank,C.W. Grafting of Poly(γ-benzyl-L-glutamate) on Chemically Modified Silicon Oxide Surfaces. *Langmuir* **1996**, *12*, 5824-5829.

167) Wieringa,R.H.; Siesling,E.A.; Geurts,P.F.M.; Werkman,P.J.; Vorenkamp,E.J.; Erb,V.; Stamm,M.; Schouten,A.J. Surface Grafting of Poly(L-glutamates). 1. Synthesis and Characterization. *Langmuir* **2001**, *17*, 6477-6484.

168) Chang,Y.C.; Frank,C.W. Vapor Deposition-Polymerization of α-Amino Acid N-Carboxy Anhydride on the Silicon(100) Native Oxide Surface. *Langmuir* **1998**, *14*, 326-334.

169) Wang,Y.; Chang,Y.C. Grafting of Homo- and Block Co-polypeptides on Solid Substrates by an Improved Surface-Initiated Vapor Deposition Polymerization. *Langmuir* **2002**, *18*, 9859-9866.

170) Lee,N.H.; Christensen,L.M.; Frank,C.W. Morphology of Vapor-Deposited Poly(α-amino acid) Films. *Langmuir* **2003**, *19*, 3525-3530.

171) Wang,Y.; Chang,Y.C. Synthesis and Conformational Transition of Surface-Tethered Polypeptide: Poly(L-glutamic acid). *Macromolecules* **2003**, *36*, 6503-6510.

172) Wang,Y.; Chang,Y.C. Synthesis and Conformational Transition of Surface-Tethered Polypeptide: Poly(L-lysine). *Macromolecules* **2003**, *36*, 6511-6518.

173) Pauling,L.; Corey,R.B. Structure of synthetic polypeptides. *Proc.Natl.Acad.Sci.U.S.A.* **1951**, *37*, 241-250.

174) Merrifield,R.B. Solid phase peptide synthesis. I. The synthesis of a tetrapeptide. *J.Am.Chem.Soc.* **1963**, *85*, 2149-2154.

175) Deming,T.J. Polypeptide materials. New synthetic methods and applications. *Adv.Mater.(Weinheim, Ger.)* **1997**, *9*, 299-311.

176) Ballard,D.G.H.; Bamford,C.H. Polymerization of alpha -benzyl-L-glutamate-N-carboxy anhydride. *J.Am.Chem.Soc.* **1957**, *79*, 2336-2338.

177) Deming,T.J. Facile synthesis of block copolypeptides of defined architecture. *Nature (London)* **1997**, *390*, 386-389.

178) Deming,T.J. Transition Metal-Amine Initiators for Preparation of Well-Defined Poly(gamma -benzyl L-glutamate). *J.Am.Chem.Soc.* **1997**, *119*, 2759-2760.

179) Deming,T.J. Amino Acid Derived Nickelacycles: Intermediates in Nickel-Mediated Polypeptide Synthesis. *J.Am.Chem.Soc.* **1998**, *120*, 4240-4241.

180) Cheng,J.; Deming,T.J. Screening of Optically Active Nickel Initiators for Enantioasymmetric Polymerization of gamma -Benzyl Glutamate-N-Carboxyanhydride. *Macromolecules* **1999**, *32*, 4745-4747.

181) Goodwin,A.A.; Bu,X.; Deming,T.J. Reactions of alpha -amino acid-N-carboxyanhydrides (NCAs) with organometallic palladium(0) and platinum(0) compounds: structure of a metallated NCA product and its role in polypeptide synthesis. *J.Organomet.Chem.* **1999**, *589*, 111-114.

182) Deming,T.J.; Curtin,S.A. Chain Initiation Efficiency in Cobalt- and Nickel-Mediated Polypeptide Synthesis. *J.Am.Chem.Soc.* **2000**, *122*, 5710-5717.

183) Brzezinska,K.R.; Deming,T.J. Synthesis of ABA Triblock Copolymers via Acyclic Diene Metathesis Polymerization and Living Polymerization of alpha -Amino Acid-N-Carboxyanhydrides. *Macromolecules* **2001**, *34*, 4348-4354.

184) Seidel,S.W.; Deming,T.J. Use of Chiral Ruthenium and Iridium Amido-Sulfonamidate Complexes for Controlled, Enantioselective Polypeptide Synthesis. *Macromolecules* **2003**, *36*, 969-972.

185) Bellomo,E.G.; Davidson,P.; Imperor-Clerc,M.; Deming,T.J. Aqueous Cholesteric Liquid Crystals Using Uncharged Rodlike Polypeptides. *J.Am.Chem.Soc.* **2004**, *126*, 9101-9105.

186) Deming,T.J. Cobalt and Iron Initiators for the Controlled Polymerization of alpha -Amino Acid-N-Carboxyanhydrides. *Macromolecules* **1999**, *32*, 4500-4502.

187) Yu,M.; Nowak,A.P.; Deming,T.J.; Pochan,D.J. Methylated Mono- and Diethyleneglycol Functionalized Polylysines: Nonionic, alpha -Helical, Water-Soluble Polypeptides. *J.Am.Chem.Soc.* **1999**, *121*, 12210-12211.

188) Balik,C.M.; Hopfinger,A.J. Quantization of the solvent effect on the adsorption of poly-gamma -benzyl-L-glutamate. *J.Colloid Interface Sci.* **1978**, *67*, 118-126.

189) DeLong,L.M.; Russo,P.S. Thermodynamic and dynamic behavior of semiflexible polymers in the isotropic phase. *Macromolecules* **1991**, *24*, 6139-6155.

190) Ferretti,J.A.; Ninham,B.W. Nuclear magnetic resonance investigation of the helix to random coil transformation in poly(α-amino acids). II. Poly(γ-benzyl L-glutamate). *Macromolecules* **1970**, *3*, 30-33.

191) Roots,J.; Edsman,K.; Nystroem,B. Helix-coil transition of poly(gamma -benzyl-L-glutamate) in a mixture of dichloroacetic acid/1,2-dichloroethane. *Makromol.Chem.* **1980**, *181*, 2395-2400.

192) Doty,P.; Yang,J.T. Polypeptides. VII. Poly-gamma -benzyl-L-glutamate: the helix-coil transition in solution. *J.Am.Chem.Soc.* **1956**, *78*, 498-500.

193) Karasz,F.E.; O'Reilly,J.M. Enthalpy changes in the helix-coil transition of poly(gamma -benzyl L-glutamate). *Biopolymers* **1967**, *5*, 27-35.

194) Sugai,S.; Kamashima,K.; Nitta,K. Poly(gamma -alkyl L-glutamates). II. Optical rotatory dispersion studies in organic solvents. *J.Polym.Sci., Part A-2* **1968**, *6*, 1065-1081.

195) Ben Ishai,D.; Berger,A. Cleavage of N-carbobenzoxy groups by dry hydrogen bromide and hydrogen chloride. *Journal of Organic Chemistry* **1952**, *17*, 1564-1570.

196) Idelson,M.; Blout,E.R. Polypeptides. XXI. High molecular-weight poly(α,L-glutamic acid): preparation and optical rotation changes. *Journal of the American Chemical Society* **1958**, *80*, 4631-4634.

197) Blout,E.R.; Idelson,M. Polypeptides. VI. Poly-α-L-glutamic acid: preparation and helix-coil conversions. *Journal of the American Chemical Society* **1956**, *78*, 497-498.

198) Blout,E.R.; Idelson,M. Polypeptides. XXII. Compositional effects on the configuration of water-soluble polypeptide copolymers of L-glutamic acid and L-lysine. *Journal of the American Chemical Society* **1958**, *80*, 4909-4913.

199) Hayashi,T.; Emi,S.; Nakajima,A. Helix-coil transition of poly(ε-carbobenzyloxy-L-lysine) in m-cresol. *Polymer* **1975**, *16*, 396-400.

200) Nakamoto,K.; Suga,H.; Seki,S.; Teramoto,A.; Norisuye,T.; Fujita,H. Solution properties of synthetic polypeptides. XIX. Heat capacity measurements on the system of poly(ε-

carbobenzyloxy-L-lysine) and m-cresol in the helix-coil transition region. *Macromolecules* **1974**, *7*, 784-788.

201) Nishioka,N.; Maekawa,A.; Teramoto,A. Solution properties of synthetic polypeptides. XXI. Solvent effect on the helix-coil transition of poly(e-carbobenzoxy L-lysine). *Biopolymers* **1978**, *17*, 665-675.

202) Matsuoka,M.; Norisuye,T.; Teramoto,A.; Fujita,H. Solution properties of synthetic polypeptides. XV. Helix-coil transition in poly(e-carbobenzyloxy-L-lysine). *Biopolymers* **1973**, *12*, 1515-1532.

203) Omura,I.; Teramoto,A.; Fujita,H. Dielectric dispersion of polypeptide solutions. II. Helix-coil transition of poly(e-carbobenzoxy-L-lysine) in m-cresol. *Macromolecules* **1975**, *8*, 284-290.

204) Stokrova,S.; Fiser,V.; Blaha,K. Helix-coil transition of poly(Ne-carbobenzoxy-L-lysine) in solutions containing trifluoroacetic acid. *Macromolecules* **1973**, *6*, 523-525.

205) Zhang,J.H.; Zhan,P.; Wang,Z.L.; Zhang,W.Y.; Ming,N.B. Preparation of monodisperse silica particles with controllable size and shape. *J.Mater.Res.* **2003**, *18*, 649-653.

206) Daly,W.H.; Poche,D. The preparation of N-carboxyanhydrides of α-amino acids using bis(trichloromethyl) carbonate. *Tetrahedron Letters* **1988**, *29*, 5859-5862.

207) Poche,D.S.; Moore,M.J.; Bowles,J.L. An unconventional method for purifying the N-carboxyanhydride derivatives of γ-alkyl-L-glutamates. *Synthetic Communications* **1999**, *29*, 843-854.

208) Berne,B.; Pecora,R.*Dynamic Light Scattering*; Wiley: New York, 1976;

209) Razink,J.J.; Schlotter,N.E. Correction to "Preparation of monodisperse silica particles: Control of size and mass fraction" by G.H. Bogush, M.A. Tracy and C.F. Zukoski IV, Journal of Non-Crystalline Solids 104 (1988) 95-106. *J.Non-Cryst.Solids* **2007**, *353*, 2932-2933.

210) Wieringa,R.H.; Siesling,E.A.; Werkman,P.J.; Angerman,H.J.; Vorenkamp,E.J.; Schouten,A.J. Surface Grafting of Poly(L-glutamates). 2. Helix Orientation. *Langmuir* **2001**, *17*, 6485-6490.

211) Kricheldorf,H.R.; Von Lossow,C.; Schwarz,G. Tertiary amine catalyzed polymerizations of alpha -amino acid N-carboxyanhydrides: the role of cyclization. *J.Polym.Sci., Part A: Polym.Chem.* **2006**, *44*, 4680-4695.

212) Zhao,X.B.; Ji,X.H.; Zhang,Y.H.; Lu,B.H. Effect of solvent on the microstructures of nanostructured Bi2Te3 prepared by solvothermal synthesis. *J.Alloys Compd.* **2004**, *368*, 349-352.

213) Cazaux,J. Recent developments and new strategies in scanning electron microscopy. *J.Microsc.(Oxford, U.K.)* **2005**, *217*, 16-35.

214) Stokes,D.J. Recent advances in electron imaging, image interpretation and applications: environmental scanning electron microscopy. *Philos.Trans.R.Soc.London, Ser.A* **2003**, *361*, 2771-2787.

215) Sheiko,S.S.; da Silva,M.; Shirvaniants,D.; LaRue,I.; Prokhorova,S.; Moeller,M.; Beers,K.; Matyjaszewski,K. Measuring Molecular Weight by Atomic Force Microscopy. *J.Am.Chem.Soc.* **2003**, *125*, 6725-6728.

216) Amelinckx,S.; van Dyck,D.; van Landuyt,J.; van Tendeloo,G.*Electron Microscopy: Principles and Fundamentals*; VCH: 1997;

217) Wittemann,A.; Drechsler,M.; Talmon,Y.; Ballauff,M. High Elongation of Polyelectrolyte Chains in the Osmotic Limit of Spherical Polyelectrolyte Brushes: A Study by Cryogenic Transmission Electron Microscopy. *J.Am.Chem.Soc.* **2005**, *127*, 9688-9689.

218) Danino,D.; Bernheim-Groswasser,A.; Talmon,Y. Digital cryogenic transmission electron microscopy: an advanced tool for direct imaging of complex fluids. *Colloids Surf., A* **2001**, *183-185*, 113-122.

219) Meyer,H.W.; Richter,W. Freeze-fracture studies on lipids and membranes. *Micron* **2001**, *32*, 615-644.

220) Hayat,M.A.*Basic Electron Microscopy Techniques*; Van Nostrand Reinhold: 1972;

221) Hayat,M.A.*Basic Techniques for Transmission Electron Microscopy*; Academic Press: 1986;

222) Ogawa,E. Vapor pressure, surface tension and density of osmium tetroxide. *Bull.Chem.Soc.Jpn.* **1931**, *6*, 302-317.

223) Fojta,M.; Kostecka,P.; Trefulka,M.; Havran,L.; Palecek,E. "Multicolor" Electrochemical Labeling of DNA Hybridization Probes with Osmium Tetroxide Complexes. *Anal.Chem.* **2007**, *79*, 1022-1029.

224) Havran,L.; Fojta,M.; Palecek,E. Voltammetric behavior of DNA modified with osmium tetroxide 2,2'-bipyridine at mercury electrodes. *Bioelectrochemistry* **2004**, *63*, 239-243.

225) Ferretti,J.A.; Paolillo,L. Nuclear magnetic resonance investigation of the helix to random coil transformation in poly(alpha -amino acids). I. Poly-L-alanine. *Biopolymers* **1969**, *7*, 155-171.

226) McCormick,M.; Reimer,J.A. NMR Studies of Structural Phase Transitions in Random Copolymers. *Macromolecules* **2003**, *36*, 477-485.

227) Goodman,M.; Toda,F.; Ueyama,N. Apparent helix-coil transition for poly (L-alanine) as measured by nuclear magnetic resonance. *Proc Natl Acad Sci U S A* **1973**, *70*, 331-333.

228) Tran-Dinh,S.; Neumann,J.M.; Huynh-Dinh,T.; Genissel,B.; Igolen,J.; Simonnot,G. DNA fragment conformations. Proton NMR studies of helix-coil transition, conformations and dynamic structures of the self-complementary deoxyhexanucleotide d(A-C-A-T-G-T) in aqueous solution. *Eur.J.Biochem.* **1982**, *124*, 415-425.

229) Orekhov,V.Y.; Korzhnev,D.M.; Diercks,T.; Kessler,H.; Arseniev,A.S. 1H-15N NMR dynamic study of an isolated alpha -helical peptide (1-36)-bacteriorhodopsin reveals the equilibrium helix-coil transitions. *J.Biomol.NMR* **1999**, *14*, 345-356.

230) Sun,J.; Chen,X.; Deng,C.; Yu,H.; Xie,Z.; Jing,X. Direct formation of giant vesicles from synthetic polypeptides. *Langmuir* **2007**, *23*, 8308-8315.

231) Temussi,P.A.; Goodman,M. Conformational transition in oligopeptides. NMR spectroscopic study. *Proc.Nat.Acad.Sci.U.S.* **1971**, *68*, 1767-1772.

232) Tewari,U.S.; Vasudevan,P.; Ramakrishna,V. Viscosity behavior of o-, m-, and p-cresol melts. *Indian J.Chem.* **1975**, *13*, 720-721.

233) Kirsch,S.; Doerk,A.; Bartsch,E.; Sillescu,H.; Landfester,K.; Spiess,H.W.; Maechtle,W. Synthesis and Characterization of Highly Cross-Linked, Monodisperse Core-Shell and Inverted Core-Shell Colloidal Particles. Polystyrene/Poly(tert-butyl Acrylate) Core-Shell and Inverse Core-Shell Particles. *Macromolecules* **1999**, *32*, 4508-4518.

234) Matsuura,S.; Niu,C.h.; Cohen,J.S. Pyridinium polyhydrogen fluoride, a deprotecting reagent in peptide chemistry. *J.Chem.Soc., Chem.Commun.* **1976**, 451-452.

235) Temyanko,E.; Russo,P.S.; Ricks,H. Study of Rodlike Homopolypeptides by Gel Permeation Chromatography with Light Scattering Detection: Validity of Universal Calibration and Stiffness Assessment. *Macromolecules* **2001**, *34*, 582-586.

236) Russo,P.S.; Miller,W.G. On the nature of the poly(gamma -benzyl glutamate)-dimethylformamide "complex phase". *Macromolecules* **1984**, *17*, 1324-1331.

237) Kokufuta,E.; Ogawa,K.; Doi,R.; Kikuchi,R.; Farinato,R.S. Geometrical Characteristics of Polyelectrolyte Nanogel Particles and Their Polyelectrolyte Complexes Studied by Dynamic and Static Light Scattering. *J.Phys.Chem.B* **2007**, *111*, 8634-8640.

APPENDIX A SUPLEMENTAL MATERIAL FOR CHAPTER 5

Temyanko from our research group studied PBLG in DMF by gel permeation chromatography (GPC).[235] The grade of the solvent was Gold Label™ from Aldrich. The vendor does not offer DMF Gold Label™ grade anymore. It is assumed that the Gold Label™ grade was of high purity and low water content. In the study by Temyanko *et al.* efforts were made to keep the highly hygroscopic DMF dry. Russo and Miller reported that even small amounts of water can alter the phase behavior of PBLG in DMF.[236] Keeping DMF dry throughout the GPC run requires an extreme amount of care such as purging the solvent with helium, having a closed system with a dry nitrogen atmosphere, *etc*. The experiment can be simplified if a salt such as LiBr is added to the DMF.[177;178]

A broad range of PBLG was studied by GPC using anhydrous grade DMF as well as 0.1 M LiBr in DMF as mobile phases. Additionally, a mobile phase that included a large concentration of water of 1% (v/v) (~ 10,000 ppm) was used in order to verify the tolerance of the 0.1 M LiBr in DMF mobile phase to water. The tandem of detectors included differential refractive index (DRI), static light scattering (SLS), dynamic light scattering (DLS) and viscosity. This allowed obtaining information such as molecular weight (MW), radius of gyration (R_g), hydrodynamic radius (R_h) and intrinsic viscosity ([η]).

Figure A1 shows the conformation plot (R_g *vs* molar mass) for PBLG in the three mobile phases explored. PBLG in DMF is in a rodlike conformation.[235] The expected curve for a perfect rod is given by equation A1.[237]

$$R_g = \left(\frac{L^2}{12} + \frac{r^2}{2} \right)^{\frac{1}{2}} \qquad \text{Equation A1}$$

where *L* is the length of the rod and *r* is the radius of the rod. For PBLG *r* = 0.8 nm [189] and *L* is given by equation A2. [93]

$$L = \left(\frac{M}{M_0} \right) x\, 0.15\, nm \qquad \text{Equation A2}$$

where M is the molecular weight of the polymer, M_0 is the molecular weight of the repeating unit of PBLG, 219 g-mol^{-1}.

The expected line for a rod fits the conformation plots well up to a molar mass of ~ 300,000 g-mol^{-1}. At higher molar masses the plots deviate from the predicted R_g for a rod. The largest deviation is observed when anhydrous DMF is the mobile phase. This may indicate some bending or aggregation of the PBLG.

Figure A2 shows a graph of R_h *vs* molar mass of PBLG in different mobile phases. The expected curve for a rod is given by Equation A3.[237]

$$R_h = \frac{L}{2s - 0.19 - \frac{8.24}{s} - \frac{12}{s^2}} \qquad \text{Equation A3}$$

where $s = \ln\left(\frac{L}{r} \right)$.

L and r are the length and radius of the rod respectively. *L* is given by Equation A2 and *r* = 0.8 nm for PBLG.

The expected curve for R_h of a rod fits well the experimental data up to a molar mass of ~ 600,000 g-mol^{-1}. The behavior of the deviations is similar to the observed in the conformation plots. The largest deviation is observed when anhydrous DMF is the mobile phase. This may indicate some bending or aggregation of the PBLG.

Figure A3 shows a merged graph of R_g and R_h *vs* molar mass for PBLG in different mobile phases. R_g is larger than R_h at almost all molar masses regardless of the mobile phase. The purpose of this plot is just to aid the observation and comparison of the R_g *vs* molar mass and R_h *vs* molar mass plots.

Figure A4 shows the Mark-Howink plot ([η] *vs* molar mass) for PBLG in different mobile phases. Equation A4 is the Mark-Houwink equation.

$$[\eta] = KM^{\alpha} \qquad \text{Equation A4}$$

By taking the logarithm in both sides, the equation takes the form of a linear equation in which *K* is the intercept and α is the slope.

For the curve of PBLG in anhydrous DMF a linear fit was performed between molar masses of ~ 60,000 g-mol^{-1} and 400,000 g-mol^{-1}. The results of the fitting were *K* = -6.72 ± 0.15 and α = 1.70 ± 0.03. For the curve of PBLG in 0.1 M LiBr in DMF a linear fit was performed between molar masses of ~ 20,000 g-mol^{-1} and 600,000 g-mol^{-1}. The results of the fitting were *K* = -4.60 ± 0.009 and α = 1.29 ± 0.002. For the curve of PBLG in 0.1 M LiBr in DMF a linear fit was performed between molar masses of ~ 20,000 g-mol^{-1} and 500,000 g-mol^{-1}. The results of the fitting were *K* = -4.92 ± 0.009 and α = 1.39 ± 0.002.

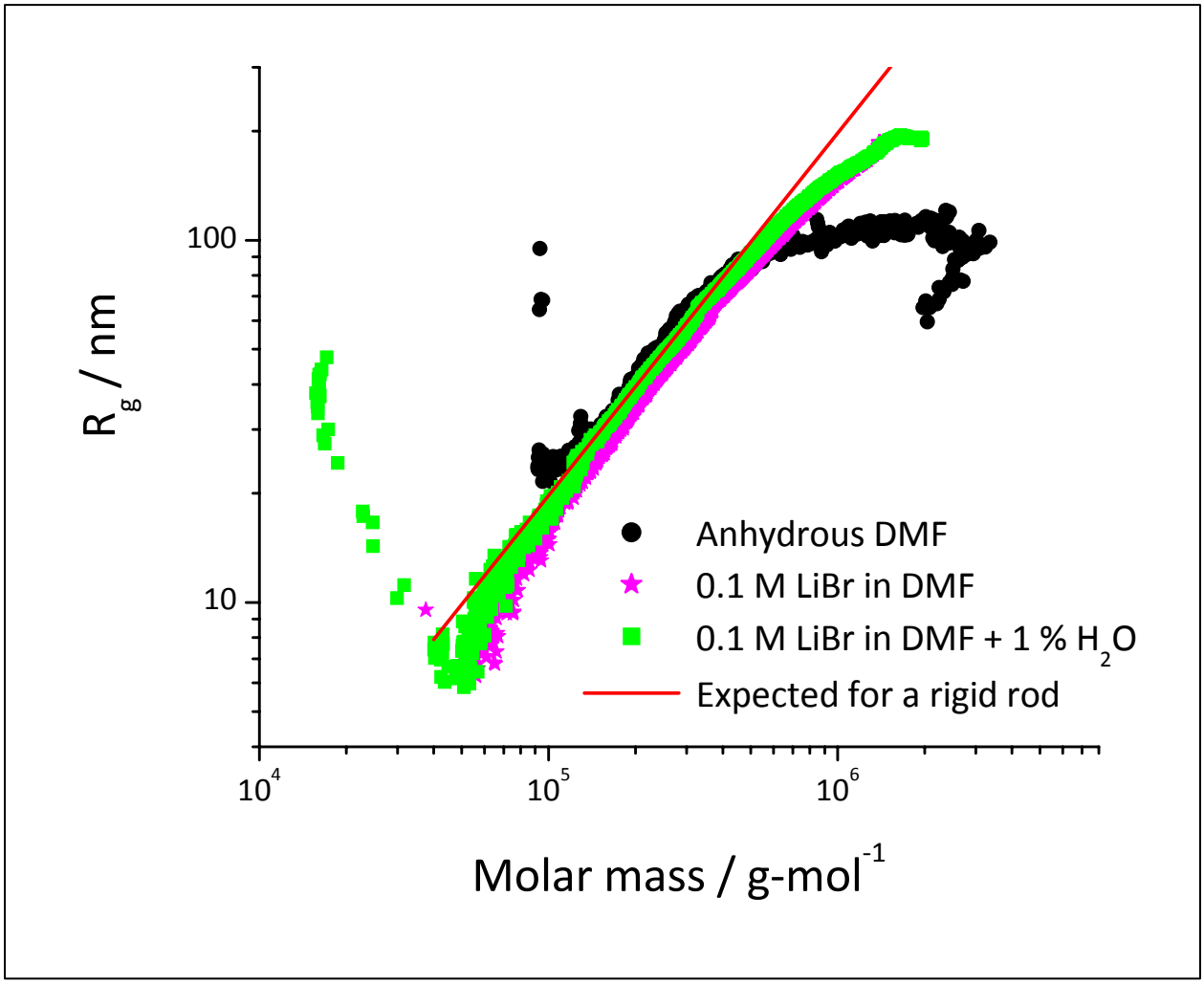

Figure A1 Graph of R_g *vs* molar mass of PBLG in different mobile phases: anhydrous DMF (●), 0.1 M LiBr in DMF (★) and 0.1 M LiBr in DMF + 1% water added (■). The red line is the predicted curve for a rod.

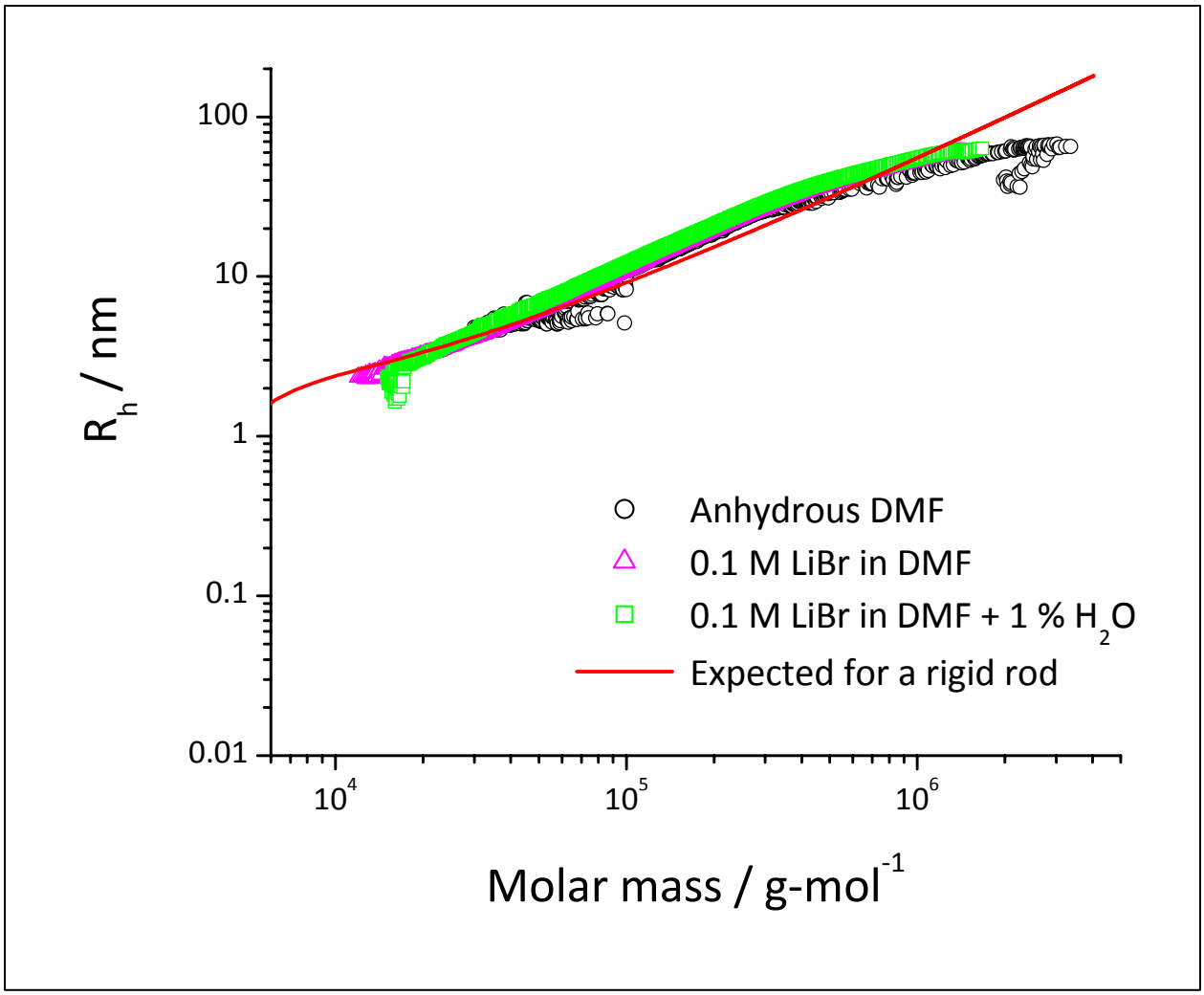

Figure A2 Graph of R_h *vs* molar mass of PBLG in different mobile phases: anhydrous DMF (○), 0.1 M LiBr in DMF (△) and 0.1 M LiBr in DMF + 1% water added (□). The red line is the expected curve for a rod.

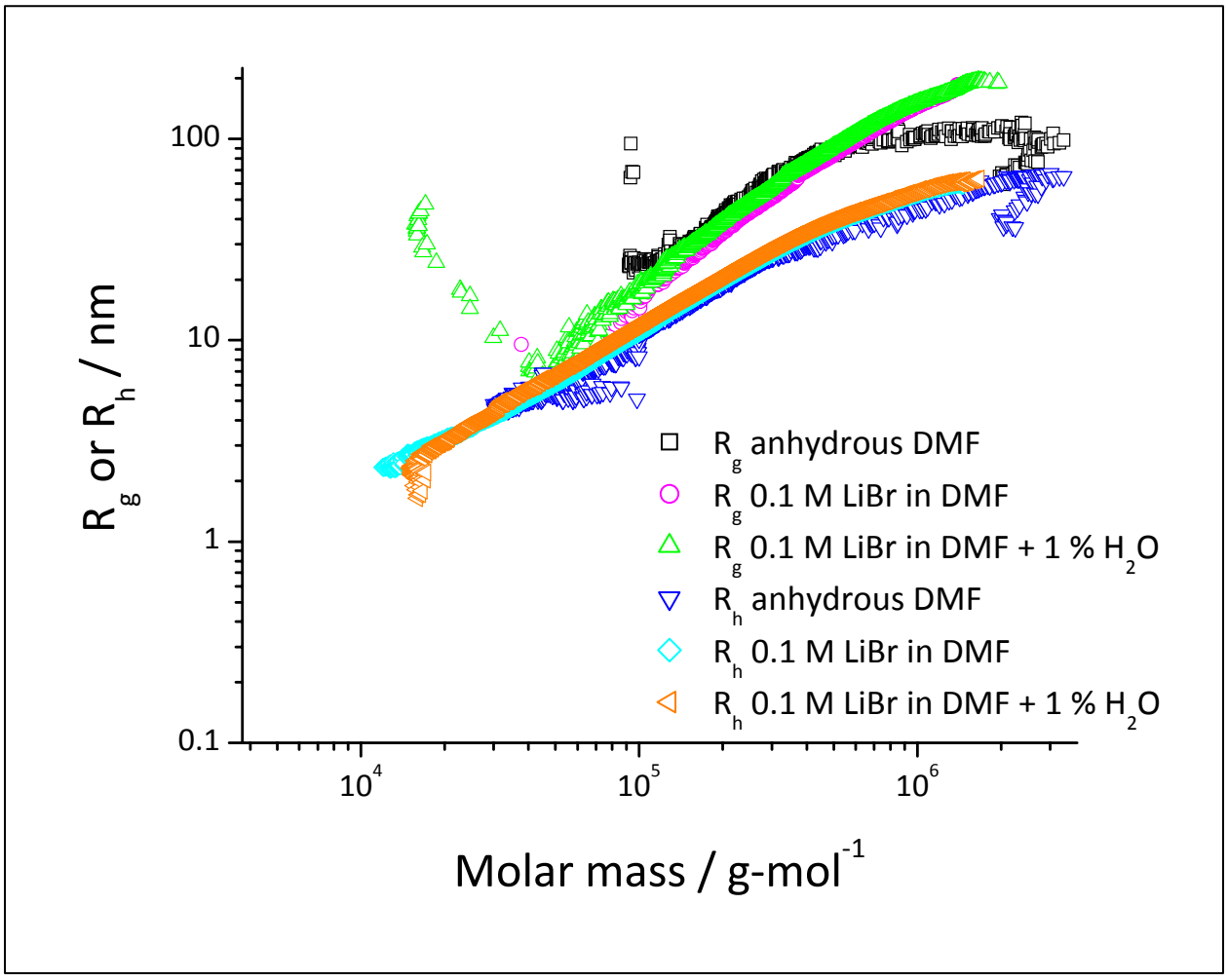

Figure A3 Graph of R_g or R_h *vs* molar mass of PBLG (merged) in different mobile phases: R_g in anhydrous DMF (□), R_g in 0.1 M LiBr in DMF (○), R_g in 0.1 M LiBr in DMF + 1% water added (△), R_h in anhydrous DMF (▽), R_h in 0.1 M LiBr in DMF (◇) and Rh in 0.1 M LiBr in DMF + 1% water added(◁).

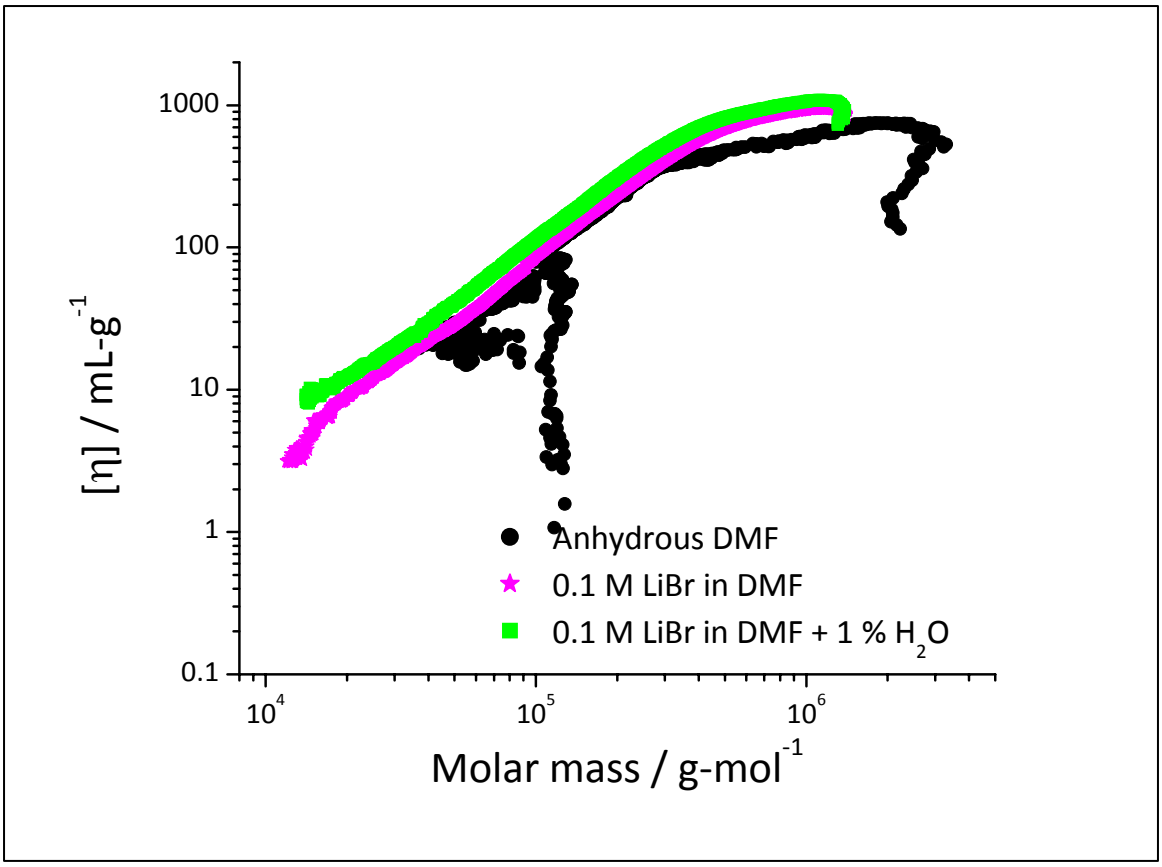

Figure A4 Mark-Houwink plot of PBLG in different mobile phases: anhydrous DMF (●), 0.1 M LiBr in DMF (★) and 0.1 M LiBr in DMF + 1% water added (■).

APPENDIX B PERMISSION

From: "Grad School ETD" <gradetd@lsu.edu>
To: "Erick Soto-Cantu" <esotoc1@lsu.edu>
CC:
Subject: RE: Question about copyright
Date: Wednesday, September 24, 2008 6:54:47 AM

Contact her major professor who should have her email address. She can grant you copyright permission.

From: Erick Soto-Cantu [mailto:esotoc1@lsu.edu]
Sent: Mon 9/15/2008 4:18 PM
To: Grad School ETD
Subject: Question about copyright

Hi,

I am writting my dissertation and I would like to use a figure from a dissertation from a group member that already graduated. The author is Sibel Turksen (we have the same research advisor in the department of Chemistry), she graduated in 2004 and her dissertation is still witheld from web publishing. How can I request to use the material on my dissertation?

Thanks,

Erick Soto-Cantu
Ph.D. Candidate
236 Choppin Hall
Louisiana State University
Baton Rouge, LA 70803

From: "Selcuk, Sibel" <Sibel.Selcuk@heritage-enviro.com>
To: "Erick Soto-Cantu" <esotoc1@lsu.edu>
CC:
Subject: FW: RE: Question about copyright
Date: Thursday, September 25, 2008 2:42:04 PM

Dear Erick Soto-Cantu,

Permission Granted:

I hereby acknowledge that I have the right to grant the permission requested in this electronic mail. I hereby grant to Erick Soto-Cantu the right to use Figure 4.33 from my Louisiana State University Doctoral Dissertation entitled "Synthesis and Characterization of Superparamagnetic Silica-Homopolypeptide Composite Particles".

By: Dr. Sibel Selcuk (Turksen) Date: 09-25-2008

SIBEL SELCUK, PhD
Research Analytical Chemist
Heritage Research Group
7901 W. Morris St. Indianapolis IN 46231
Phone (317) 390-3136
Fax (317) 486-2985
sibel.selcuk@heritage-enviro.com

From: Erick Soto-Cantu [mailto:esotoc1@lsu.edu]
Sent: Wednesday, September 24, 2008 3:22 PM
To: Selcuk, Sibel
Subject: Fw: RE: Question about copyright

Dear Dr. Turksen-Selcuk,

I would like to request permission to use Figure 4.33 from the 2004 Louisiana State University dissertation entitled "Synthesis and Characterization of Superparamagnetic Silica-Homopolypeptide Composite Particles" of which you are the author. It will be used as dissertation material for illustrative purposes.

Sincerely,

Erick Soto-Cantu
Ph.D. Candidate
232 Choppin Hall
Department of Chemisty
Louisiana State University

VITA

Erick Isael Soto Cantu was born in Obregón, México. He attended CBTis 37 for high school education. He was recruited by his chemistry teacher, Gloria Lobo, for training to participate in the Chemistry Olympiad. Erick won first place in the state competition and second place in the national contest in Monterrey, México, in 1996. Later that year, Erick returned to Monterrey and enrolled at Universidad Autónoma de Nuevo León (UANL). Erick earned his bachelor's degree in chemistry in 2001. He obtained the highest GPA among chemistry majors. Erick inquired and learned about the possibility of graduate studies at Louisiana State University from his polymer lab instructor, Prof. Javier Macossay. Erick worked in research and development at a coatings manufacturer in Monterrey. In 2002, he enrolled in the chemistry doctoral program at Louisiana State University where he joined Prof. Paul Russo's group. Erick won the Colgate-Palmolive teaching scholar award for his work in chemistry 2364 and 4010. In 2008 he won the Dow award for excellence in macromolecular studies. Erick is a doctoral candidate and is expected to receive the degree of Doctor of Philosophy in the December 2008 commencement.